Reviewed Preprint
v1 • October 3, 2025
Not revised

Reviewed Preprint
v2 • June 11, 2026
Revised by authors

Oxytocin neurons signal state-dependent transitions from rest to thermogenesis and behavioral arousal in social and non-social settings

Morgane Vandendoren[1,#], Jason G Landen[1,#], Joseph F Rogers[1,#], Samantha Killmer[1], Baizar Alamiri[1], Celeste Pohlman[1], Glenn J Tattersall[2], Nicole L Bedford[1], Adam C Nelson[1]

[1]Department of Zoology and Physiology, University of Wyoming, Laramie, United States • [2]Department of Biological Sciences, Brock University, St Catharines, Canada

For correspondence: anelso74@uwyo.edu

[#] These authors contributed equally

Competing interests: No competing interests declared

Reviewing editor: Moriel Zelikowsky, University of Utah, United States

© 2025, Vandendoren et al. This article is distributed under the terms of the Creative Commons Attribution License, which permits unrestricted use and redistribution provided that the original author and source are credited.

eLife Assessment

This study presents an **important** finding regarding the role of oxytocin neurons in thermogenesis and behavioral thermoregulation. The use of numerous converging methods, including behavior, fiber photometry, optogenetics, thermal recordings, metabolic analyses, and more, produces a multi-dimensional dataset delivering findings that provide **solid** support for the conclusions. The conclusions could be further strengthen by more extensive analyses of behavior and determining whether it is the release of oxytocin (rather than co-release of glutamate) from the PVN that is critical for the transition between behavioral states, nevertheless, the manuscript had many strengths, the findings are novel, and this work opens new doors for understanding the role of the PVT in thermoregulation. This work will be of strong interest to the thermoregulation, social behavior, and oxytocin signaling communities.

https://doi.org/10.7554/eLife.108212.2.sa4

Abstract

Core body temperature (Tb) is defended within narrow limits through thermoregulatory behaviors like huddling, nesting, and physical activity as well as autonomic responses like brown fat thermogenesis. While Tb displays regulated fluctuations across different behavioral states and rest/arousal cycles, the neural control of these transitions is poorly understood. Here, we investigate the relationship between oxytocin neurons of the paraventricular hypothalamus (PVN^{OT}) and behavioral and autonomic thermoeffector pathways across physiological states in mice. First, we show that PVN^{OT} neurons are activated during social thermoregulation. We then demonstrate that *in vivo* PVN^{OT} calcium dynamics align with transitions from rest to thermogenesis and behavioral arousal. Counter to our initial hypothesis, these dynamics were observed in both social and non-social contexts. Using a computer vision model to track thermoeffector pathways, we demonstrate that precisely timed stimulation of PVN^{OT} neurons during low-Tb resting states increases thermogenesis followed by behavioral arousal. We therefore suggest a model in which PVN^{OT} neurons facilitate homeostatic state-dependent transitions in thermo-behavioral states.

Introduction

Maintaining a relatively constant core body temperature (Tb) is a vital homeostatic need. While excessive deviations (e.g. >2°C) from the typical mammalian Tb of approximately 37°C can be harmful[1], Tb normally fluctuates within a narrow range (typically 0.5 - 1°C) across sleep-wake cycles and behavioral states [2–4]. These fluctuations often exhibit bimodal or multimodal

distributions, indicating distinct thermal states. Additionally, Tb variations are increasingly understood not as passive outcomes of animal physiology, but as regulated, brain-initiated transitions between defended Tb "balance-points" [2,5–7]. For example, the transition from the rest to the active balance-point involves modulation of both autonomic and behavioral thermoeffector pathways (i.e., regulated heat loss and production) to meet the energetic demands of movement and arousal [2,7,8]. However, the neural mechanisms that govern these physiological transitions remain incompletely understood [8,9].

Thermoregulation is orchestrated by the integration of autonomic and behavioral effectors. Autonomic outputs, such as brown adipose tissue (BAT) thermogenesis and vasomotor tone, are well-characterized at the circuit level. This pathway integrates sensory signals from peripheral thermosensors in the preoptic area of the hypothalamus (POA), then relays this information to the dorsomedial hypothalamus (DMH), and then to sympathetic efferent neurons of the rostral medullary raphe (rMR) [5,10]. By contrast, the neuronal substrates of behavioral thermoregulation—such as huddling, nesting, or physical activity [7,11–13]—and how they integrate with autonomic outputs are less well defined. Although recent studies have made progress in identifying brain regions underlying some of the associated neural pathways [14–17], much remains unknown about how animals behaviorally thermoregulate.

Behavioral thermoregulation strategies are naturally organized into alternating sequences across bouts of arousal and quiescence and are modulated by environmental conditions (including social context) and internal state [8,9,12,16,18–20]. In the social context, huddling provides thermal and energetic benefits through shared body heat and reduction of heat loss [21–24]. During mild cold stress, huddling among mice facilitates both entry into, and exit from, an energy-saving, low-Tb quiescent state [12]. In the non-social context, physical activity and nesting are two behavioral strategies to generate and retain body heat as temperature decreases [13,25–27]. These patterns suggest active neural regulation of behavior and sympathetic arousal in tandem; however, the brain circuits that support this coordination remain unidentified.

Oxytocin (OT)-producing neurons in the paraventricular nucleus of the hypothalamus (i.e., PVN^{OT}) are a compelling candidate for such coordination [28]. PVN^{OT} neurons have been implicated in autonomic arousal [29], energy expenditure [30], and thermoregulation—including activation of BAT thermogenesis [31–33]. The oxytocin system is also classically associated with social behaviors [34] including physical touch [35]—a key element of huddling. Indeed, OT-mutant rat pups display deficits in both warm-seeking and huddling behavior [36], and OT neurons display bursts of pulsatile activity during bouts of lactation and direct physical contact with pups [37]. Yet, whether PVN^{OT} neural activity is functionally associated with the rhythmic patterning of thermoregulatory states is not known.

Here, we set out to identify the relationship between PVN^{OT} activity and daily patterns of behavioral thermoregulation in mice. We initially observed that PVN^{OT} activity is linked to huddling states. Then, we discovered that PVN^{OT} calcium dynamics during huddling are predictive of transitions to body warming and arousal. Intriguingly, in a parallel fashion, PVN^{OT} activity also tracks transitions from rest to arousal in solo animals. Last, using automated thermal feature tracking and optogenetics, we demonstrate that PVN^{OT} stimulation initiates state-dependent transitions that coordinate physiological warming with behavioral arousal. These findings reveal a previously unrecognized role for PVN^{OT} neurons in regulating dynamic, context-dependent thermo-behavioral strategies.

Results

PVN^{OT} neural activity is associated with huddling substates

Mice use huddling to facilitate thermoregulatory state transitions. We sought to identify huddling-associated brain regions in groups of adult females, which show stronger huddling-associated Tb changes than male groups [12]. Using a home-cage surveillance system that eliminates direct human-animal interaction [12] in conjunction with FOS immunohistochemistry (IHC), we examined patterns of cellular FOS activity in 18 brain regions. We focused on regions associated with

thermoregulation, social behavior, and identified to be FOS-activated during huddling substates in preliminary studies (Fig. 1A-B). We examined animals engaged in active huddling (close physical contact while displaying some physical activity), quiescent huddling (close physical contact with no physical activity) and—as a control for physical touch in the absence of social contact—solo-housed animals engaged in self-grooming. For IHC, we scored cellular FOS activity after the animals had been engaged in state-specific behavior (i.e., active huddle, quiescent huddle, solo-groom) for at least 15 minutes.

We initially focused on active huddling-associated FOS expression because this state requires that an animal actively maintain close physical contact with another individual. We identified three regions that were activated 90 minutes after the onset of active-huddling: the dorsal medial hypothalamus (DMH), the rostral lateral septum (LS), and the paraventricular nucleus of the hypothalamus (PVN) (Fig. 1C-F and S1A-F; all statistical results are reported in Table S1). The DMH and the PVN are areas associated with energy regulation and thermoregulation, with inputs to the rMR [5,38,39]. The LS is associated with a variety of functions, from motivation to fear responses [40,41] and is strongly associated with the control of social behavior [42]. These results suggest active huddling recruits brain regions with known roles in thermoeffector and social interaction pathways.

The PVN is one of two primary locations of OT-producing neurons [39]. Given the established associations of PVN^{OT} neurons with thermoregulation and social behavior, we asked whether they were activated during active and quiescent huddling. To increase the temporal resolution of our assay from the timescale of protein translation to that of mRNA transcription, we used single-molecule fluorescence *in situ* hybridization (smFISH) to identify PVN^{OT} neurons that became *Fos*-positive 30 minutes after the onset of a behavioral state. We quantified neurons in the dorsal and ventral PVN, which have unique cyto-architectures and projection patterns[43] (Fig. 1G-I). PVN^{OT} neurons were *Fos*-positive during both active huddling and quiescent huddling. During active huddling, the dorsal population was more *Fos*-positive than the ventral population ($t = 4.31$, $p = 1.01X\ 10^{-3}$, LMM, Table S1), and this dorsal population displayed greater *Fos* activity during active compared to quiescent huddling (Fig. 1I) ($t = 3.30$, $p = 3.94X\ 10^{-2}$, LMM, Table S1).

These results suggest the PVN is a huddling-associated brain region and that PVN^{OT} neurons are activated during huddling substates. Given the coarse timescale of *Fos* dynamics (≥30 minutes for transcription and ~60-90 minutes for translation) compared to the faster timescale of rest-arousal cycles in mice (minutes; [44,45]), we next employed in vivo calcium recordings to capture finescale population-level dynamics of PVN^{OT} neurons.

PVN^{OT} Ca^{2+} peaks track rest and arousal behavior states in social and non-social conditions

Behaviorally, mice modulate body temperature through physical activity, nesting, and huddling [7,11–13,25]. In a longitudinal study accounting for individual variance in physiology and behavior, we next asked how calcium activity in PVN^{OT} neurons was associated with real-time behavior during social thermoregulation [46] in different thermal conditions (Fig. 2A-C). As a control for social context, we also examined solo-housed animals. Experiments were conducted at three floor temperatures: cold (15°C), cool (23°C; room temperature), and a temperature near the "lower critical temperature" (29°C; the transition point between energy-requiring and energy-neutral thermoregulatory mechanisms [11,47,48]). We tracked six behaviors in the solo condition and 10 behaviors in the paired condition (Fig. 2B).

We used an AAV encoding the calcium indicator GCaMP (pGP-AAV9-syn-FLEX-jGCaMP8s-WPRE) [49] and fiber photometry using an optical fiber implanted above the PVN (Fig. 2A-D). GCaMP AAVs have been validated to transfect OT neurons in OT-Cre mice [50–52] and, in this study, showed co-labelling with OT-immunoreactive neurons (Fig. S2A-B). Neural-photometric recordings were conducted during the light/rest phase, when rhythmic episodes of rest and activity make the distinction between different thermoregulatory states readily discernable [12]. We observed large

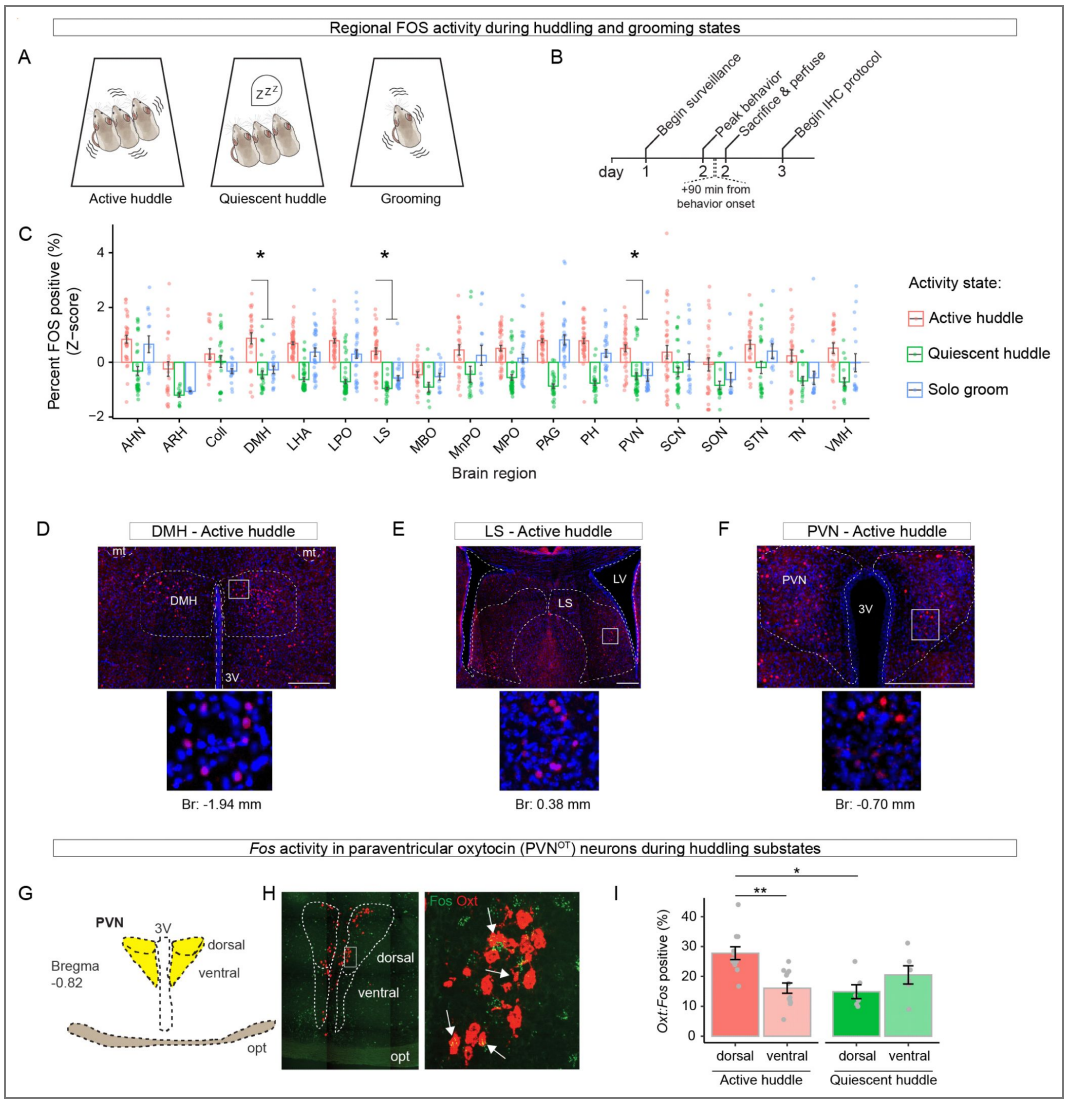

Figure 1. The PVN and PVN^{OT} neurons are FOS activated during huddling substates.

(A - B) Experimental design to identify state-specific activity in 18 brain regions. Behavioral states **(A)**. Experimental timeline **(B)**. **(C)** Quantification of percent FOS - DAPI colocalized cells across brain regions for each behavior. Regional FOS percentages are z-scored on a per experiment basis. N = 15 mice/1530 ROIs. Each datapoint is an ROI. Asterisks denote regions in which active huddle FOS activity is greater than both quiescent huddle and solo groom. P-values adjusted for multiple comparisons using the Holm method. **(D - F)** Representative histology images showing active huddling associated FOS expression in the DMH **(D)**, LS **(E)**, and PVN **(F)**. 3V: third ventricle; mt: mammillothalamic tract; LV: lateral ventricle. Scale bar equals 500 µm. Insets show FOS (red) and DAPI (blue). **(G)** Schematic of the PVN. Opt: optic tract. **(H)** Representative histology images showing mRNA expression of *Fos* and *Oxt* in the PVN. **(I)** Quantification of percent *Oxytocin:Fos* colocalized cells in dorsal and ventral subregions of the PVN during active huddling and quiescent huddling (N = 8 mice). Each datapoint is an ROI. **C:** linear model with Tukey's post-hoc tests. **I:** linear mixed effect model. Data are mean ±SEM. P < 0.05 *, P < 0.01 **, P < 0.001 ***. Full statistical analysis in Table S1.

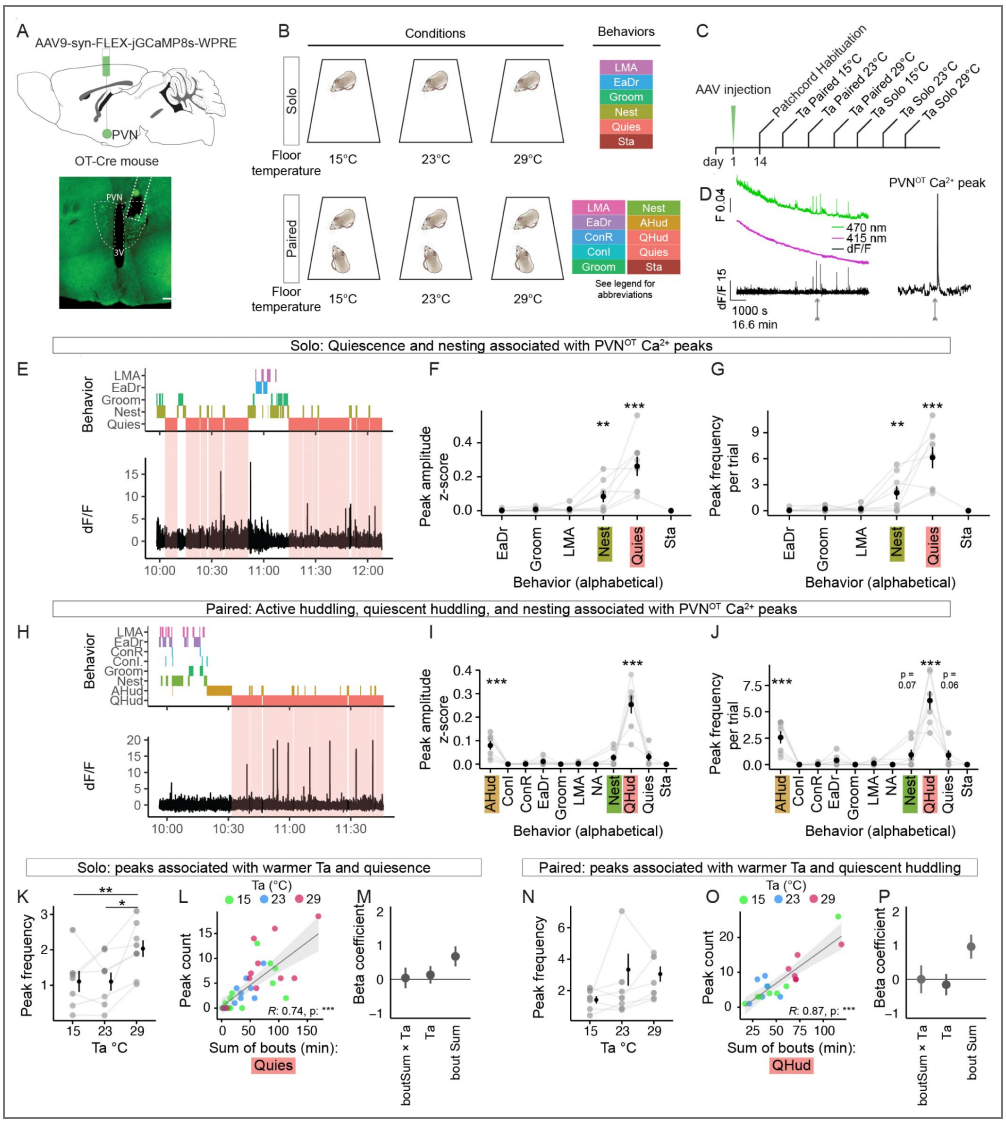

Figure 2. PVN^{OT} peaks track rest and arousal behavior states in social and non-social conditions.

(A - C) Fiber photometric recordings of PVN^{OT} cells in different social contexts and floor temperature conditions. Scheme of GCaMP AAV injections (top) and histology showing GCaMP-positive neurons in the PVN optic fiber placement (bottom) Scale bar 200 µm. **(A)**. Floor temperature and social context conditions, and behaviors analyzed **(B)**. Scheme of the timeline. Order of the social and floor temperature conditions was pseudo-randomized **(C)**. **(D)** Example traces of calcium-dependent (470 nm) and calcium-independent (415 nm) channels, and the post-processed dF/F trace (bottom), from a two-hour recording. Example PVN^{OT} Ca^{2+} peak, denoted by arrow, is expanded (right). **(E - G)** Behaviors associated with PVN^{OT} peaks in solo condition. Example ethogram aligned to photometric recording. Soft red shaded areas align with the quiescent state **(E)**. PVN^{OT} peak amplitude **(F)** and frequency **(G)** according to behavioral state across solo trials. **(H - J)** Behaviors associated with PVN^{OT} peaks in paired condition. Example ethogram aligned to photometric recording. Soft red shaded areas align with quiescent huddling **(H)**. PVN^{OT} peak amplitude **(I)** and frequency **(J)** according to behavioral state across paired trials. **(K - M)** Effect of floor temperature and quiescence on PVNOT peaks in solo animals. Peak frequency according to floor temperature (Ta) **(K)**. Peak count according to total duration of quiescent bouts **(L)**. Beta coefficients from a model of the effect of floor temperature, total duration of bouts (boutSum), and the Ta*boutSum interaction on peak count **(M)**. **(N - P)** Effect of floor temperature and quiescence huddling on PVNOT peaks in paired animals. PVNOT peak frequency according to floor temperature **(N)**. Peak count according to total duration of quiescent bouts **(O)**. Beta coefficients from a model of the effect of floor temperature, total duration of bouts (boutSum), and the Ta*boutSum interaction on peak count **(P)**. **F,G,I,J,K,L,M,N,O,P**: linear mixed model. N = 8 mice/50 recordings. **M** and **P** show means plus confidence interval; all else shows mean ±SEM. P < 0.05 *, P < 0.01 **, P < 0.001 ***. Full statistical analysis in Table S1. Abbreviations: LMA (Locomotor Activity), EaDr (Eating or Drinking), Groom (Grooming), Nest (Nesting or Nest Building), Quies (Quiescence), Sta (Stationary), ConI (Contact Initiated), ConR (Contact Received), AHud (Active Huddle), QHud (Quiescent Huddle).

calcium transients (hereafter "peaks") that appeared to be similar to those previously reported in lactating female mice [37,51] (Fig. 2D). Further analyses focused on peaks that were at least six standard deviations above baseline.

We first examined the effect of social context (i.e., paired- vs. solo-housed) on calcium peak amplitude and frequency across the three floor temperatures. While there was no effect of social context on peak amplitude (Fig. S2C), there was an increase in peak frequency in paired animals (Fig. S2C-D) (t = 2.455, p = 1.82X 10^{-2}, LMM, Table S1). To our surprise, in both social and nonsocial contexts, PVN^{OT} peaks were strongly linked to specific behaviors. In the solo context, peak amplitude and frequency were associated with nesting (t = 2.83, p = 7.64X 10^{-3}, LMM, Table S1) and quiescence (i.e., motionless rest) (t = 8.85, p = 1.98X 10^{-10}, LMM, Table S1) (Fig. 2E-G). In the paired context, peaks were associated with active (t = 5.26, p = 2.35X 10^{-6}, LMM) and quiescent huddling (Video S1) (t = 16.74, p = 1.84X 10^{-23}, LMM) and, to a lesser extent, nesting (Fig. 2H-J, Table S1). We next examined the behavioral associations of PVN^{OT} peaks within each floor temperature. The behavior-state associations with calcium peaks were largely preserved across all three floor temperatures (Fig. S2G-J). Linear mixed model (LMM) analysis of calcium peak amplitude and frequency revealed main effects of quiescence and nesting in the solo context (Fig. S2G,I), and main effects of active huddling, quiescent huddling, and nesting in the paired context (Fig. S2H,J). Thus, PVN^{OT} peaks are associated with distinct resting and waking behavioral states in social and non-social contexts.

Next, we analyzed the relationship between peak frequency and floor temperature and behavioral bout length across the two social contexts (Fig. 2K-P). For resting behaviors (quiescence and quiescent huddling), peaks were more frequent at 29°C for solo (Fig. 2K) animals, and trended (non-significantly) upward in paired animals (Fig. 2N, Table S1). In mice, sleep is more common at warmer ambient temperatures [8]. To disambiguate whether PVN^{OT} peaks display warm sensitivity vs. arousal-state dependency, we performed multiple regression analysis relating the number of peaks to floor temperature and the duration of rest bouts. In solo and paired conditions calcium peak counts were strongly related to rest bout duration (Fig. 2L,O), and quiescence and quiescent huddling bouts appeared longer at 29°C (Fig. 2L,O, red dots). Analysis of the contribution of bout length and floor temperature to peak counts showed that, in solo and paired contexts, increased peak counts at 29°C could be explained by longer rest bout lengths (Fig. 2M and 2P). We then examined active behaviors associated with PVN^{OT} peaks. For active huddling, peak counts were positively correlated with bout length, but not temperature (Fig. S2K-L). For nesting, peak counts were not associated with bout length nor floor temperature (Fig. S2M-N).

Together, these results suggest PVN^{OT} peaks track distinct resting and active behaviors in social and non-social settings and are enhanced in the social context. In addition, PVN^{OT} peaks are largely unaffected by the floor temperature conditions tested; we therefore pooled data from the three floor temperatures in subsequent analyses.

PVN^{OT} neurons predict increased likelihood of transitions towards thermogenesis and behavioral arousal in social and non-social contexts

PVN^{OT} peaks track two rest states (quiescence and quiescent huddling), and two active states (i.e., nesting and active huddling) (Fig. 2). Notably, each of these states are in part thermoregulatory and are naturally organized into alternating sequences of bouts across rest/active cycles [8,9,12,16,18–20]. To address how PVN^{OT} dynamics align with these sequences, we quantified peaks relative to the onset and offset of behavior bouts, as well as to changes in physical activity and core body temperature (Fig. 3A).

We first examined physical activity (as measured by frame-to-frame pixel changes). Physical activity increased following PVN^{OT} peaks in both solo (t = 3.37, p = 0.012, LMM) and paired (t = 6.82, p = 0.001, LMM, Table S1) conditions,. This increase began at the approximate time of the peak and persisted through the subsequent 400 seconds (6.6 min) (Fig. 3B-E).

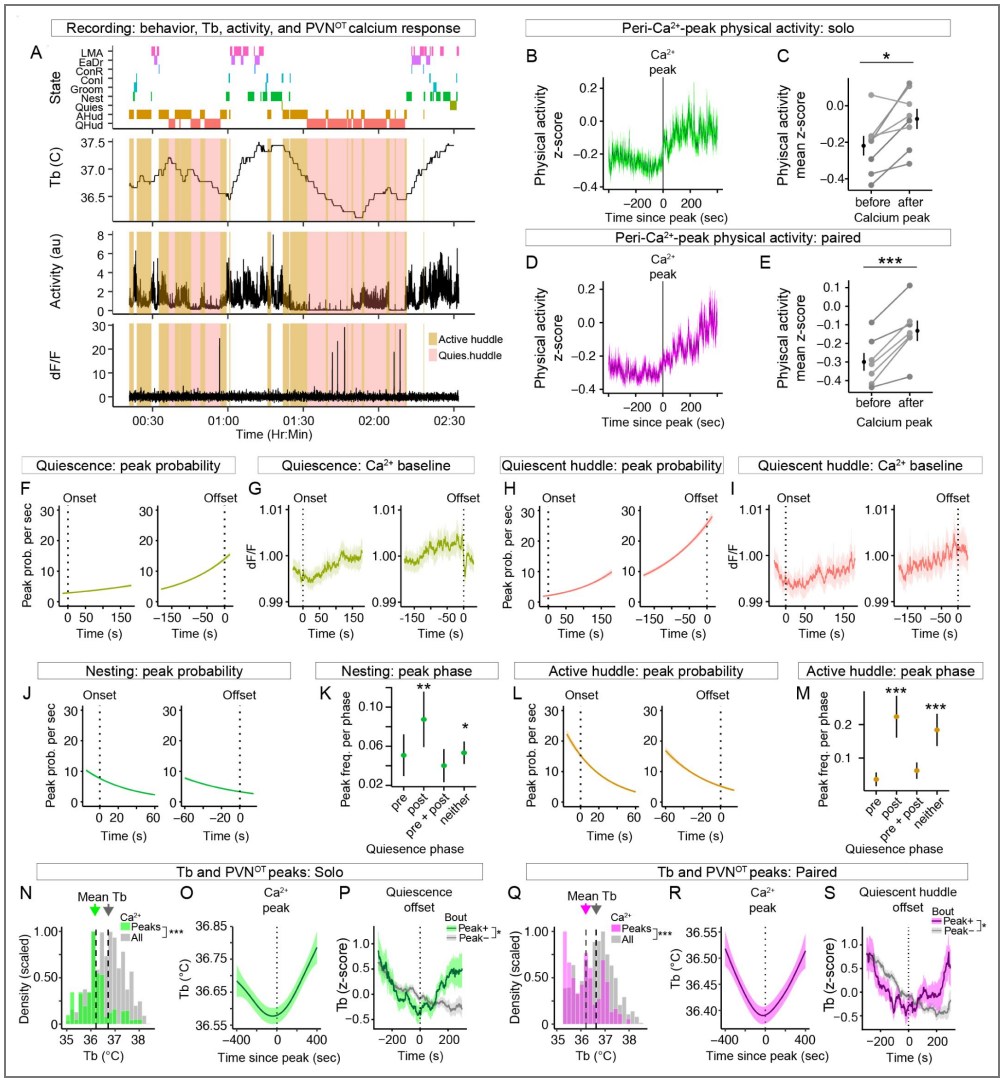

Figure 3. PVN^{OT} peaks predict transitions to behavioral arousal and thermogenesis.

(A) Individual, example trace of alignment of behavioral state, body temperature, physical activity, and dF/F from an experiment in the paired context. Bouts of active- and quiescent-huddle are color coded. **(B - E)** Physical activity around the time of PVN^{OT} peaks. Peri-event time histogram of activity before and after PVN^{OT} peaks in solo mice **(B)**. Per-individual means before and after PVN^{OT} peaks in solo mice **(C)**. Peri-event time histogram of activity before and after peaks in paired mice **(D)**. Per-individual means before and after peaks in paired mice **(E)**. **(F - I)** PVN^{OT} Ca^{2+} dynamics during onset and offset of rest-behavior bouts. Quiescence onset/offset: peak probability **(F)** and Ca^{2+} baseline average **(G)**. Quiescent huddle onset/offset: peak probability **(H)** and Ca^{++} baseline average **(I)**. **(J - M)** PVN^{OT} Ca^{2+} dynamics during onset and offset of active-behavior bouts. Nesting onset/offset: peak probability **(J)**. Nesting-associated peak frequency according to quiescence phase. "Neither" refers to bouts not adjoining bouts of quiescence **(K)**. Active huddle onset/offset: peak probability **(L)**. Active-huddle-associated peak frequency according to quiescence phase. "Neither" refers to bouts not adjoining bouts of quiescence **(M)**. **(N - S)** Relationship between core body temperature (Tb) and PVNOT Ca++ dynamics and behavioral transitions. **(N-P)** Tb dynamics in solo animals. Histogram of Tb during minutes containing a calcium peak (green) vs. baseline (grey) data in solo animals **(N)**. Event-triggered average of Tb before and after PVNOT peaks in solo animals **(O)**. Scaled Tb transitions around quiescence offset for bouts with PVNOT peaks (Peak+) and without peaks (Peak-). Event-triggered average of z-scored body temperature aligned to the time of quiescence offset (0 s). Peak+ bouts had a Ca2+ peak within 100 s preceding bout offset. Lines show mean z-Tb; shaded ribbons indicate SEM **(P)**. **(Q – S)** Tb dynamics in paired animals (similar to N-P). Histogram of Tb during minutes with a peak vs baseline **(Q)**. Event-triggered average of Tb before and after PVNOT peaks **(R)**. Event-triggered average of Tb aligned to quiescent huddle offset during bouts with and without peaks **(S)**. **C,E,K,M,N,P,Q**: linear mixed model. **F,H,J,L**: logistic regression. N = 8 mice/50 recordings, except for **N-S**, N = 5 mice/24 recordings. **O** and **R** :predicted values of a general additive model ±SEM; **P** and **R**: linear mixed model. All data shows mean ±SEM. P < 0.05 *, P < 0.01 **, P < 0.001 ***. Full statistical analysis in Table S1.

We next examined the density (i.e., frequency of peaks per time bin) of calcium peaks with respect to the onset and offset of the two resting states: quiescence and quiescent huddling. For both behaviors, there was a higher density of peaks in the minutes prior to bout offset compared to onset (Fig. S3A-C). Moreover, there was a positive relationship between bout length and the number of peaks per bout, indicating that longer rest bouts are more likely to have peaks (Fig. S3B,D). To better understand the relationship between PVN^{OT} dynamics and bouts of quiescence and quiescence huddling, we next examined (1) the per-second probability of observing a peak relative to bout onset/offset using logistic regression, and (2) changes in calcium baseline (Fig. 3F-M).

For bouts of quiescence, peak probability was approximately 2.7% near the time of onset and 14.0% near the time of offset (Fig. 3F). For bouts of quiescent huddling, peak probability was approximately 2.1% near the onset and around 25.6% near the time of offset (Fig. 3H). In accordance with the peak density and probability data, baseline calcium in PVN^{OT} neurons was higher in the minutes leading to rest offset compared to onset in all animals (Fig. 3G,I, see also S3M-N). Thus, PVN^{OT} neural activity strongly predicts (i.e., probabilistically) quiescence/quiescent huddling offset compared to onset by at least five-fold, and signals an increase in physical activity —a correlate of behavioral arousal [53] and a means of increasing metabolic rate and Tb [26].

We next examined PVN^{OT} peak density and probability during the onset and offset of the two active states: nesting and active huddling (Fig. 3J-M, and S3E-H). In contrast to the two resting states, peak density in both states was higher near bout onset compared to offset (Fig. S3E,G). Moreover, there was only a weak relationship between peak count and bout length for both states, indicating that longer bouts are not more likely to have peaks (Fig. S3F,H). Logistic regression analysis of nesting bouts showed that PVN^{OT} peak probability was approximately 7.7% near the time of onset and 3.3% near the time of offset (Fig. 3J). For active huddling bouts, peak probability was approximately 15.3% near the time of onset and 5.2% near the time of offset (Fig. 3L). Thus, for nesting and active huddling, PVN^{OT} peaks are two- to three-fold more likely to predict bout onset than offset. Notably, within the paired condition, there was a higher peak probability for active huddling compared to nesting (Poisson regression, nesting vs. active huddling peaks counts, $P < 0.001$), suggesting that social interaction enhances the probability of PVN^{OT} activity.

Because the pre-onset and post-offset periods can be composed of multiple different behaviors, the calcium analyses described above were restricted to the time-window of the behavioral bouts themselves (i.e., between onset and offset) plus a small (30 sec) margin. To provide a broader view of PVN^{OT} activity across the extended peri-event period, we examined baseline calcium for three minutes before and after the onset and offset of each type of behavior (Fig. S3I-L). For the two resting states (quiescence and quiescent huddling), baseline calcium reached a minimum near bout onset and a maximum near offset (Fig. S3I-J), whereas for the two active states (nesting and active huddling) baseline calcium showed the opposite pattern, with the maximum near onset and the minimum near offset (Fig. S3K–L). Thus, despite heterogeneity in the peri-bout periods, PVN^{OT} baseline calcium exhibits consistent state-dependent dynamics around the offset of rest and onset of active behaviors.

Nesting and active huddling often occur immediately before or after (or in between) bouts of quiescence (i.e., the peri-quiescent phase) [12,16,19,20]. We next examined the quiescence phase for PVN^{OT} peaks associated with nesting and active huddling. PVN^{OT} peaks were more likely to occur during the post-quiescence phase for both nesting (Fig. 3K) ($t = 2.97$, $p = 0.005$, LMM) and active huddling (Fig. 3M) ($t = 4.08$, $p = 1.58X\ 10^{-4}$, LMM, Table S1). Notably, although nesting and active huddling are commonly expressed during the pre-quiescent phase, these two behaviors are rare during the post-quiescent phase (Fig. S3O-P). Thus, even though nesting and active huddling are relatively rare during the post-quiescent phase, those are precisely the active state-phases during which PVN^{OT} activity increases. This suggests that PVN^{OT} neurons distinguish nesting/active huddling in the post-quiescent phase from these same behaviors in the pre-quiescent phase.

Together these results suggest that elevated PVN^{OT} activity dynamics predict within approximately 100 seconds the offset of two rest states (quiescence and quiescent huddling) and within around 20 seconds the onset of two post-quiescence active states (nesting and active huddling) in solo and paired mice, respectively.

PVN^{OT} peaks occur during low Tb (~36.2°C) and prior to body warming

In rodents, transitions from rest to arousal are thought to result, in part, from an ultradian (i.e., occurring on cycles < 24 hr), brain-driven switch of the defended body temperature from a rest balance-point (i.e., lower bound) to an awake balance-point (i.e., upper bound) [2,7]. Because PVN^{OT} calcium peaks aligned with transitions from resting to active states, we examined Tb dynamics in relation to different behavioral states and the timing of PVN^{OT} calcium peaks.

We first measured the relationship between core Tb and behavioral bout length (i.e., duration) using regression (Fig. S3Q-V). For bouts lasting two or more minutes, Tb was not associated with active huddling, eating/drinking, grooming self, or quiescence. In contrast, Tb was negatively correlated with the length of quiescence huddling bouts (Fig. S3V). This finding supports our previous demonstration that quiescent huddling is an energy saving state in mice [12].

We then examined Tb dynamics before, during, and after PVN^{OT} calcium peaks (Fig. 3N-S). PVN^{OT} peaks occurred when Tb was around 0.5°C lower than baseline (baseline-Tb: 36.7°C; peri-peak-Tb: 36.2°C) (Fig. 3N,Q) in both solo (t = −38.85, p < 0.0001, LMM) and paired (t = −42.78, p < 0.0001, LMM, Table S1) conditions. Moreover, PVN^{OT} peaks aligned with the low point of a U-shaped body temperature profile: on average, Tb decreased before, and increased after, the time of the calcium peak in both solo and paired conditions (Fig. 3O,R). Together, these results suggest that PVN^{OT} peaks occur during a low Tb and predict a forthcoming increase in Tb.

We next examined rest-to-active transitions, and asked whether the thermogenic trajectory differed depending on whether a PVN^{OT} calcium peak occurred prior to rest offset. We extracted peri-transition temperature traces (±300 s) aligned to the offset of quiescence and quiescent-huddling bouts and classified each transition as Peak+ if it contained one or more PVN^{OT} peaks in the 100 s preceding bout offset, and Peak− otherwise. To control for inter-animal differences in Tb balance point, temperature was z-scored within mouse (Fig. 3P,S). Analysis revealed that transitions preceded by PVN^{OT} peaks exhibited larger post-offset increases in body temperature than transitions lacking peaks for both quiescence (PeakPlus effect: F(1, 161) = 4.60, p = 0.033) and quiescent huddling (F(1, 113) = 5.64, p = 0.019, Table S1). Together, these results indicate that although PVN^{OT} peaks are not present before every rest offset, when they do occur it is associated with an enhanced thermogenic rise during the ensuing rest-to-active transition.

Lactation as a functional validation of PVN^{OT} recordings

We next sought to verify the oxytocinergic identity of recorded GCaMP cells in the PVN using IHC. Unexpectedly, we found variable overlap between oxytocin immunoreactivity and AAV-GCaMP-positive cells. For example, in PVN tissue slices from one individual the percentage of OT^{+},GCaMP^{+} cells ranged from 80% to 69%, while the percentage of GCaMP^{+},OT^{+} cells ranged from 51% to 24% (Fig. S4A-F). Notably, in slices with low overlap between OT and GCaMP markers there was pronounced OT reactivity in the processes lining the third ventricle, particularly the ventral side and the lumen (Fig. S4D). These observations are in accord with reports that OT IHC can reflect release-competent processes, including those contacting or lining the ventricle [54,55], and that OT IHC staining between the ventricle and PVN soma can vary by time of day [56]. We therefore turned to physiology recordings to verify the cellular identity of the GCaMP recorded cells.

PVN^{OT} neurons display characteristic pulsatile activity bursts during lactation and direct contact with pups, with heightened intensity and broadening waveforms during late-stage lactation (PPD 8 to 14) compared to early-stage lactation (PPD 2-7) [37,51,57]. Whether this type of activity in PVN^{OT} neurons is exclusive to lactation and nursing events is poorly understood [37,50,58]. To address

whether calcium peaks occurring during transitions from quiescence to active states resemble those during lactation, we recorded from virgin females as described above and then allowed them to reproduce and nurse their young (Fig. 4A-C). As documented in other studies [37,51], PVN^{OT} neurons displayed peaks that increased in frequency and amplitude from early-stage to late-stage lactation. This observation provides a physiological verification of the oxytocinergic identity of the recorded neurons in our system (Fig. 4D-E and Video S2). PVN^{OT} peaks in virgin females appeared similar in amplitude in early-stage compared to late-stage lactation and appeared narrower overall (Fig. 4F-I).

Systematic comparisons of peak kinetics revealed that virgin female calcium peaks displayed narrower full-width half maximum (FWHM) values than either early-stage or late-stage lactation (Fig. 4I-J). Next, while virgin and early-stage lactation peak amplitudes were equivalent, both were less than that of late-stage lactation (Fig. 4K). Finally, while virgin interpeak intervals (IPIs) were equivalent to early-stage lactation, they were longer than those of late-stage lactation (Fig. 4L) (all statistics in Table S1).

Together, these results provide a physiological validation of the oxytocinergic identity of the recorded neurons. They suggest that calcium peaks observed in virgin females during rest-wake behaviors (this study) share similar kinetics to PVN^{OT} peaks during early-stage lactation. As such, this data uncovers a behavioral and physiological context in which PVN^{OT} neurons display calcium burst-like peaks.

PVN^{OT} peaks signal increases in BAT thermogenesis and changes in regional surface temperature

Our data suggest PVN^{OT} peaks signal transitions towards thermogenesis and arousal as measured by core Tb and physical activity. However, core Tb represents the integration of several different thermoeffector pathways like BAT thermogenesis and peripheral thermal regulation (e.g., cutaneous blood flow. We therefore sought to automate a computational strategy that uses video thermography in freely moving animals to approximate BAT thermogenesis and regional surface temperatures at sub-second resolution—a timescale relevant to sympathetic activity.

We developed a computer vision system called Skeleton-Guided Bodypart Segmentation (SGBS) that uses deep learning to record the surface temperature of three thermal features of an animal: the surfaces over (1) interscapular brown fat (BAT), (2) the rump, and (3) the entire dorsal surface (Fig. 5A). Our pipeline integrates DeepLabCut-based animal tracking [59] and Mask R-CNN technologies [60] in a Python framework [61] to process high-resolution thermography (FLIR) videos. An attention layer integrates 10 anatomical skeleton keypoints (e.g., head, nose, shoulders and tail) with a model trained on manual annotations of the three thermal features. Leveraging these keypoints, SGBS can precisely localize and delineate thermal features for mask prediction (Fig. 5B). SGBS detects above-average temperatures in the BAT region and below-average temperatures for the rump region without the need for shaving the back—a manipulation that alters heat loss and can alter behavioral and autonomic thermoregulation [62] (Fig. 5C). We compared the training loss (log scale) for SGBS to an unmodified Mask R-CNN trained under identical conditions. The SGBS model converged more rapidly and reached an approximately 100-fold lower final loss than the baseline network, indicating that incorporating DLC-derived keypoint heatmaps enhance segmentation performance in thermographic images (Fig. 5D). We used SGBS to segment BAT, rump, and dorsal surface features on a frame-by-frame basis, extracting the mean temperature for each feature (Fig. 5A and Video S3). SGBS data were synchronized with timestamps and integrated with other data streams, including calcium traces and behavior tracking. For these analyses, solo-housed females were used to eliminate the confounding effects of heat exchange with social partners.

To test the performance of SGBS, we used thermal recordings from the fiber photometry experiments. We examined the temporal dynamics of pairwise combinations of the three thermal features with respect to core Tb and identified the lag time that gives the best correlation (i.e., cross-correlation analysis) (Fig. 5E). Core Tb and dorsal surface temperatures were very similar

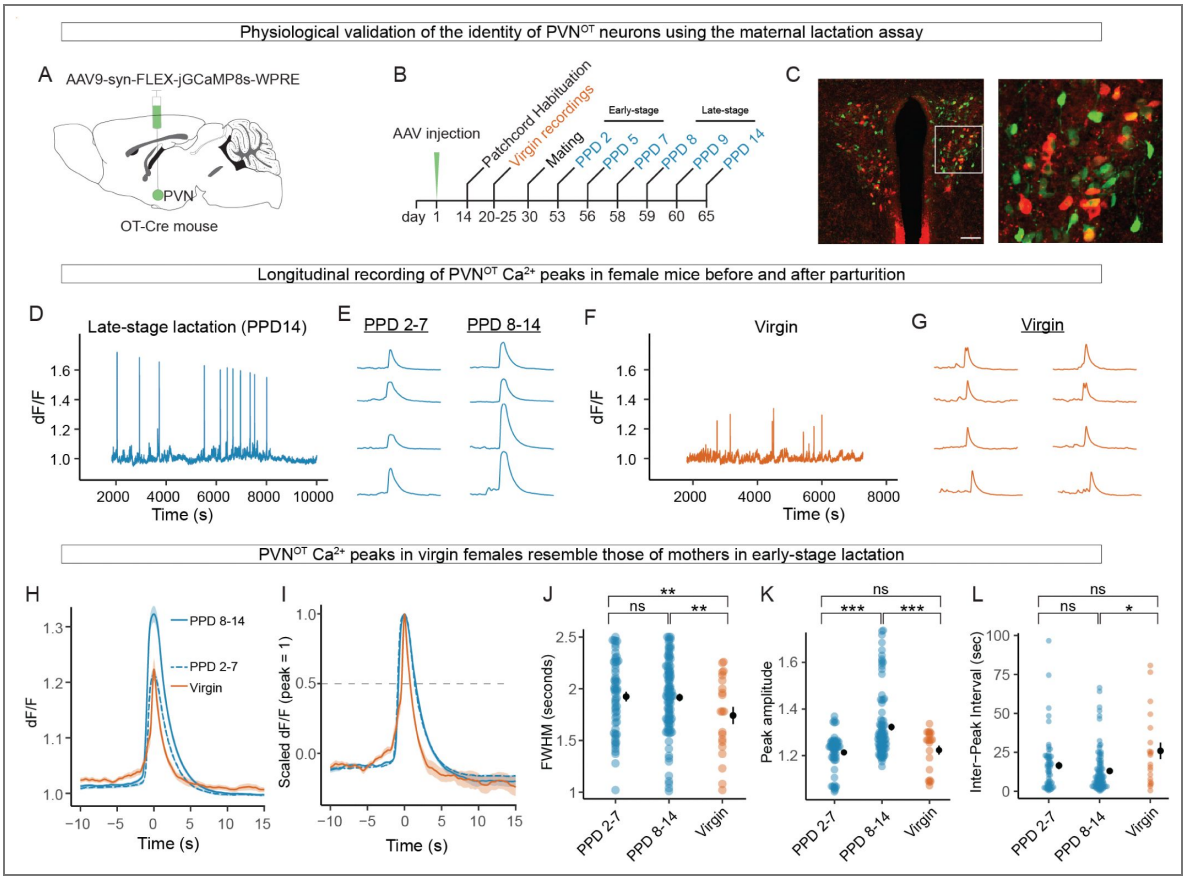

Figure 4. Validation experiment: PVN^{OT} peaks observed in virgin females share similarities with peaks seen in lactating mothers.

(A - C) Longitudinal fiber photometry recordings of PVN^{OT} cells in virgin-to-lactating mice. Scheme of GCaMP8s AAV injections **(A)** and recording timeline **(B)**. Typical histology section showing PVN stained with anti-OT (red) and GCaMP8s expression (green). Scale bar 100 µm. **(C)**. **(D - G)** PVN^{OT} Ca^{++} peaks in virgin females and in mothers during early-stage (PPD 2-7) and late-stage (PPD 8-14) lactation. Example of a post-processed dF/F trace from a two-hour recording on PPD 14 **(D)**. Representative peaks from PPD 2-7 and PPD 8-14 **(E).** Example of a post-processed dF/F trace from a two-hour recording of a virgin female **(F)**. Representative peaks **(G)**. **(H - L)** PVN^{OT} Ca^{++} peak kinetics in virgins and lactating mothers. Average dF/F over time of peaks according to condition shown as raw data **(H)** and scaled (peak-normalized with amplitude = 1) **(I)**. Full-width of half maximum (FWHM) **(J)**, peak amplitude **(K)**, and interpeak interval **(L)** according to female condition. N = 2 females, N = 24 recordings, N = 174 peaks. Full statistical analysis in Table S1.

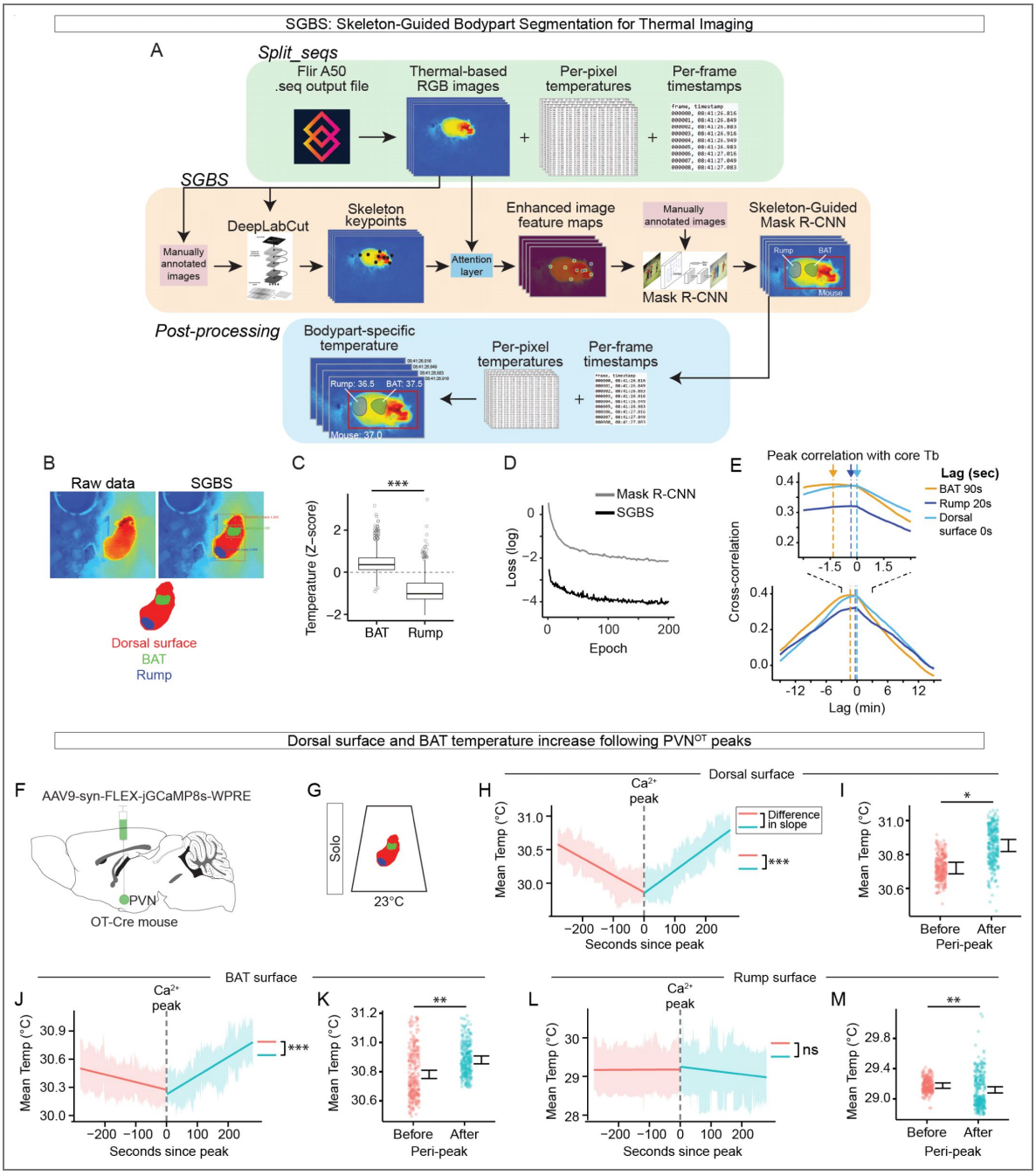

Figure 5. A computer vision model for tracking thermal features during Ca^{++} imaging.

(A) SGBS model architecture. Three main modules are involved in thermographic identification of surface temperature features: processing raw FLIR .seq files (*Split_seqs*); segmentation of anatomical regions (*SGBS*); overlaying temperatures onto segmented regions for each frame (*Post-processing*). **(B)** Example image showing segmentation of three anatomical thermal features. **(C)** Boxplot shows per-minute mean temperatures (BAT-surface, rump-surface) scaled on a per-mouse basis. **(D)** Loss values between *SGBS* and traditional Mask R-CNN. **(E)** Cross-correlation analysis of core body temperature (Tb) and thermal features (BAT, rump, dorsal surfaces). Data are from light-only control animals recorded for two hours (N = 4). A negative value in the time-shift axis means the thermal features are shifted behind relative to Tb. **(F-G)** Alignment of SGBS thermal feature data with calcium imaging. Viral strategy **(F)** and experimental condition **(G)**. **(H-M)** Peristimulus time histograms (PSTH) of SGBS thermal feature data in relation to the time of PVN^{OT} calcium peaks (time 0). Dorsal surface PSTH slopes **(H)** and means **(I)**. BAT surface PSTH slopes **(J)** and means **(K)**. Rump surface PSTH slopes **(L)** and means **(M)**. N = 4 mice; N = 12 recordings. **H, J, L** slope-lines are fitted values from a linear mixed model. **I, K, M** are per-frame means; statistics from a linear mixed model. **G-M** show means ±SEM. P < 0.05 *, P < 0.01 **, P < 0.001 ***. Full statistical analysis in Table S1.

with no lag. Next, changes in core Tb lagged changes in BAT by approximately 90 seconds, a result consistent with a previous report [63]. Finally, rump temperature lagged core Tb by 20 seconds. Thus, SGBS captures the dynamics of thermoregulatory features at the resolution of seconds. These results support the notions that (1) core and dorsal surface temperatures are highly correlated because they both integrate multiple thermoeffector pathways, (2) BAT thermogenesis can drive temperature increases in the mouse body on the order of minutes, and (3) rump surface temperature changes, which may partly reflect vasomotor processes, track Tb on a relatively faster timescale (i.e., seconds)[64]. Finally, the alignment between the SGBS-derived thermal feature trajectories with independently recorded thermologger core Tb data provides an external physiological validation of the SGBS segmentation pipeline (Fig. 5E).

We next used SGBS to align thermal feature data with PVN^{OT} calcium peaks from fiber photometry recordings (Fig. 5F-M). Consistent with our previous core Tb measurements (Fig. 3N-S), thermal feature temperatures trended downward before the calcium peak but increased afterward for both BAT surface and dorsal surface, a shift confirmed by a significant difference in slope before *vs*. after the peak (Fig. 5H,J) (Table S1). Moreover, BAT ($t = 2.72$, $p < 0.0065$, LMM) and dorsal surface ($t = 2.48$, $p < 0.0133$, LMM) temperatures were significantly greater after the peak compared to before (Fig. 5I,K). By contrast, although rump temperature showed no difference in slope before *vs*. after peak, the mean temperature was lower after the peak compared to before (Fig. 5L-M) ($t = -3.13$, $p < 0.0018$, LMM) (all statistics in Table S1). Together, these results suggest that PVN^{OT} activation is followed with an onset of BAT thermogenesis and a concurrent decrease in rump surface temperature, consistent with sympathetically-driven peripheral heat conservation.

Optogenetic activation of PVN^{OT} neurons initiates thermogenic responses

To elucidate the functional link between PVN^{OT} activity during quiescence and thermoeffector outputs, channelrhodopsin (AAVDJ-EF1a-DIO-hChR2(H134R)-EYFP-WPRE-pA) was expressed in the PVN of Oxytocin-Cre mice (ChR2+) to allow for optogenetic stimulation of PVN^{OT} neurons (Fig. 6A). To control for potential warm-sensitive physiological responses due to heat from light stimulation, a "light-only" cohort of Oxytocin-Cre mice received optic fiber implants over the PVN. These experiments were conducted at room temperature (23°C) in solo-housed females to focus on the precise physiology of PVN^{OT} neurons and to eliminate confounding effects of social-partners. Blue light stimulation (10 Hz; 20 ms pulse width (20% duty cycle); 10 mW power; 10 or 20 sec pulse train) was delivered after solo animals had been quiescent for at least two minutes (a condition similar to when PVN^{OT} calcium peaks occur).

We first examined the effect of blue light stimulation of PVN^{OT} neurons on core Tb. Approximately 400 sec (6.6 min) after a 20 sec, but not a 10 sec, pulse train, Tb increased in ChR2+ but not light-only controls (Fig. S5A).

Further examination of Tb data revealed that, by chance, some blue light stimulations were delivered during a relatively high Tb—in contrast to the low Tb context in which PVN^{OT} calcium peaks naturally occur (Fig. 3N-S). To address a possible mismatch in internal physiology during optogenetic stimulations vs. endogenous calcium peaks, we stratified the data according to whether Tb was above or below average (per-mouse) at the time of stimulation (i.e., Tb-T0). The low Tb-T0 distribution was similar to the Tb distribution observed during PVN^{OT} calcium peaks in solo animals (Fig. 6B blue line, cf. Fig. 3N). We then examined the effect of 20 sec optogenetic stimulation in the stratified data and found ChR2+ stimulation caused increased Tb in the low Tb-T0 context but not the high Tb-T0 context; this increased Tb was observable 420 sec after stimulation ($t = 2.235$, $p < 0.025$, LMM) and persisted at least for several minutes (Fig. 6C) (Table S1). Thus, precisely timed, context-dependent stimulation of PVN^{OT} neurons is sufficient to increase core Tb.

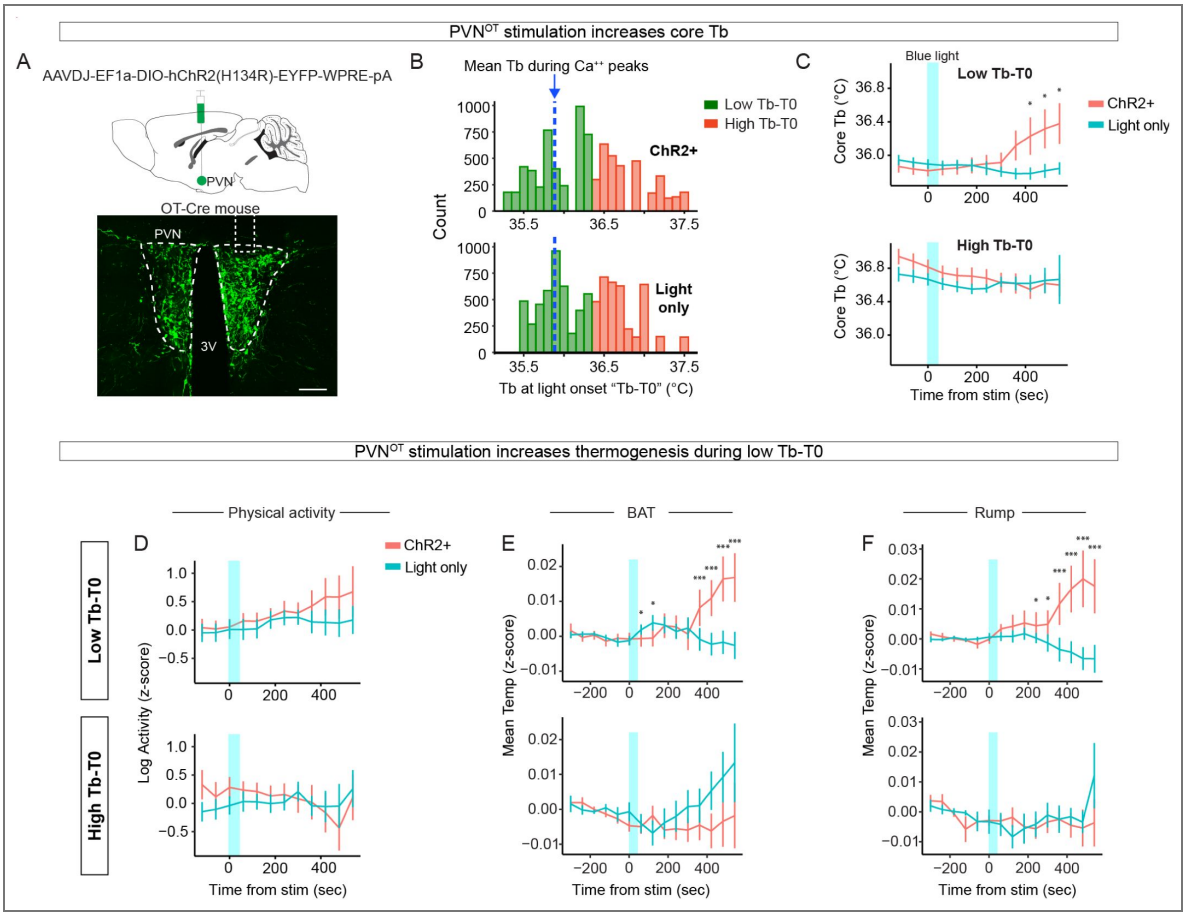

Figure 6. Optogenetic stimulation of PVN^{OT} neurons at a low Tb increases behavioral arousal and thermogenesis.

(A) Viral strategy for ChR2 transfection. **(B)** Histograms showing core body temperature (Tb) during light stimulations in ChR2+ (top) and light-only controls (bottom). Tb-T0 is the Tb at the onset of light stimulation pulse-trains. Low Tb-T0 (green) refers to stimuli during low Tb, and High Tb-T0 (red) refers to stimuli during high Tb. Blue dotted line denotes the mean Tb at which PVN^{OT} Ca^{++} occur (from Fig. 3N). **(C)** Blue light stimulation (time 0; shaded blue rectangle) increases core Tb during low Tb-T0 in ChR2+ animals compared to light-only animals (top). No effect during high Tb-T0 (bottom). **(D - F)** PVN^{OT} stimulation increases thermogenesis in ChR2+ but not light-only controls. Shown are effects during low Tb-T0 (top row) and high Tb-T0 (bottom row). Optogenetic stimulation (time 0; shaded blue rectangle) effects on physical activity **(D)**, BAT surface temperature **(E)**, and rump surface temperature **(F)** in ChR2+ compared to light-only control animals. **C-F**: linear mixed model on data binned per-minute. Data show means ±SEM. N = 6 mice (3 ChR2+ animals and 3 light-only controls); N = 12 experiments; N = 73 light stimuli. P < 0.05 *, P < 0.01 **, P < 0.001 ***. Full statistical analysis in Table S1.

Next, we examined the effect of PVN^{OT} stimulation on physical activity and behavior (Fig. 6D, S5B-C). While no significant differences were detected between ChR2+ and controls, ChR2+ mice showed a trend toward increased physical activity over time in the low Tb-T0 context (Fig. 6D) (Table S1). A separate slope-based analysis of post-stimulation activity revealed that ChR2+ animals exhibited a steeper increase in physical activity compared to light-only controls in the low (but not high) Tb-T0 context. (Fig. S5C). Analysis of manually-annotated behaviors suggested that PVN^{OT} stimulation did not activate a specific motor pattern output but instead resulted in combined increases in the time spent in nesting (LMM estimate coefficient of ChR2+ stimulation: +38.0 sec), locomotion (+54.0 sec), and grooming (+14.5 sec), but not in eating/drinking (-0.4 sec) (Fig. S5B).

We next examined the effect of light stimulation on thermal features using SGBS. Compared to light-only controls, 20 sec pulse trains triggered increased BAT surface ($t = 3.427$, $p < 6.09\times10^{-4}$, LMM) and rump surface ($t = 6.921$, $p < 4.48\times10^{-12}$, LMM) temperatures in the low (but not high) Tb-T0 context approximately 360 sec post stimulus (Fig. 6E-F) (all statistics in Table S1). Moreover, in the low Tb-T0 context, blue light stimulation in ChR2+ animals increased the slopes of the surface temperatures of BAT and rump surface temperatures compared to light-only control animals (Fig. S5D-F). In contrast, in the high Tb-T0 context, blue light stimulation did not affect the BAT or rump surface temperatures and caused a slight decrease in the dorsal surface temperature (Fig. S5D-F) (Table S1).

To better understand the temporal ordering of thermogenic pathways with and without optogenetic stimulation, we next turned to two analyses using cross-correlation and lagged regression. In the first analysis, we examined this progression across all mice in the optogenetic cohort, similar to the analysis of the fiber photometry cohort. Here, we computed peak cross-correlation lags between the derivatives of Tb (i.e., dTb/dt), BAT-surface, and physical activity, and found that, in most mice (five out of six, 83%), BAT surface temperature changes preceded changes in dTb/dt , whereas activity did not consistently precede dTb/dt and often followed it (Fig. S5G). Because this dataset is enriched for repeated rest bouts during the inactive phase, this finding is consistent with the idea that during natural rhythms of rest and arousal thermogenesis precedes increases in physical activity [2,7].

In a second analysis, we quantified the time course by which optogenetic stimulation influenced core temperature while accounting for concurrent changes in physical activity and BAT surface temperature. We modeled the rate of change in core temperature (dTb/dt) using a mixed-effects lagged regression in which stimulation was represented as a brief input whose influence could persist and decay over 30 seconds. To control for behavioral and thermal contributions, we included activity and BAT surface temperature terms measured at the current time and at preceding time points (0–60 s in 10 s steps). We then compared this to an identical model without the stimulation term. Adding the stimulation term significantly improved model fit (likelihood ratio test, $\chi^2 = 7.15$, $p = 0.0056$; Fig. S5H), indicating that stimulation-associated changes in dTb/dt are not fully explained by activity and BAT surface dynamics.

Together, these data suggest that 20 seconds of PVN^{OT} stimulation during the low Tb-T0 resting states is sufficient to trigger a sustained increase in Tb, and to a lesser extent, an increase in physical activity. Thus, PVN^{OT} neurons signal state dependent transitions in thermogenesis and behavioral arousal. These findings are consistent with the notion that natural rhythms of rest to arousal transitions are initiated by a brain-driven switch to a higher defended Tb of the awake state, and that these transitions are often driven by step-wise activation of thermogenic pathways and physical activity [7].

PVN^{OT} cellular projections to the rMR

We next asked what pathways could PVN^{OT} neurons promote transitions towards thermogenesis and physical activity. rMR efferent neurons regulate non-shivering thermogenesis, cutaneous vasoconstriction, and heart rate [5], and the surrounding gigantocellular reticular nucleus (GiA) regulates locomotion and movement [65,66]. In rats, PVN^{OT} to rMR projections ($PVN^{OT} \rightarrow$ rMR)

stimulate thermogenesis and cardiovascular responses in an oxytocin receptor (OXTR)-dependent fashion [31]. To investigate possible $PVN^{OT}\rightarrow$rMR cell types in mice, we used tracing tools to disambiguate magno- vs. parvocellular PVN^{OT} projections [67] (Fig. S6A-C). The majority of $PVN^{OT}\rightarrow$rMR projections were non-magnocellular cells located in the caudal and lateral PVN, suggesting they are parvocellular (i.e., $PVN^{OT(parvo)}$) (Fig. S5C), consistent with previous studies [31,67,68]. In addition, we observed OXTR-positive neurons in the rMR and GiA (i.e., rMR^{OXTR}) using smFISH (Fig. S5D). Thus, $PVN^{OT(Parvo)}\rightarrow rMR^{OXTR}$ neurons are a candidate pathway underlying transitions towards thermogenesis and behavioral arousal in mice.

Discussion

State-dependent PVN^{OT} activity during thermo-behavioral transitions

This study identifies a distinct pattern of state-dependent PVN^{OT} activity during natural patterns of thermoregulatory and arousal behaviors. We initially set out to define the role of PVN^{OT} neurons in huddling-associated rest and wake states, but long-duration in vivo recordings revealed large calcium transients ("peaks") in both social and non-social contexts. These peaks were temporally aligned with transitions from resting states (quiescence and quiescent huddling) to active states (nesting, active huddling, and physical activity), as well as with increases in thermogenesis. Notably, the PVN^{OT} activity patterns and kinetics observed in virgin female mice resembled the well-characterized bursts seen during early lactation [37,51,69], suggesting that this pattern of activity has a broader physiological role in coordinating transitions between thermoregulatory and behavioral states. Thus, although oxytocin is often associated with social behavior, our findings indicate that PVN^{OT} neurons provide a state-dependent signal for thermo-behavioral transitions that generalizes beyond the social context.

PVN^{OT} peak dynamics were temporally aligned with the offset of low-Tb resting states. In the minutes preceding the end of a rest bout, baseline calcium increased to a local maximum (Fig. S3I-J) and peaks occurred probabilistically: the per-second probability of a peak rose to approximately 14–25% near rest offset, compared with only ~2–3% near rest onset (Fig. 3F,H). Logistic regression further supported the conclusion that PVN^{OT}activity increases the likelihood of a rest-to-active state transition (Fig. 3F,H,J,L). The presence of peaks that do not immediately precede overt behavior, as seen in the individual trace in Fig. 3A, is consistent with this probabilistic model and suggests that PVN^{OT} activity biases the system toward transition rather than acting as a deterministic trigger.

PVN^{OT} peaks occurred most consistently when core Tb was relatively low, around 36.2°C, approximately 0.5°C below the average rest-phase Tb of C57BL/6 mice in our colony [12]. In mice, Tb follows ultradian, limit-cycle-like oscillations between biologically constrained lower and upper bounds [2,7], and 36.2°C may approximate the lower bound from which the transition toward the active-state upper bound is initiated [7]. Consistent with this idea, although PVN^{OT} peaks were not present before every rest offset, bouts that did contain peaks showed a steeper thermogenic rise during the ensuing rest-to-active transition. Likewise, both endogenous calcium activity and optogenetic stimulation during a low-Tb (but not high-Tb) rest state signaled increases in Tb, BAT-surface, and locomotor activity within minutes, supporting a state-dependent role for PVN^{OT} neurons in promoting thermogenesis and arousal (Fig. 7).

An apparent contrast emerged between our FOS and fiber photometry results. Whereas FOS expression in the PVN was elevated during active huddling (Fig. 1), photometry showed that PVN^{OT} peaks occurred predominantly during quiescence, immediately before the transition out of rest (Fig. 3). We interpret this difference as a consequence of temporal resolution. Fiber photometry resolves activity on the sub-second timescale and therefore captures transient events occurring while the animal is still behaviorally quiescent. By contrast, FOS integrates neural activity over approximately 30–90 minutes, reflecting cumulative activity across the broader peri-transition period that includes active huddling. Because active huddling is often preceded by

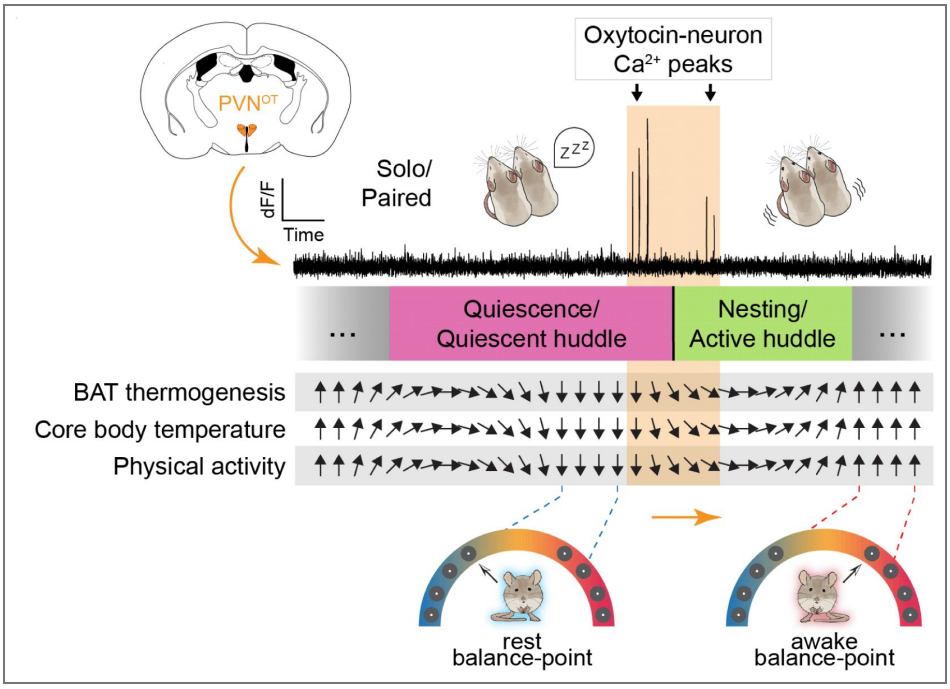

Figure 7. Graphical summary.

Increased calcium activity in PVN^{OT} neurons signals the end of rest and the onset of thermogenesis and behavioral arousal. Both the frequency of large amplitude peaks and baseline calcium levels increase approximately two minutes before the end of rest (i.e., quiescence and quiescent huddle). Calcium peaks briefly continue into two post-quiescent active states: nesting and active huddling. Optogenetic stimulation of PVN^{OT} neurons during rest triggers increased BAT thermogenesis, core body temperature (Tb) and physical activity. Arrows indicate transitions between the low-Tb rest balance point (downward vertical arrows) and the high-Tb active balance point (upward vertical arrows).

quiescent huddling, the associated FOS signals can become intermixed. These findings highlight the complementary strengths of the two approaches and underscore the importance of high-temporal-resolution recordings for identifying neural signals that precede thermo-behavioral state transitions.

The PVN^{OT} activity patterns identified in this study were not specific to social interaction. For example, brief, non-thermoregulatory encounters such as dyadic sniffing did not recruit PVN^{OT} activity, in contrast to the robust peaks observed during transitions out of rest (Fig. S2H; Table S1). However, some aspects of PVN^{OT} activity were enhanced in the social context. For example, peak probability and frequency were higher in the paired compared to solo context (Fig. 3F-I, Fig. S2D). This finding is likely related to our observation that quiescent huddling (paired) bouts were associated with stronger body temperature regulation compared to solo quiescence and other behavioral states (Fig. S3M-R). Thus, we uncover a homeostatic function of PVN^{OT} neurons that is social context independent, but nevertheless modulated between the two conditions. Future experiments should attempt to disentangle the effects of PVN^{OT} light stimulation on social vs. non-social aspects of these behavioral state transitions.

Thermal tracking and validation of PVN^{OT} recording specificity

Our deep-learning pipeline (SGBS) enabled millisecond-resolution tracking of thermal features, including dorsal surface, intrascapular BAT surface, and rump surface temperatures. We detected increases in BAT surface temperature following calcium peaks and optogenetic stimulation, supporting a role for PVN^{OT} neurons in promoting state-dependent transitions toward thermogenesis. Although infrared thermography measures surface radiance rather than tissue temperature directly, the consistent temperature differences between the BAT surface and surrounding dorsal and rump regions (Fig. 5C), together with the temporal lead of BAT surface changes relative to those regions (Fig. 5E and S5G), support the interpretation that the intrascapular BAT region acts as an active heat source during behavioral transitions. While direct telemetry or implanted thermocouples would provide greater precision, our noninvasive approach allowed us to study natural state transitions in freely moving, undisturbed animals. A limitation of the current SGBS system is that it was not designed to track tail temperature, a commonly used index of vasomotor responses.

The lactation model (Fig. 4) served as a functional validation of recording specificity. Although GCaMP expression was driven by an OT-Cre line, co-localization with OT immunoreactivity varied across brain slices (Fig. S4), consistent with prior reports using OT-Cre lines [70]. We note that the animals were perfused at ~ZT4–8, before we were aware that somatic OT immunoreactivity in PVN neurons reaches a daily low during the early light phase [56]. Together with the fact that oxytocin is released from soma and dendrites and must be resynthesized rather than locally recycled [71], this timing may have reduced detectable intracellular peptide levels, leading us to underestimate the full OT-expressing population. Nevertheless, PVN^{OT} neurons undergo well-characterized changes in firing dynamics during lactation to support milk ejection [37,51,69], and the emergence of these characteristic changes in our recorded population (Fig. 4I-L) provides functional evidence that we were primarily recording oxytocin neurons.

PVN^{OT} neurons in context of arousal and peptidergic PVN cell-types

Several neural populations that promote transitions from sleep to wake have been described [72], including populations directly involved in thermoregulation [9]. Together with a prior report showing that chemogenetic activation of PVN^{OT} neurons increases wakefulness [29], our data place PVN^{OT} neurons as a key node in the initiation of thermogenic and behavioral arousal from rest. We therefore propose a model, consistent with prior work, in which the transition from rest to arousal begins with a change in neural activity that drives thermogenesis and is either coincident with, or followed by, increased physical activity [7,63] (Fig. 7). The ~400 s latency between optogenetic PVN^{OT} stimulation and the rise in Tb (Fig. 6) is consistent with the timescale of

peptidergic neuromodulation, as oxytocin is released from large dense-core vesicles and can exert prolonged, diffuse effects [71,73,74]. Our decision to perform optogenetic stimulation in isolated animals was motivated both by the social-context independence of PVN^{OT} activity during rest-to-arousal transitions (Figs. 2 and 3) and by the technical limitation that close physical contact between huddling mice prevents accurate SGBS segmentation of individual thermal profiles.

Other peptidergic PVN populations, particularly CRF and AVP neurons, are unlikely to account for the activity pattern described here. Although their roles in huddling have not been directly tested, available evidence distinguishes both populations from PVN^{OT} neurons. CRF signaling appears to oppose oxytocin in social-care contexts, as chemogenetic activation of PVN^{CRF} neurons impairs maternal care [75], and central CRF administration suppresses maternal care [76]. AVP likewise shows separable functions: intracerebroventricular AVP inhibited nest building but not huddling in *Peromyscus* [77], and PVN^{AVP} neurons promote wakefulness via lateral hypothalamic orexin neurons [78]. Consistent with our findings, Adahman et al. [79] also reported reduced PVN^{OT} c-Fos at thermoneutrality relative to cooler conditions in a study of AVP-dependent maternal thermoregulatory behavior. Importantly, chemogenetic activation of PVN^{AVP} neurons did not recruit PVN^{OT} neurons [80], indicating these populations can operate independently. The synchronized, pulsatile bursting that validated our calcium peaks appears specific to oxytocin neurons: lactation-induced burst upregulation occurs in magnocellular OT neurons, but not AVP neurons, in the PVN [81], whereas AVP neurons exhibit asynchronous phasic bursting associated with antidiuretic rather than neuroendocrine-pulsatile functions [82,83]. To our knowledge, comparable synchronized burst activity has not been reported in PVN CRF neurons during lactation or rest.

Limitations and caveats

Caveats of this study should be considered. First, we did not directly link in vivo PVN^{OT} calcium activity or optogenetic stimulation to endocrine oxytocin release. Throughout, we refer to "PVN^{OT} neurons" rather than "oxytocin" to emphasize that our manipulations targeted the cell type, not the neuropeptide itself. The observed effects could be mediated partly or wholly by glutamate release from PVN^{OT} neurons in addition to oxytocin signaling [84]. That said, we provide anatomical evidence consistent with a peptidergic mechanism, including PVN^{OT} projections to the rostral medullary raphe and oxytocin receptor mRNA expression in this region (Fig. S6). Dissecting the relative contributions of oxytocin and glutamate is a next step, requiring receptor-targeted pharmacology or genetic loss-of-function approaches. Second, although some experiments were conducted in relatively few animals, we nevertheless observed robust within-animal associations between PVN^{OT} activity and thermo-behavioral state changes; future studies with larger cohorts should better resolve inter-individual and state-dependent variation. We focused here on females because their thermo-behavioral states were readily discernable, but future work should test whether similar mechanisms operate in males, where the neural basis of collective thermoregulatory huddling has recently begun to be defined [85]. Third, although we show that PVN^{OT} neurons are sufficient to drive thermogenic and behavioral transitions (Fig. 6), we did not perform acute loss-of-function experiments. Such experiments are warranted because decreases in baseline PVN^{OT} calcium activity were associated with transitions toward the onset of quiescence (Fig. 3I-L), suggesting this system may bidirectionally regulate thermo-behavioral state. Finally, our thermal manipulations relied on conductive floor temperature changes rather than whole-chamber ambient air temperature. While floor cooling provided a reliable and well-controlled stimulus that elicited thermoregulatory behavior without altering airflow or humidity, it may recruit peripheral thermoreceptor populations differently than ambient temperature manipulations. Future studies using chamber-wide temperature control would therefore provide an important complement.

Ideas and Speculation

How might PVN^{OT} neurons detect or define the "rest balance-point," and contribute to shifting the brain toward an "awake balance-point"? We envision a circuit model in which PVN^{OT} neurons integrate afferent thermosensory information from both peripheral and internal sources to monitor when core Tb approaches a critically low threshold during rest cycles. The lateral parabrachial nucleus (LPB), which serves as a major relay for ascending cutaneous thermosensory information [5], is a likely source of peripheral thermal input to the PVN. The preoptic area (POA) contains thermosensitive neurons that monitor brain temperature [5] and is poised to relay information to the PVN^{OT} neurons, which receive monosynaptic input [86]. When Tb drops towards the lower bound of the resting-state thermal range, peripheral and central thermal input may trigger the characteristic pulsatile pattern of PVN^{OT} activity. This activity would then engage downstream effectors, including the rostral medullary raphe, where we detect projections and oxytocin receptor mRNA expression, to initiate BAT thermogenesis and behavioral arousal. Notably, whole-brain projectome mapping has revealed that PVN^{OT} neurons send dense projections to both the parabrachial nucleus and medial preoptic area [86]. This suggests that PVN^{OT} neurons are not just receiving thermosensory information, but may also modulate LPB and POA in a state-dependent manner through reciprocal feedback.

Broader Implications

Overall, these findings extend the role of in vivo PVN^{OT} neural activity dynamics beyond social behavior [35,50,87,88], parturition/lactation [58], maternal behavior [89], sexual behavior [74], and stress responses [52], and highlight their contribution to daily patterns of rest/wake transitions, thermoregulation, and energy balance. In our model PVN^{OT} neurons respond to internal physiological conditions, such as core body temperature, to coordinate autonomic and behavioral outputs necessary for adaptive thermoregulation. These insights open new directions for understanding the neural circuits that integrate social context, internal state, and metabolic demands to regulate mammalian behavior.

Methods

Animals

OT and FOS histology. C57B6/J (Strain #: 000664) female mice were purchased from Jackson Laboratory and were 8 to 11 weeks old during the experimental period. Virgin, group-housed females were used for all trials unless otherwise specified.

PVN^{OT} manipulation and recording. Oxytocin-Ires-Cre mice were purchased from Jackson Laboratory (Strain #: 024234) [96]. Animals were bred and maintained at the University of Wyoming. Experimental female mice ranged from 9-20 weeks old during the experimental period. All experimental mice were group-housed with *ad libitum* access to food and water in a room maintained at 23±2°C with a standard 12 h light / dark cycle (light: 6:00-18:00; dark: 18:00-6:00) until they were used for surgery or experiments. Animals were housed in Optimice® IVC cage systems; cages were enriched with red huts, nestlets, and a mix of cob and pine bedding. Mice used were 18-26g during the experimental period. Animal genotyping was outsourced to Transnetyx using ear tissue biopsies. All procedures were approved by the University of Wyoming Institute Animal Care and Use Committee (IACUC) in compliance with NIH guidelines for the care and use of laboratory animals.

FOS/*Fos* behavior assays

To measure FOS protein expression across brain regions, mice were placed into the home cage recording suite as described [91] for at least 24 hours prior to behavior being monitored, with the cage's camera being connected to a Zoom meeting. After 24 hours, and at the beginning of the light cycle when huddling is most frequent, a human observer monitored behavior from another room without interrupting natural behavior. Once the target behavior was observed for a minimum of

15 consecutive minutes, 90 minutes were counted from the onset of the behavior, and animals were pulled from the recording suite for histology. Animals were not excluded if they exhibited both active and quiescent huddling during the recording session.

To determine *Fos* transcription in PVN^{OT} neurons during different huddling states, C57B6/J female mice that were 10 weeks old were housed in home cages in trios. Mice were habituated to the conditions, handling, and the cage lid camera set up for ~5 days prior to recording. Animals were split into two groups: active huddle (N=6) and quiescent huddle (N=3). To capture active huddle *Fos* transcription, mice were recorded using the cage lid camera connected to a Zoom meeting. The time of active huddle onset was documented, and mice were sacrificed 30 minutes later. To determine quiescent huddle *Fos* transcription, mice were recorded as described above. Mice were sacrificed 30 minutes after the onset of quiescent or active huddle. All brains were dissected, embedded in OCT (Fisher Scientific, #23-730-571) and stored in −80°C.

Animal Surgery

Pre- and post-surgical procedures. Prior to surgery, animals were given an analgesic dose of carprofen (20 mg/kg, s.c.). Mice were deeply anesthetized using a mixture of ketamine and xylazine (100 mg/kg and 10 mg/kg, respectively, administered i.p.). Post-surgery, the mice were returned to a warm and clean home cage. For post-operative care, antibiotic ointment (Neomycin and Polymyxin B Sulfates and Dexamethasone Ophthalmic Ointment, Bausch + Lomb) was topically applied to the incision, animals received 20 mL/Kg of lactated ringer's solution s.c., and closely observed until active. Upon emergence from anesthesia, 1 mg/kg of buprenorphine extended-release solution was administered subcutaneously between the shoulder blades. Animals were housed with cagemates and monitored daily. Carprofen was administered for three days post-surgery.

Temperature logger implants. To continuously measure internal body temperature, laparotomies were performed to implant mice with Star-Oddi DST nano-T temperature loggers. The loggers were sterilized with glutaraldehyde and rinsed with sterile PBS prior to being implanted. Mice received pre-operative care and were anesthetized as described above. A one-centimeter incision was made in the skin and underlying peritoneum, and the temperature logger was placed into the abdominal cavity. The peritoneum was sutured with PGA absorbable sutures, while the skin was closed with nylon (nonabsorbable) sutures. Mice received post-surgical care as described above.

Stereotaxic GCaMP injections and fiber implants. For fiber photometry recordings, oxytocin-Ires-Cre heterozygous, pair-housed, female mice at 8-12 weeks of age underwent stereotaxic surgery in which pGP-AAV9-syn-FLEX-jGCaMP8s-WPRE (#162377, Addgene, titer: 2.7 x 10^{13} gc/mL) was delivered to the PVN. Mice were head-fixed on a digital mouse stereotax (Stoelting, 51730D). For added analgesia, a local anesthetic (5% lidocaine) was delivered subcutaneously along the incision site before cutting. A midline incision was made along the top of the skull, the periosteum was cleared with 3% hydrogen peroxide, and the skull was dried off with canned air. Vertical measurements of bregma and lambda were taken and aligned to the same plane (DV of ± 0.05 mm). The AAV was delivered using a programmable nanoliter injector, (Nanoject III, Drummond Scientific) (300nL per side: 6 cycles of 50nL delivered at 2nL/s with 10 second delays). To allow for proper diffusion of solution into brain tissue, the needle was left in for 10 minutes before retracting. PVN coordinates relative to bregma and DV measured from the top of the brain: AP = −0.76mm, ML= ±0.19mm, DV= - 4.62mm.

A fiber-optic cannula (Ø1.25mm ferrule, Ø200 µm core, NA = 0.37, L= 6.5 mm, Neurophotometrics Ltd.) was then lowered into the injection site until the tip was located ~ 0.02 mm above the viral injection. The cannula was anchored in place with dental cement (C&B Metabond) such that a dome-shaped cap was halfway up the black ceramic ferrule and covered the entire incision. Post-operative care and recovery took place as described above. Two weeks post recovery, animals were tested for GCaMP signal using the Neurophotometrics photometry system (as described in

"**Fiber photometry recordings**"). If a signal was detected, animals underwent a laparotomy to implant a temperature logger as described above. Animals with no detectable signal were excluded from recordings.

ChR2 injection & optic fiber implant. For optogenetic stimulation of PVN^{OT} neurons, Oxytocin-Ires-Cre heterozygous, pair-housed, female mice at 8-12 weeks of age were split into two different groups: ChR2+ and control (ChR2-) animals. ChR2+ animals underwent stereotaxic injections with AAVDJ-EF1a-DIO-hChR2(H134R)-EYFP-WPRE-pA (Salk, titer: 4.03×10^{13} gc/mL) using the stereotaxic surgical procedure described above. Viral vectors were delivered using a programmable nanoliter injector, (Nanoject III, Drummond Scientific) (200nL per side: 4 cycles of 50nL delivered at 1nL/s with 10 second delays). Both ChR2+ and control animals were implanted with a fiber optic cannula (Ø1.25mm ferrule, Ø200 µm core, NA = 0.37, L= 6.5 mm, Neurophotometrics Ltd.). All optogenetic animals were given a minimum of seven days to recover before undergoing a laparotomy to implant a temperature logger.

Stereotaxic DREADD, CTB and FluoroGold injections. To identify PVN^{OT} projections to rMR, a subset of mice received two stereotaxic injections: one of AAV5-hSyn-DIO-hM3D(Gq)-mCherry (#44361, Addgene, titer: 2.6×10^{13} gc/mL) in the PVN and one of cholera toxin subunit B conjugated with Alexa Fluor 647 (Invitrogen, C34778). Using the same surgical procedure and PVN coordinates as mentioned above, 300 nL of AAV was delivered per side (6 cycles of 50nL delivered at 2nL/s with 10 second delays). The incision was closed using absorbable PGA suture threads and antibiotic ointment was applied topically along the incision. Animals recovered for two weeks to maximize viral expression. A second stereotaxic surgery was performed to deliver a volume of 10 nL of 0.5% CTB into the rMR. RMR coordinates relative to bregma and DV measured from the top of the brain: AP = - 5.80mm, ML= 0.00mm, DV= −4.95mm. Mice received post-operative care as described above and recovered for 3-4 days. To distinguish between peripheral-projecting magnocellular and central-projecting parvicellular neurons, mice received 15 uL intravenous injection of 4% Fluoro-Gold (Fluorochrome) diluted in 100 uL of sterile saline. Prior to injection, mice were given an analgesic dose of carprofen (20 mg/kg, s.c.). Mice were briefly restrained using a modified 50 mL conical tube, in which holes were drilled to allow for proper air flow and respiration. Mouse tails were interposed between two heating pads to enhance visibility of the tail vein. Tails were wiped down with 70% ethanol and FG was administered via either right or left lateral tail vein using a 0.5 mL 28G syringe. Mice were sacrificed 24- 48 hours post-FG administration.

Histology

FOS Immunohistochemistry. For quantitative analysis of FOS expression, mice were given a lethal dose of isoflurane after removal from the home cage recording suite. Animals were then transcardially perfused with 1X PBS and 4% paraformaldehyde (PFA) in PBS. Brains were removed and kept in 4% PFA overnight at 4°C. Brains were sliced into 60 um sections using a vibratome (Leica VT1000S) and every other slice was saved in 48-well plates, wrapped in parafilm in 1X PBS, overnight at 4°C. The next day, 0.3 mL of block solution (0.20% triton, 10% natural goat serum (NGS) (Jackson ImmunoResearch 005-000-121), in 1X PBS) was placed into each well and incubated for one hour at room temperature on a plate shaker. Block was removed and replaced with freshly made primary antibody solution (c-Fos (9F6) Rabbit mAb, Cell Signaling, 14609, 1:1000 dilution in block solution) and incubated for 48 hours on a shaker at 4°C. Slices were washed three times with 1X PBS for 15 minutes. Slices were then incubated in secondary antibody solution (Goat anti-Rabbit IgG, Alexa Fluor Plus 555, Thermo Scientific, A32732, 1:500 dilution in block) for 2 hours on a shaker at room temperature and protected from light. Wash steps were repeated with 1X PBS. Slices were then mounted on Superfrost Plus slides using a paintbrush and stained with DAPI mounting medium (Vectashield H-2000). Slides were imaged with a Zeiss Axio Scan.Z1 fluorescent microscope. Regions were identified by finding all locations that displayed FOS expression and cropped using ImageJ alongside the Allen Brain Atlas. The quantity of cells and overlap was calculated using a custom CellProfiler 4.2.1 script.

Fluorescent *in situ* hybridization (RNAscope). For quantitative analysis of *Oxt* and *Fos* overlap in PVN^{OT} mice were anesthetized with a lethal amount of isoflurane. Brains were extracted, embedded in OCT and stored at −80°C. Brains were sectioned at 16 µm using a cryostat and subsequently stored at −80°C. For *in situ,* slides containing brain sections were placed in 4% PFA for 45 minutes and then were dehydrated in 50%, 70% and 100% ethanol for 5 minutes each at RT. Slides dried for 5 minutes after dehydration and hydrogen peroxide was added for 10 minutes at RT. Slides were then treated with Protease III for 30 minutes at RT to allow for antigen accessibility. The probe cocktail contained *Oxt* (ACD Bio, #493171) and *Fos* (ACD Bio, #316921) and was diluted at 1:2 ratio with probe diluent. An aliquot of 40µL of probe cocktail was added to each section and incubated in a 40°C oven for two hours. For amplification, 40µL of AMP 1 was added each slice and placed in the 40°C oven for 15 minutes. AMP 2 was then added to each slice and slides were again incubated at 40°C for 15 minutes. Finally, 2-3 drops of AMP 3 were added to each slice and slides were incubated at 40°C for 30 minutes.

Fluorophores were added to each channel and diluted at 1:1500. Each fluorophore was added by first opening the channel using 2-3 drops of HRP on each slice and incubating at 40°C for 15 minutes. The fluorophore was added at a volume of 40 µL to each slice and slides were incubated at 40°C for 30 minutes. To close the channel, 2-3 drops of blocker were added to each slice and incubated for 15 minutes. Lastly, a drop of DAPI (ACD Bio, #320858) was added to each slice for 30-45 seconds. DAPI was allowed to dry for approximately 3 minutes before immediately coverslipping with 1-2 drops of ProLong Gold (Invitrogen, P36930). Slides were protected from any surrounding light, left to dry overnight and imaged with a Zeiss Axio Scan.Z1.

AAV expression. To verify AAV injection sites, animals who had received stereotaxic DREADD, GCaMP8s, or CHR2 injections were sacrificed at ≤18 weeks. Mice were deeply anesthetized with a lethal amount of isoflurane and perfused with 4% PFA. Extracted brains were then stored in 4% PFA overnight at 4°C before being sliced at 60 µm using a vibratome (Leica VT1000S). PVN regions were identified via the Allen Brain Atlas. PVN slices were stained with a DAPI mounting medium (200 µl/slide, Vectashield H-2000) and scanned using a Zeiss Axio Scan.Z1. Images were enhanced and/or pseudo-colored using ImageJ.

Fiber photometry recordings

Recording setup. The Neurophotometrics fiber photometry system (FP3001), operating with Bonsai (Version 2.72) software, was used to acquire photometric data with concurrent video recordings (Arducam, OV9281). Patchcords (MBF Bioscience, NPM-BPC-4) were attached to the fiber ferrules, and held in place by either ceramic sleeves or by a quick-release interconnecter (ThorLabs, ADAL3). Calcium dependent GCaMP fluorescence signals were recorded with light from a 470-nm LED that was band-pass filtered, narrowed with a collimator, reflected by a dichroic mirror, and focused on the sensor of a CCD camera by a 20x objective. To account for auto-fluorescence and possible motion artifacts, a 415-nm LED for calcium-independent isosbestic fluorescence signal was used. The recorded signals were acquired with a sampling rate of 30 Hz for each channel at 100% duty cycle. LED light power was calibrated prior to every recording using a power meter (ThorLabs, PM100USB and S120C). LED light was delivered at a power that resulted in 60µW of 415-nm light, and 85 µW of 470-nm light at the tip of the patchcord.

Recording conditions. Photometric recordings occurred in the home cage, with the cage-lid replaced by a custom-fit metal sleeve that extended the cage wall height to 16”. Optic fiber-implanted mice and their pair-housed sister were habituated to the connector and patchcord prior to commencement of experimental schedule. Habituation periods ranged from several days to a week depending on individual animal reaction to the patchcord and to sufficiently aversion train the cagemate. Aversion training was performed during habituation periods by lightly coating the patchcord with diluted capsaicin (EMD Millipore, 211275). The cagemate and implant mouse were observed, and training was repeated until the cagemate associated the unpleasant sensation of capsaicin with chewing of the patchcord. Recordings were approximately 2-hours and were conducted at three different floor temperatures (15C°, 23C° and 29°C), with and without the sister cage-mate. Floor temperature was controlled by placing the home-cage onto a custom aluminum

chassis that attached to the Hot/Cold Plate (Ugo Basile, 35300), temperature was then validated by a temperature logging iButton (DS1922L-F5, Embedded Data Systems) placed inside the home-cage. A portion of the nesting material was removed before experiments to prevent occlusion of the animals during the recording (see Supplementary Video 1 for typical amount of bedding left in cage).

Validation trials using the lactation assay. To verify the bursting activity of PVN oxytocin neurons observed in photometry recordings, virgin females were crossed with stud males after completing at least two photometry trials (as described above). The dams and pups were housed in their home cages throughout the trial period. Dams were recorded during nursing and lactation. Maternal oxytocin neural activity was recorded at the following timepoints: postpartum day (PPD) 2, 5, 7, 8, 9, and 14. For this experiment the minimum peak amplitude was set to be > 7 standard deviations (sds) above the mean. This threshold was obtained by examining peaks in mothers that clearly displayed pulsatile activity bursts during lactation and closely resembled the peak dynamics that have been previously described during lactation [37, 69, 51].

Behavioral characterization. Videos were uploaded to Noldus Ethovision XT 16, where the physical activity of the mice (calculated total percentage of pixel change between frames) and behaviors were identified. Activity in the paired context was defined as the summed activity for both animals.

The behaviors for solo photometry animals were manually scored as follows: Locomotor Activity (LMA), Eating or Drinking (EaDr), Grooming (Groom), Nesting or Nest Building Nest (Nest) where the animal engaged in nest-building behavior or activity within its nest other than grooming, Quiescence (Quies) where the animal is inactive inside its nest, and Stationary (Sta) which was defined as animal inactivity outside of the nest.

The behavior of the photometry animal for paired assays was manually scored as follows: Locomotor Activity (LMA), Eating or Drinking (EaDr), contact initiated (ConI), contact received (ConR), Grooming (Groom), Nesting or Building Nest (Nest) characterized by the photometry animal engaging in nest-building behavior or its activity inside the nest while its cagemate engaged in nest-building behavior, Active huddle (AHud) defined as physical contact and activity between both animals in the nest, Quiescent Huddle (QHud) referred to physical contact and inactivity between both animals in the nest, Quiescence (Quies) where the photometry animal was engaging in inactivity alone in the nest, and Stationary (Sta).

Behavior and activity data was exported at 10 frames per second as a .csv file and imported to R for analysis.

Calcium data preprocessing. Fluorescent signal data preprocessing was done with a custom R script as follows: 415 and 470 channels de-interleaved; 470 channel filtered to remove high-frequency noise using a 4th-order Butterworth filter [95] modified to remove end-effect transients; trimmed to remove approximately the first six minutes of data (to mitigate the effect of photobleaching); if necessary, further trimmed to remove effects of disruptions to the patchcord (chewing or twisting); smoothed with a sliding window function (rollapply; width = 9) [97].

To correct the calcium-dependent signal from effects of photobleaching and heat-mediated LED decay, we first extracted the “fitted values” from the linear relationship between the 470 (calcium-dependent) and 415 (calcium independent) fluorescent signals. Next, to calculate dF/F we divided the 470 signal by these fitted values. Because we observed occasional artifactual shifts in baseline dF/F values, we baseline corrected dF/F using the iterative least squares method [92]. The Z-scored dF/F was calculated as $Z = (\chi - \mu)/\sigma$, where μ is the mean dF/F and σ is the standard deviation of dF/F. To define peaks, we used the findpeaks function [90], with the minimum peak distance set at two seconds and the minimum peak height set at six standard deviations above the mean dF/F. Photometric data were aligned to behavioral data (exported from Noldus Ethovision) and Tb data (exported from Mercury) using common centisecond-resolution timestamps and reduced to a sampling frequency of 10 frames per second.

Peri-event data oriented on specific events (i.e., calcium peaks or start/stop frames of behavioral bouts) were extracted using a custom function that (1) extracts the indices of the events and (2) generates a list of vectors for a specified number of rows before and after the event.

To compare longitudinal physiological patterns of activity in PVN^{OT} neurons in virgin females (primary subjects of this study) compared to nursing and lactation, we made the following modifications to the protocol as described above. First, to quantify PVN^{OT} peak characteristics (amplitude, full width half maximum, interpeak interval) before linear normalization and baseline correction, (i.e., to better describe the dynamics of their native characteristics), we corrected the calcium-dependent signal from effects of photobleaching and heat-mediated LED decay using an exponential decay model. Specifically, we used a self-starting nls (nonlinear least squares) function in R to fit the isosbestic data with the following model: y(t) ~ SSasymp(timeS, yf, y0, log_alpha), where the measured isosbestic value y starts at y0 and decays towards yf at a rate α. SSasymp is a shortcut that guesses its own parameters; instead of fitting the rate constant α directly, it searches for the logarithm of α: y(t)~yf+(y0−yf)e^−exp(logα)t. We then linearly scaled this fitted decay to the calcium-dependent data using robust regression (MASS::rlm with the psi function set to bisquare); finally, we divided the calcium-dependent data by this scaled fit to get a corrected signal.

In accordance with previous work, we examined three epochs in the same animals: virgin females; early-stage lactation (PPD 2-7); and late-stage lactation (PPD 8-14). To calculate the full-width half maximum (FWHM) of PVN^{OT} peaks, we used a custom function that performs the following steps: finds each peak; determines the half-max value; interpolates where the signal crosses the half-max value; computes the FWHM as the difference between these crossing points. To enable visual comparison of waveform width across groups in dependent of amplitude differences, we derived peak-normalized average waveforms using a normalization procedure for every peak prior to averaging.

Specifically, for each peak we (1) baseline-subtracted the trace by subtracting the mean fluorescence in a pre-peak baseline window, and then (2) divided the baseline-subtracted waveform by its own maximum value to scale the event amplitude to 1. We then computed the mean ± SEM of these peak-normalized waveforms across events within each group. To calculate the interpeak interval (IPI), we used the lead function in R to compute the time (in seconds) from one peak to the next on a per-recording basis.

Computer vision analysis

Processing Flir .seq files. RGB videos, timestamps, and thermal data were extracted from Flir thermographic .seq files using a Python-based adaptation of *ThermImageJ* [3]. Raw images were obtained via Flirpy [4], converted to RGB, and merged into AVI video files. Metadata, including timestamps and frame rates, was extracted using *Exiftool* [5]. This workflow provided thermal images for model training, AVI videos for analysis, and timestamps and temperature data for integration with behavioral information. The processing script is available at *https://github.com/j-landen/seq_process*.

Skeleton-Guided Bodypart Segmentation (SGBS) for thermographic temperature extraction. To quantify region-specific surface temperature from FLIR thermography videos in awake mice, we developed Skeleton-Guided Bodypart Segmentation (SGBS), a two-stage computer vision pipeline that combines DeepLabCut (DLC) keypoint tracking with an instance-segmentation network (Mask R-CNN) (code: *https://github.com/j-landen/SGBS*). First, a DLC model was trained on 1,800 manually labeled frames to detect 10 dorsal keypoints (nose, head tip, implant, neck base, center back, tail base, mid-tail, patchcord, and left/right shoulder). For each thermography frame, these keypoints were converted to a set of per-keypoint spatial heatmaps and fused with the thermal image as additional channels that guide segmentation (i.e., a skeleton-conditioned attention/fusion step that biases the network toward anatomically plausible regions even when posture, bedding, or patchcords alter thermal texture). Second, a custom Mask R-CNN model was trained on 457 manually annotated images (Darwin/V7) to segment three regions of interest: interscapular BAT, rump, and the full dorsal surface.

Model performance was evaluated on a held-out validation set not used for training (20% of annotated images), using standard segmentation accuracy metrics (per-class intersection-over-union and Dice/F1) and by visual inspection of predicted masks overlaid on raw frames. As an additional control, we trained an unmodified Mask R-CNN (same backbone initialization, same training/validation split, and identical training schedule) and compared loss curves and validation performance between the baseline and skeleton-guided models. Loss is calculated as the sum of three components: (1) a classification loss (cross-entropy) that assesses how accurately each body part is identified, (2) a bounding box regression loss that measures how close the predicted box is to the ground truth, and (3) a mask loss (binary cross-entropy) that evaluates pixel-by-pixel agreement between the predicted mask and the ground truth mask. Finally, masks were mapped to radiometric pixel values to extract per-frame temperature statistics (mean, min, max, SD) for each region. To establish physiological (external) validity independent of segmentation training, SGBS-derived temperature trajectories were temporally aligned with simultaneously recorded core body temperature from implanted thermologgers; thermologger data were not used for model training. SGBS measures showed strong positive correspondence with core temperature dynamics and reproduced expected temporal relationships among BAT, dorsal, and rump signals (e.g., BAT changes preceding core temperature, consistent with thermogenic physiology).

Optogenetic stimulation

Recording setup. Blue light (450 nm) stimulation was delivered using the Neurophotometrics fiber photometry system (FP3001), with simultaneous video and thermal recording. Mono-filament patchcords (Doric Lenses, MFP_200/220/900-0.37_3m_FC-MF1.25) were attached to the fiber ferrules and held in place by a quick-release interconnecter (ThorLabs, ADAL3). Optogenetic laser power was measured prior to every recording using a power meter (ThorLabs, PM100USB and S120C). Optogenetic activation used a frequency of 10 Hz, with a 20 ms pulse width (20% duty cycle) and 10 mW of power measured at the tip for either 10- or 20-second trains.

Optogenetic recordings occurred in the home cage, with the same setup as fiber photometry recordings, described above. Mice were pair-housed until recording. One animal was tested at a time, while the other animal was placed in a holding cage for the duration of the experiment. During experiments, animals were observed remotely from a different room. The human observer turned on blue light stimulation after the animal had been inactive for a minimum of two minutes. Stimulations were a minimum of ten minutes apart from one another. Experiments were two hours long, averaging four to seven stimulations. Every animal was tested at least twice using each stimulation time (10s and 20s), until a minimum of 10 total stimulations occurred per animal, per stimulation time.

Optogenetic data preprocessing. For each stimulation, data spanning 5 min (–300 s) before to 10 min (+600 s) after light onset were extracted, with the onset designated as time 0. Core body temperature (Tb) data was recorded once every five seconds for the duration of the experiment. We therefore subset all other data to the same rate for core Tb analyses.

Activity levels were measured at a rate of 10 Hz, so all data were subset to the same rate for activity analyses. As activity is measured using percent pixel movement over the entire image, activity was first set to a logarithmic scale, to measure small differences in change, then normalized using a Z score across mouse IDs to account for differences in baseline activity levels.

Feature-specific surface temperatures using SGBS were measured at a rate of around 20-30 Hz, depending on the Flir A50's output. As previously described, all surface temperature data was subset to 10 Hz and aligned to surface temperature data based on the nearest timestamps when the laser was turned on (< 0.1s deviation). To eliminate the effect of outliers originating from an incorrect segmentation output, all surface temperature data were smoothed with a rolling average over one half of a second. To eliminate differences in baselines per animal, every value was baseline-normalized using $\Delta T/T$, where each temperature value was expressed as a change from the pre-stimulation mean (3-minutes prior to light on) relative to that baseline.

To assess whether optogenetic effects varied with initial thermal state, core body temperature at the onset of each blue-light pulse (Tb-T0) was recorded. Because Tb-T0 values were generally higher than those observed during spontaneous PVNOT calcium peaks, stimulations were stratified for each mouse into “low Tb-T0” and “high Tb-T0” trials using that animal’s mean Tb-T0 as the cutoff. The two strata were then analyzed separately.

Statistics

Statistical results are reported in Table S1.

Effect of behavior state on FOS expression. To determine the effect of behavior on FOS expression, brain ROIs (divided into left and right sides, where appropriate) were scanned by CellProfiler 4.2.1 to determine the total number of cells, as marked by DAPI. DAPI ROIs were shrunk to a point and then expanded by a factor of 6, and classified as being either FOS-positive or FOS-negative, as marked by presence of the secondary antibody (Alexa Fluor 555), using the same parameters for every slice. These per-ROI portions were then standardized using a Z-score between different histology days, to account for any batch effects of antibody binding or fluorescence. A linear regression model was used on a per-ROI basis, and a post-hoc tukey test was used to determine the effect of behavior on FOS expression, for each brain region. P-values were adjusted for multiple comparisions using the Holm method.

Relationship between PVN^{OT} calcium activity and behavior state, activity, and body temperature. To determine the effect of different behavioral states on calcium peak amplitude and frequency, we fit LMMs with amplitude or frequency as the dependent variable, behavioral state as the independent variable, and mouseID as a random effect. These models were run for both solo and paired conditions.

To determine the effect of social context and floor temperature on calcium peak amplitude and frequency, we fit LMMs with amplitude or frequency as the dependent variable, social context or floor temperature as the independent variable, and mouseID as a random effect.

To determine how calcium peak frequency is affected by behavioral state bout length (i.e., for quiescence and quiescent-huddle) and floor temperature, we fit a LMM with per-bout peak counts as the dependent variable; bout-length, floor temperature, and their interactions as the independent variables; and mouseID as the random effect. We subsequently extracted the standardized beta coefficients using the sjPlot package [93].

To determine how locomotor activity changed during a 300 sec. interval of time surrounding calcium peaks (i.e., peri-peak time), we first z-scored the activity data (estimated at 10 Hz), then smoothed it according to the mean using the rollapply function [97], and finally calculated the per-second mean for each individual. Next, we calculated normalized activity data across the 600 sec interval, including the mean normalized activity before and after each peak (i.e., “before-after”). Last, we fit a LMM with normalized activity as the dependent variable, “before-after” as the independent variable, and mouse-ID as a random effect.

To determine peak probability during defined behaviors we used logistic regression. First, we used custom R code to (1) extract the onset and offset of behavioral bouts, and (2) label rows of data (at 10 frames per second) according to whether they occurred within a minute containing (or not containing) a calcium peak (i.e., PeakMinute). Next, we fit a binomial generalized linear model with PeakMinute as the dependent variable; the independent variable was the time span before, during, and after the behavioral epoch of interest (e.g., quiescence offset). Next, we extracted the per-frame predicted values (including standard error) from this model.

To compare the statistical distributions of Tb during calcium peaks *vs*. baseline, we plotted Tb according to the PeakMinute designation described above. We then used a LMM with Tb as the dependent variable; the independent variables were PeakMinute and mouseID as a random effect.

To determine whether PVN^{OT} peaks were associated with enhanced thermogenic changes at rest-to-active transitions, we performed transition-aligned analyses of body temperature followed by linear mixed modeling. First, we extracted 600 sec peri-transition segments (−300 to +300 sec; sampled at 10 Hz) aligned to the offset of quiescence and quiescent-huddle bouts. Each transition

was categorized as Peak+ if one or more PVN^{OT} peaks occurred within the 100 sec interval preceding bout offset (−100 to 0 sec), and Peak− otherwise. To account for inter-individual variability in Tb set point, temperature was z-scored within mouse prior to analysis. For each transition, we quantified the post-offset change in scaled body temperature (Δz-Tb) by subtracting a pre-offset baseline (mean z-Tb from −60 to 0 sec) from the mean post-offset value (mean z-Tb from 0 to 300 sec). We then fit separate LMMs for quiescence offsets and quiescent-huddle offsets with Δz-Tb as the dependent variable, PeakPlus (Peak+ vs. Peak−) as the independent variable, and mouseID as a random effect.

PVN^{OT} peak characteristics: before mating *vs*. early/late stages of lactation. To determine the effect of life-history phase (virgin, early-stage and late-stage lactation) on peak amplitude, FWHM, and interpeak interval we used LMMs with epoch (PPD 2-7; PPD 8-14; virgin) as a fixed effect and mouseID as a random effect to control for repeated measures. We performed posthoc tukey comparisons for each pairwise combination of fixed effect level using the emmeans package.

Effect of optogenetic stimulation on thermal profile. To determine the effect of light stimulation on Tb in ChR2+ and light-only controls separately, Tb data were binned per minute, with each value representing the mean of the 60 seconds following. We used a linear mixed-effects model (LMM) with Tb as the dependent variable, the interaction between light-status and minute as independent variables, and mouseID as a random effect. A post-hoc tukey test was used to determine per-minute differences.

To determine the effect of light stimulation on physical activity in ChR2+ vs. light-only controls separately, activity was binned per minute, and we used the same LMM as above, but with activity as the dependent variable.

To determine the effect of light stimulation on surface temperatures (BAT, rump, or dorsal surface) in ChR2+ vs. light-only controls separately, each surface temperature was analyzed separately, first by binning temps per minute, and then using the same LMM as above, with surface temps as the dependent variable.

To further determine the effect of light stimulation on direction of temperature change, slopes before and after light onset were analyzed with a second LMM that included fixed effects of time, proximity to stimulation (pre vs. post), and their interaction, plus a random intercept for mouse ID; frame-level weights were set to the inverse of each frame's temperature SD. A significant interaction term indicated that temperature trajectories differed between ChR2+ and control groups across the stimulation boundary.

To assess the effect of light stimulation on behavior in ChR2+ versus light-only controls, we quantified cumulative time spent in each behavioral state following stimulation. First, linear regression models were applied to individual arousal behaviors to evaluate their contribution to group differences. As no single behavior showed a significant effect, all arousal behaviors were grouped, and a second linear regression model was used to assess whether total arousal time differed between groups.

To quantify the temporal progression by which optogenetic stimulation influenced core body temperature while accounting for concomitant changes in locomotor activity and BAT surface temperature, we used lagged regression and cross-correlation analyses of thermal dynamics. First, we performed lagged regression analyses on the derivative of core Tb (dTb/dt). For these analyses, frame-level data were first restricted to a peri-stimulus window (time-from-stimulation onset: −270 to +570 s) and then aggregated into 1 s bins within each trial. Within each trial, we computed first differences for Tb and BAT surface temperature ($dTb(t) = Tb(t) - Tb(t-1)$; $dBAT(t) = BAT(t) - BAT(t-1)$). Photostimulation was represented as a binary 1 s time series (stim(t) = 1 during seconds containing any LightOn frames, else 0) and transformed into an impulse-response regressor using a kernel (τ = 30 s), producing a decaying stimulation effect term (stim_k(τ)). We then fit a LMM, "mod_nonstim", with dTb as the dependent variable and fixed effects including stim_k(t), distributed lags of activity (Activity(t−L)) and BAT derivative (dBAT(t−L)) over L = 0–60 s (10 s increments), and random intercepts for mouse ID and trial. Predictors were z-scored to facilitate

model convergence and comparison of effect sizes. (mod_nostim: dTb_z ~ Act_L0 + Act_L10 + Act_L20 + Act_L30 + Act_L40 + Act_L50 + Act_L60 + dBAT_L0 + dBAT_L10 + dBAT_L20 + dBAT_L30 + dBAT_L40 + dBAT_L50 + dBAT_L60 + (1 | mouseID) + (1 | trial)).

To test whether stimulation explained variance in dTb beyond that captured by activity and BAT surface dynamics, we compared the full mod_nonstim model to an otherwise identical model excluding the stimulation parameter (stim_k(τ)) using a likelihood-ratio test.

To assess temporal ordering of changes in BAT surface temperature and activity relative to changes in core temperature, we computed trial-wise cross-correlation functions between derivative time series (dBAT vs. dTb; Activity derivative vs. dTb) within the peri-stimulus window, using a lag search range of ±180 s. For each trial, we extracted the lag corresponding to the peak cross-correlation coefficient (peak-lag), where positive lags indicate that the predictor time series precedes dTb. Peak-lags were summarized across trials within each mouse.

Resource availability

Lead contact

For further information or requests, contact should be directed towards the lead contact, Adam Nelson (*anelso74@uwyo.edu*).

Materials availability

This study did not generate any new reagents.

Supplementary Tables

	Group	Model	Dep. Variable	Ind. Variable	Rndm effect	DF	T value	P-Val.
Fig. 1C								Adj:Holm
AHN	AH - QH	Linear Mod	%FOS(Zscore)	Behavior state	NA	78	5.09	2.96E-04
AHN	AH - SG	Linear Mod	%FOS(Zscore)	Behavior state		78	0.60	1.000
AHN	QH - SG	Linear Mod	%FOS(Zscore)	Behavior state		78	-3.30	0.146
ArcHN	AH - QH	Linear Mod	%FOS(Zscore)	Behavior state		50	3.29	0.173
ArcHN	AH - SG	Linear Mod	%FOS(Zscore)	Behavior state		50	2.92	0.422
ArcHN	QH - SG	Linear Mod	%FOS(Zscore)	Behavior state		50	-0.45	1.000
COLL	AH - QH	Linear Mod	%FOS(Zscore)	Behavior state		59	1.06	1.000
COLL	AH - SG	Linear Mod	%FOS(Zscore)	Behavior state		59	2.26	1.000
COLL	QH - SG	Linear Mod	%FOS(Zscore)	Behavior state		59	1.33	1.000
DmHN	AH - QH	Linear Mod	%FOS(Zscore)	Behavior state		64	5.80	2.80E-05
DmHN	AH - SG	Linear Mod	%FOS(Zscore)	Behavior state		64	4.43	4.22E-03
DmHN	QH - SG	Linear Mod	%FOS(Zscore)	Behavior state		64	-0.68	1.000
LH	AH - QH	Linear Mod	%FOS(Zscore)	Behavior state		150	12.72	0.00E+00
LH	AH - SG	Linear Mod	%FOS(Zscore)	Behavior state		150	2.73	0.568
LH	QH - SG	Linear Mod	%FOS(Zscore)	Behavior state		150	-7.94	6.62E-11
LPO	AH - QH	Linear Mod	%FOS(Zscore)	Behavior state		139	11.43	5.94E-13
LPO	AH - SG	Linear Mod	%FOS(Zscore)	Behavior state		139	3.28	0.136
LPO	QH - SG	Linear Mod	%FOS(Zscore)	Behavior state		139	-7.13	7.15E-09
LSR	AH - QH	Linear Mod	%FOS(Zscore)	Behavior state		105	11.28	1.68E-12
LSR	AH - SG	Linear Mod	%FOS(Zscore)	Behavior state		105	7.33	7.15E-09
LSR	QH - SG	Linear Mod	%FOS(Zscore)	Behavior state		105	-2.87	0.418
MamN	AH - QH	Linear Mod	%FOS(Zscore)	Behavior state		125	6.91	2.99E-08
MamN	AH - SG	Linear Mod	%FOS(Zscore)	Behavior state		125	2.18	1.000
MamN	QH - SG	Linear Mod	%FOS(Zscore)	Behavior state		125	-4.32	3.62E-03
MePO	AH - QH	Linear Mod	%FOS(Zscore)	Behavior state		46	2.39	1.000
MePO	AH - SG	Linear Mod	%FOS(Zscore)	Behavior state		46	0.43	1.000
MePO	QH - SG	Linear Mod	%FOS(Zscore)	Behavior state		46	-1.80	1.000
MPO	AH - QH	Linear Mod	%FOS(Zscore)	Behavior state		53	2.46	1.000
MPO	AH - SG	Linear Mod	%FOS(Zscore)	Behavior state		53	0.52	1.000
MPO	QH - SG	Linear Mod	%FOS(Zscore)	Behavior state		53	-1.67	1.000
PAG	AH - QH	Linear Mod	%FOS(Zscore)	Behavior state		101	10.15	1.86E-12
PAG	AH - SG	Linear Mod	%FOS(Zscore)	Behavior state		101	-0.18	1.000
PAG	QH - SG	Linear Mod	%FOS(Zscore)	Behavior state		101	-9.64	2.03E-12
PH	AH - QH	Linear Mod	%FOS(Zscore)	Behavior state		99	10.96	1.03E-08
PH	AH - SG	Linear Mod	%FOS(Zscore)	Behavior state		99	3.07	0.249
PH	QH - SG	Linear Mod	%FOS(Zscore)	Behavior state		99	-6.79	1.20E-07
PVN	AH - QH	Linear Mod	%FOS(Zscore)	Behavior state		101	5.42	5.21E-05
PVN	AH - SG	Linear Mod	%FOS(Zscore)	Behavior state		101	4.52	2.02E-03
PVN	QH - SG	Linear Mod	%FOS(Zscore)	Behavior state		101	-0.08	1.000
SCN	AH - QH	Linear Mod	%FOS(Zscore)	Behavior state		78	2.41	1.000
SCN	AH - SG	Linear Mod	%FOS(Zscore)	Behavior state		78	0.94	1.000
SCN	QH - SG	Linear Mod	%FOS(Zscore)	Behavior state		78	-1.02	1.000
SON	AH - QH	Linear Mod	%FOS(Zscore)	Behavior state		56	2.33	1.000
SON	AH - SG	Linear Mod	%FOS(Zscore)	Behavior state		56	1.51	1.000
SON	QH - SG	Linear Mod	%FOS(Zscore)	Behavior state		56	-0.50	1.000
SubTN	AH - QH	Linear Mod	%FOS(Zscore)	Behavior state		60	3.17	0.222
SubTN	AH - SG	Linear Mod	%FOS(Zscore)	Behavior state		60	0.72	1.000
SubTN	QH - SG	Linear Mod	%FOS(Zscore)	Behavior state		60	-1.72	1.000
TubN	AH - QH	Linear Mod	%FOS(Zscore)	Behavior state		55	2.69	0.705
TubN	AH - SG	Linear Mod	%FOS(Zscore)	Behavior state		55	2.62	0.818
TubN	QH - SG	Linear Mod	%FOS(Zscore)	Behavior state		55	-0.31	1.000
VmHN	AH - QH	Linear Mod	%FOS(Zscore)	Behavior state		57	4.07	1.60E-02
VmHN	AH - SG	Linear Mod	%FOS(Zscore)	Behavior state		57	1.69	1.000
VmHN	QH - SG	Linear Mod	%FOS(Zscore)	Behavior state		57	-2.06	1.000
Figure 1I								
PVNOT	dorAH - venAH	lmer/Tukey	% *Fos*	Region*behavior	mouseID	27.54	4.31	1.01E-03

	dorAH - dorQH	lmer/Tukey	% *Fos*	Region*behavior	mouseID	8.74	3.30	3.94E-02
	dorAH - venQH	lmer/Tukey	% *Fos*	Region*behavior	mouseID	8.74	1.81	0.333
	venAH - dorQH	lmer/Tukey	% *Fos*	Region*behavior	mouseID	8.59	0.23	0.996
	venAH - venQH	lmer/Tukey	% *Fos*	Region*behavior	mouseID	8.59	-1.30	0.587
	dorQH - venQH	lmer/Tukey	% *Fos*	Region*behavior	mouseID	27.17	-1.52	0.438

	Group	Model	Dep. Variable	Ind. Variable	Rndm effect	DF	T value	P-Val.
Fig. 2F								
Solo	EatDrink	lmer	Amplitude	Behavior	mouseID	34.75831	0.07498	0.941
	Groom	lmer	Amplitude	Behavior	mouseID	34.75831	0.26705	0.791
	LMA	lmer	Amplitude	Behavior	mouseID	34.75831	0.32409	0.748
	Nest	lmer	Amplitude	Behavior	mouseID	34.75831	2.83207	7.64E-03
	Quiescent	lmer	Amplitude	Behavior	mouseID	34.75831	8.85183	1.98E-10
	Stationary	lmer	Amplitude	Behavior	mouseID	34.77749	0.11229	0.911
Fig. 2G								
Solo	EatDrink	lmer	Frequency	Behavior	mouseID	34.62	0.09650	0.924
	Groom	lmer	Frequency	Behavior	mouseID	34.62	0.32166	0.750
	LMA	lmer	Frequency	Behavior	mouseID	34.62	0.32166	0.750
	Nest	lmer	Frequency	Behavior	mouseID	34.62	3.17483	3.14E-03
	Quiescent	lmer	Frequency	Behavior	mouseID	34.62	9.45694	4.00E-11
	Stationary	lmer	Frequency	Behavior	mouseID	34.68	0.13502	0.893
Fig. 2I								
Paired	Active huddle	lmer	Amplitude	Behavior	mouseID	56	5.25932	2.35E-06
	Contact_Init	lmer	Amplitude	Behavior	mouseID	56	0	1.000
	Contact_Rec	lmer	Amplitude	Behavior	mouseID	56	0.06867	0.945
	EatDrink	lmer	Amplitude	Behavior	mouseID	56	0.72183	0.473
	Groom	lmer	Amplitude	Behavior	mouseID	56	0	1.000
	LMA	lmer	Amplitude	Behavior	mouseID	56	0.19394	0.847
	NA	lmer	Amplitude	Behavior	mouseID	56	0	1.000
	Nest	lmer	Amplitude	Behavior	mouseID	56	1.83891	0.071
	Quiscent huddle	lmer	Amplitude	Behavior	mouseID	56	16.74134	1.84E-23
	Quiescent	lmer	Amplitude	Behavior	mouseID	56	1.88315	0.065
	Stationary	lmer	Amplitude	Behavior	mouseID	56	0	1.000
Fig. 2J								
Paired	Active huddle	lmer	Amplitude	Behavior	mouseID	56	5.25932	2.35E-06
	Contact_Init	lmer	Amplitude	Behavior	mouseID	56	0	1.000
	Contact_Rec	lmer	Amplitude	Behavior	mouseID	56	0.06867	0.945
	EatDrink	lmer	Amplitude	Behavior	mouseID	56	0.72183	0.473
	Groom	lmer	Amplitude	Behavior	mouseID	56	0	1.000
	LMA	lmer	Amplitude	Behavior	mouseID	56	0.19394	0.847
	NA	lmer	Amplitude	Behavior	mouseID	56	0	1.000
	Nest	lmer	Amplitude	Behavior	mouseID	56	1.83891	0.071
	Quiscent huddle	lmer	Amplitude	Behavior	mouseID	56	16.74134	1.84E-23
	Quiescent	lmer	Amplitude	Behavior	mouseID	56	1.88315	0.065
	Stationary	lmer	Amplitude	Behavior	mouseID	56	0	1.000
Fig. 2K							statistic	
Solo:Quies.	Ta_15 - Ta_23	lmer/Tukey	Frequency	AmbientTemp	mouseID	16.11576	-0.23860	0.969
	Ta_15 - Ta_29	lmer/Tukey	Frequency	AmbientTemp	mouseID	17.07043	-3.35101	0.010
	Ta_23 - Ta_29	lmer/Tukey	Frequency	AmbientTemp	mouseID	17.07517	-3.22980	0.013
Fig. 2N								
Paired:QH	Ta_15 - Ta_23	lmer/Tukey	Frequency	AmbientTemp	mouseID	15.27282	-1.85294	0.186
	Ta_15 - Ta_29	lmer/Tukey	Frequency	AmbientTemp	mouseID	15.60255	-1.64613	0.257
	Ta_23 - Ta_29	lmer/Tukey	Frequency	AmbientTemp	mouseID	15.53927	0.14852	0.988

	Group	Model	Dep. Variable	Ind. Variable	Rndm effect	DF	T value	P-Val.
Fig. 3C								
PeriCa2+peak	Solo	lmer	PhysicalActiv.	after vs before	MouseID	7.00	3.37	0.012
Fig. 3E								
PeriCa2+peak	Paired	lmer	PhysicalActiv.	after vs before	MouseID	6.00	6.62	0.001

Fig. 3K								
Nesting	Pre-quies.	lmer	PeakFreq	Quiesence phase	MouseID	32.26	1.71	0.097
	Post-quies.	lmer	PeakFreq	Quiesence phase	MouseID	35.28	2.97	0.005
	Pre and Post	lmer	PeakFreq	Quiesence phase	MouseID	20.54	1.96	0.064
	Neither	lmer	PeakFreq	Quiesence phase	MouseID	10.47	2.37	0.038
Fig. 3M								
Act.Huddle	Pre-quies.	lmer	PeakFreq	Quiesence phase	MouseID	65.44	0.60	0.548
	Post-quies.	lmer	PeakFreq	Quiesence phase	MouseID	50.88	4.08	0.000
	Pre and Post	lmer	PeakFreq	Quiesence phase	MouseID	26.61	1.58	0.127
	Neither	lmer	PeakFreq	Quiesence phase	MouseID	21.42	4.42	0.000
Fig. 3N								
Solo Tb	Peak: binary	lmer	BodyTemp	PeakType	MouseID	968662.28	-38.85	0.000
Fig. 3Q								
Paired Tb	Peak: binary	lmer	BodyTemp	PeakType	MouseID	764606.10	-42.78	0.000
Fig. 3P								
Solo Tb	Post-rest. +/- peak	lmer	Delta Ca post rest	PeakPlus (+/-)	MouseID	161.00	F(4.6)	0.033
Fig. 3S								
Paired Tb	Post-rest. +/- peak	lmer	Delta Ca post rest	PeakPlus (+/-)	MouseID	113.00	F(5.64)	0.019

	Group	Model	Dep. Variable	Ind. Variable	Rndm effect	DF	T value	P-Val.
Fig. 4I								
FWHM	lac_2_7 - lac_8_14	lmer	FWHM	Lactation phase	MouseID	170.07	0.63	0.806
	lac_2_7 - virgin	lmer	FWHM	Lactation phase	MouseID	170.54	3.51	1.68E-03
	lac_8_14 - virgin	lmer	FWHM	Lactation phase	MouseID	170.40	3.31	3.27E-03
Fig. 4J								
Amplitude	lac_2_7 - lac_8_14	lmer	PeakAmplitud	Lactation phase	MouseID	170.06	-5.56	4.75E-06
	lac_2_7 - virgin	lmer	PeakAmplitud	Lactation phase	MouseID	170.49	1.15	0.485
	lac_8_14 - virgin	lmer	PeakAmplitud	Lactation phase	MouseID	170.36	4.97	4.75E-06
Fig. 4K								
IPI	lac_2_7 - lac_8_14	lmer	IntrPeakIntrvl	Lactation phase	MouseID	167.90	1.24	0.431
	lac_2_7 - virgin	lmer	IntrPeakIntrvl	Lactation phase	MouseID	104.73	-1.95	0.130
	lac_8_14 - virgin	lmer	IntrPeakIntrvl	Lactation phase	MouseID	135.08	-2.92	1.15E-02

	Group	Model	Dep. Variable	Ind. Variable	Rndm effect	DF	T value	P-Val.
Fig. 5G								
Slope	Dorsal surface	lmer	Surface temp	Time* Event	MouseID	2793	7.85	5.89E-15
Fig. 5H								
Mean	Dorsal surface	lmer	Surface temp	Peri event	MouseID	2793	2.48	0.0133
Fig. 5I								
Slope	BAT surface	lmer	Surface temp	Time* Event	MouseID	2793	18.08	3.00E-69
Fig. 5J								
Mean	BAT surface	lmer	Surface temp	Peri event	MouseID	2793	2.72	0.0065
Fig. 5K								
Slope	Rump surface	lmer	Surface temp	Time* Event	MouseID	2620	0.03	0.976
Fig. 5L								
Mean	Rump surface	lmer	Surface temp	Peri event	MouseID	2620	3.13	0.0018

	Group	Model	Dep. Variable	Ind. Variable	Rndm effect	DF	T value	P-Val.
Fig. 6C								
Low Tb-T0	0 sec	lmer	Core Tb	Binned time	MouseID	Inf	-0.779	0.436
	60 sec	lmer	Core Tb	Binned time	MouseID	Inf	-0.577	0.564
	120 sec	lmer	Core Tb	Binned time	MouseID	Inf	-0.515	0.606
	180 sec	lmer	Core Tb	Binned time	MouseID	Inf	-0.097	0.923
	240 sec	lmer	Core Tb	Binned time	MouseID	Inf	-0.029	0.977
	300 sec	lmer	Core Tb	Binned time	MouseID	Inf	0.554	0.580
	360 sec	lmer	Core Tb	Binned time	MouseID	Inf	1.524	0.128
	420 sec	lmer	Core Tb	Binned time	MouseID	Inf	2.235	0.025
	480 sec	lmer	Core Tb	Binned time	MouseID	Inf	2.133	0.033
	540 sec	lmer	Core Tb	Binned time	MouseID	Inf	1.971	0.049

Fig. 6D								
Low Tb-T0	0 sec	lmer	Physical activity	Binned time	MouseID	4.45	0.452	0.673
	60 sec	lmer	Physical activity	Binned time	MouseID	4.62	0.402	0.705
	120 sec	lmer	Physical activity	Binned time	MouseID	4.66	0.627	0.560
	180 sec	lmer	Physical activity	Binned time	MouseID	4.72	0.325	0.759
	240 sec	lmer	Physical activity	Binned time	MouseID	4.80	0.833	0.444
	300 sec	lmer	Physical activity	Binned time	MouseID	5.01	0.763	0.480
	360 sec	lmer	Physical activity	Binned time	MouseID	5.22	0.774	0.472
	420 sec	lmer	Physical activity	Binned time	MouseID	5.38	1.734	0.139
	480 sec	lmer	Physical activity	Binned time	MouseID	5.48	1.389	0.219
	540 sec	lmer	Physical activity	Binned time	MouseID	6.14	1.673	0.144
Fig. 6E								
Low Tb-T0	0 sec	lmer	BAT temp	Binned time	MouseID	Inf	-0.414	0.6787
	60 sec	lmer	BAT temp	Binned time	MouseID	Inf	-2.218	0.0265
	120 sec	lmer	BAT temp	Binned time	MouseID	Inf	-2.765	0.0057
	180 sec	lmer	BAT temp	Binned time	MouseID	Inf	-0.315	0.7528
	240 sec	lmer	BAT temp	Binned time	MouseID	Inf	-0.427	0.6696
	300 sec	lmer	BAT temp	Binned time	MouseID	Inf	0.934	0.3504
	360 sec	lmer	BAT temp	Binned time	MouseID	Inf	3.427	6.09E-04
	420 sec	lmer	BAT temp	Binned time	MouseID	Inf	5.866	4.46E-09
	480 sec	lmer	BAT temp	Binned time	MouseID	Inf	8.111	5.04E-16
	540 sec	lmer	BAT temp	Binned time	MouseID	Inf	10.508	7.94E-26
Fig. 6F								
Low Tb-T0	0 sec	lmer	Rump temp	Binned time	MouseID	Inf	0.096	0.9236
	60 sec	lmer	Rump temp	Binned time	MouseID	Inf	1.495	0.1350
	120 sec	lmer	Rump temp	Binned time	MouseID	Inf	2.388	0.0169
	180 sec	lmer	Rump temp	Binned time	MouseID	Inf	2.207	0.0273
	240 sec	lmer	Rump temp	Binned time	MouseID	Inf	3.056	2.24E-03
	300 sec	lmer	Rump temp	Binned time	MouseID	Inf	4.717	2.39E-06
	360 sec	lmer	Rump temp	Binned time	MouseID	Inf	6.921	4.48E-12
	420 sec	lmer	Rump temp	Binned time	MouseID	Inf	10.140	3.66E-24
	480 sec	lmer	Rump temp	Binned time	MouseID	Inf	12.047	2.00E-33
	540 sec	lmer	Rump temp	Binned time	MouseID	Inf	12.132	7.16E-34

	Group	Model	Dep. Variable	Ind. Variable	Rndm effect	DF	T value	P-Val.
Fig. S2C								
	Paired vs. solo	lmer	Amplitude	Social context	mouseID	6.842	1.540	0.168
Fig. S2D								
	Paired vs. solo	lmer	Peak freq.	Social context	mouseID	43.298	2.455	1.82E-02
Fig. S2G								
Solo	EatDrink	lmer	Amplitude	Behavior	mouseID	57.583	-0.615	0.541
	Groom	lmer	Amplitude	Behavior	mouseID	56.462	-0.430	0.669
	LMA	lmer	Amplitude	Behavior	mouseID	56.462	-0.390	0.698
	Nest	lmer	Amplitude	Behavior	mouseID	53.692	2.346	2.27E-02
	Quiescent	lmer	Amplitude	Behavior	mouseID	53.692	8.041	8.81E-11
	Stationary	lmer	Amplitude	Behavior	mouseID	98.181	0.296	0.768
Fig. S2I								
Solo	EatDrink	lmer	Frequency	Behavior	mouseID	39.71	0.08	0.939
	Groom	lmer	Frequency	Behavior	mouseID	37.58	0.34	0.734
	LMA	lmer	Frequency	Behavior	mouseID	37.58	0.30	0.765
	Nest	lmer	Frequency	Behavior	mouseID	35.65	3.94	3.68E-04
	Quiescent	lmer	Frequency	Behavior	mouseID	35.65	10.51	1.83E-12
	Stationary	lmer	Frequency	Behavior	mouseID	100.21	0.31	0.758
Fig. S2H								
Paired	Active huddle	lmer	Amplitude	Behavior	mouseID	160	3.4057	8.34E-04
	Contact_Init	lmer	Amplitude	Behavior	mouseID	160	-0.6678	0.505
	Contact_Rec	lmer	Amplitude	Behavior	mouseID	160	-0.5620	0.575
	EatDrink	lmer	Amplitude	Behavior	mouseID	160	-0.1131	0.910
	Groom	lmer	Amplitude	Behavior	mouseID	160	-0.5501	0.583

	LMA	lmer	Amplitude	Behavior	mouseID	160	-0.5109	0.610
	NA	lmer	Amplitude	Behavior	mouseID	160	-0.0953	0.924
	Nest	lmer	Amplitude	Behavior	mouseID	160	1.0442	0.298
	Quiscent huddle	lmer	Amplitude	Behavior	mouseID	160	14.1307	6.05E-30
	Quiescent	lmer	Amplitude	Behavior	mouseID	160	0.8782	0.381
	Stationary	lmer	Amplitude	Behavior	mouseID	160	-0.3739	0.709
Fig. S2J								
Paired	Active huddle	lmer	Frequency	Behavior	mouseID	123.7290	6.1241	1.12E-08
	Contact_Init	lmer	Frequency	Behavior	mouseID	126.9801	-0.0020	0.998
	Contact_Rec	lmer	Frequency	Behavior	mouseID	126.9676	0.1419	0.887
	EatDrink	lmer	Frequency	Behavior	mouseID	126.9801	0.9498	0.344
	Groom	lmer	Frequency	Behavior	mouseID	134.2063	0.0007	0.999
	LMA	lmer	Frequency	Behavior	mouseID	126.9801	0.2926	0.770
	NA	lmer	Frequency	Behavior	mouseID	161.9678	0.0370	0.971
	Nest	lmer	Frequency	Behavior	mouseID	126.9676	2.5441	1.22E-02
	Quiscent huddle	lmer	Frequency	Behavior	mouseID	123.7290	16.1268	3.33E-32
	Quiescent	lmer	Frequency	Behavior	mouseID	131.7690	1.8253	0.070
	Stationary	lmer	Frequency	Behavior	mouseID	159.3348	-0.0252	0.980

	Group	Model	Dep. Variable	Ind. Variable	Rndm effect	DF	T value	P-Val.
Fig. S3M								
	Quiesence	lmer	NearZero dF/F	offsetVS.onset	mouseID	7	5.035	1.51E-03
Fig. S3N								
	Quies. Huddle	lmer	NearZero dF/F	offsetVS.onset	mouseID	6	3.299	1.64E-02
Fig. S3O							statistic	
Nesting	pre - post	lmer	Sum of bouts	Rest_Phase	mouseID	135.0469	3.708	1.71E-03
	pre - both	lmer	Sum of bouts	Rest_Phase	mouseID	135.0206	2.422	0.078
	pre - neither	lmer	Sum of bouts	Rest_Phase	mouseID	135.0780	-5.177	4.75E-06
	post - both	lmer	Sum of bouts	Rest_Phase	mouseID	135.0742	-1.234	0.606
	post - neither	lmer	Sum of bouts	Rest_Phase	mouseID	135.0514	-8.989	1.60E-14
	both - neither	lmer	Sum of bouts	Rest_Phase	mouseID	135.1052	-7.565	3.22E-11
Fig. S3P							statistic	
ActiveHudd	pre - post	lmer	Sum of bouts	Rest_Phase	mouseID	68.08	3.71	2.31E-03
	pre - both	lmer	Sum of bouts	Rest_Phase	mouseID	68.08	3.46	5.10E-03
	pre - neither	lmer	Sum of bouts	Rest_Phase	mouseID	68.01	-2.03	0.19
	post - both	lmer	Sum of bouts	Rest_Phase	mouseID	68.19	-0.25	0.995
	post - neither	lmer	Sum of bouts	Rest_Phase	mouseID	68.08	-5.72	1.56E-06
	both - neither	lmer	Sum of bouts	Rest_Phase	mouseID	68.08	-5.46	4.21E-06

	Group	Model	Dep. Variable	Ind. Variable	Rndm effect	DF	T value	P-Val.
Fig. S5B								
ChR2	Arousal	lmer	Cum. Time	Group	MouseID	152	1.8928	0.0603
	Quiescence	lmer	Cum. Time	Group	MouseID	152	-0.3042	0.7614
Fig. S5C								
ChR2	Low Tb-T0	lmer	Physical activity	Time * Group	MouseID	705	-2.0477	4.10E-02
	High Tb-T0	lmer	Physical activity	Time * Group	MouseID	616	1.9036	0.0574
Fig. S5D								
ChR2	Low Tb-T0	lmer	BAT temp	Time * Group	MouseID	595	-3.1796	1.55E-03
	High Tb-T0	lmer	BAT temp	Time * Group	MouseID	521	1.8330	0.0674
Fig. S5E								
ChR2	Low Tb-T0	lmer	Rump temp	Time * Group	MouseID	588	-5.7331	1.58E-08
	High Tb-T0	lmer	Rump temp	Time * Group	MouseID	520	1.2131	0.2256
Fig. S5F								
ChR2	Low Tb-T0	lmer	Dorsal temp	Time * Group	MouseID	588	-4.7657	2.37E-06
	High Tb-T0	lmer	Dorsal temp	Time * Group	MouseID	519	2.4031	1.66E-02

Table S1.

Supplementary Figures

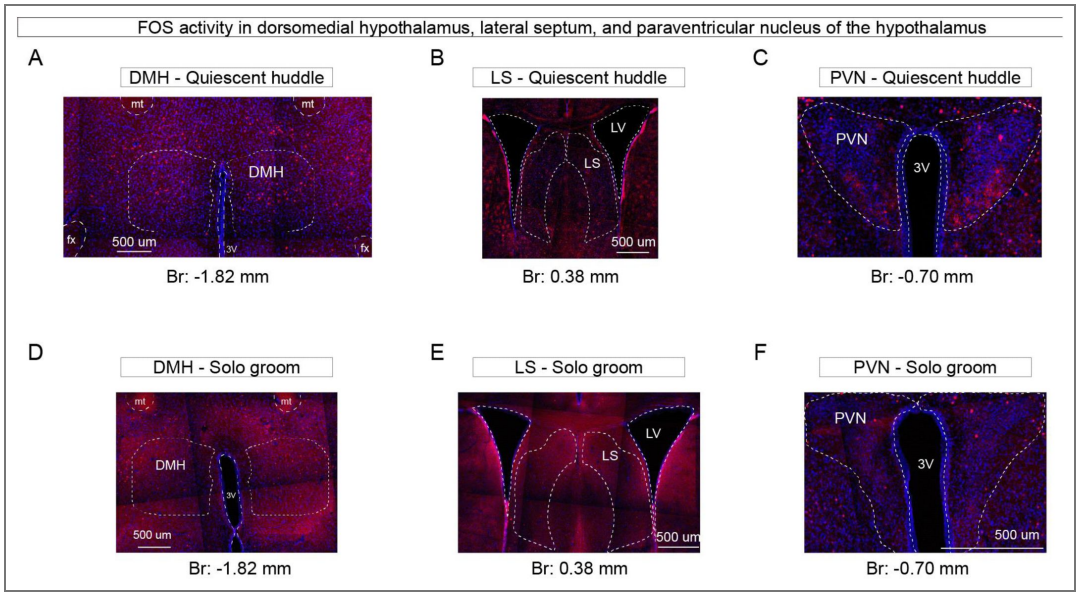

Figure S1. Histology of FOS activity in the DMH, LS, and PVN. Related to Figure 1. **(A - C)** Representative histology images showing quiescent huddling associated FOS expression in the DMH **(A)**, LS **(B)**, and PVN **(C)**. **(D – E)** Representative histology showing solo grooming associated FOS expression in the DMH **(D)**, LS **(E)**, and PVN **(F)**. Abbreviations: 3V: third ventricle; DMH dorsomedial hypothalamus; LS lateral septum; mt: mammillothalamic tract; PVN paraventricular nucleus of the hypothalamus.

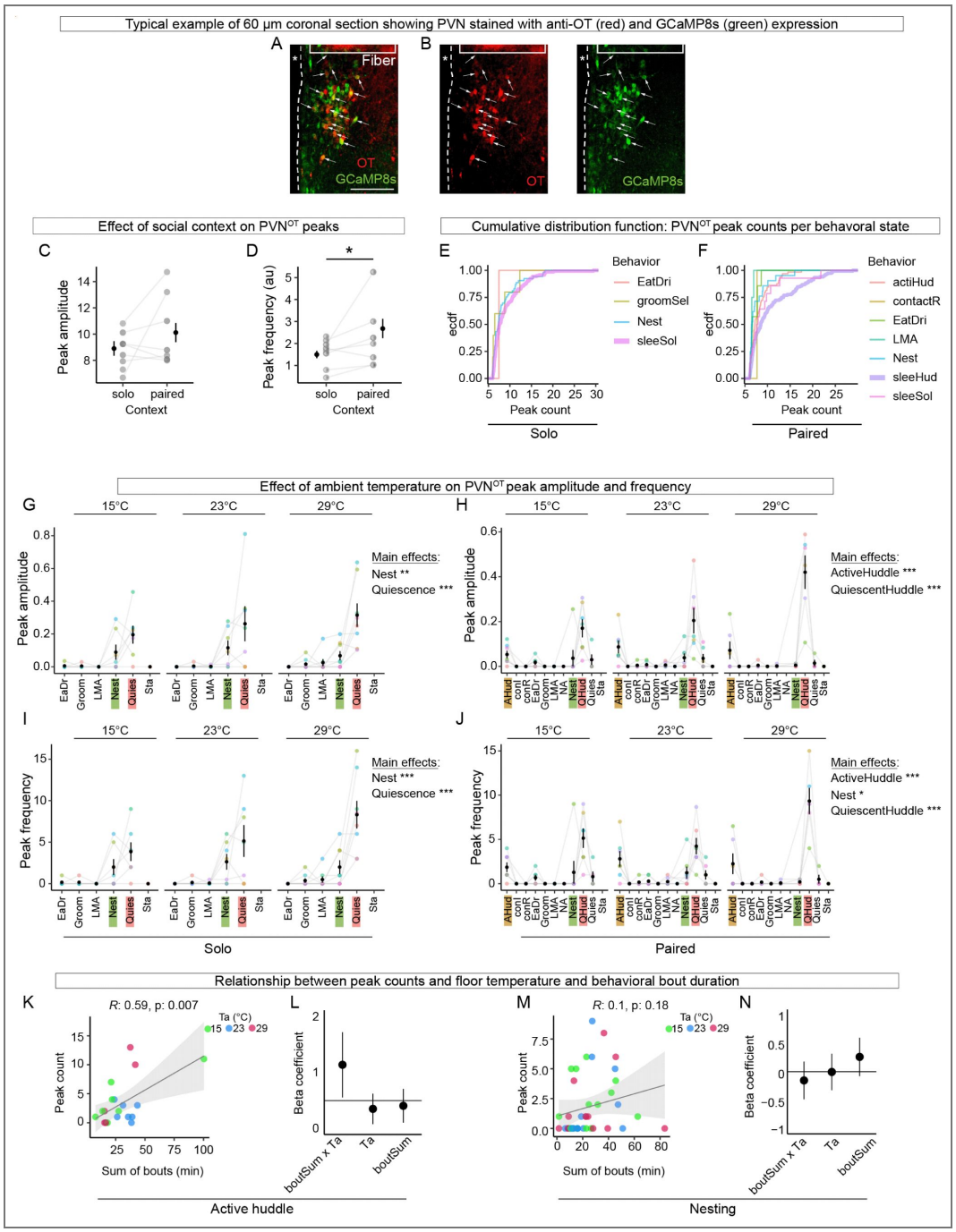

Figure S2. Characterization of PVN^{OT} Ca^{2+} peaks and their associations with behavioral states.

Related to Figure 2. **(A - B)** Representative coronal brain slice showing the location of the optical fiber and expression of oxytocin peptide (red) and GCaMP8s (green) in the PVN. Arrows indicate some cells co-labeled with GCaMP8s and anti-OT. The third ventricle is designated by "*". Scale bar 100 µm. **(C - D)** Effect of social context on PVNOT peak amplitude **(C)** and frequency **(D)**. **(E - F)** PVNOT empirical cumulative distribution functions (ecdf) of peak counts according to behavioral state in solo **(E)** and paired **(F)** conditions. **(G - H)** Effect of floor temperature on PVNOT peak amplitude. Relationship between floor temperature and behavior state in solo **(F)** and paired **(G)** females. **(I - J)** Effect of floor temperature on PVNOT peak frequency. Relationship between floor temperature and behavior state in solo **(I)** and paired **(J)** females. **(K - N)** Effect of floor temperature and active behaviors on PVNOT peak counts for active huddling **(K-L)** and nesting **(M-N)**. Peak count according to total duration of bouts per trial; *R* and p values shown at top **(K,M)**. Beta coefficients from a model of the effect of floor temperature, total duration of bouts (boutSum), and the Ta*boutSum interaction on peak count **(L,N)**. Statistical results are from linear mixed models. N = 8 solo, N = 7 paired, N = 50 recordings. Data shows mean ±SEM. P < 0.05 *, P < 0.01 **, P < 0.001 ***.

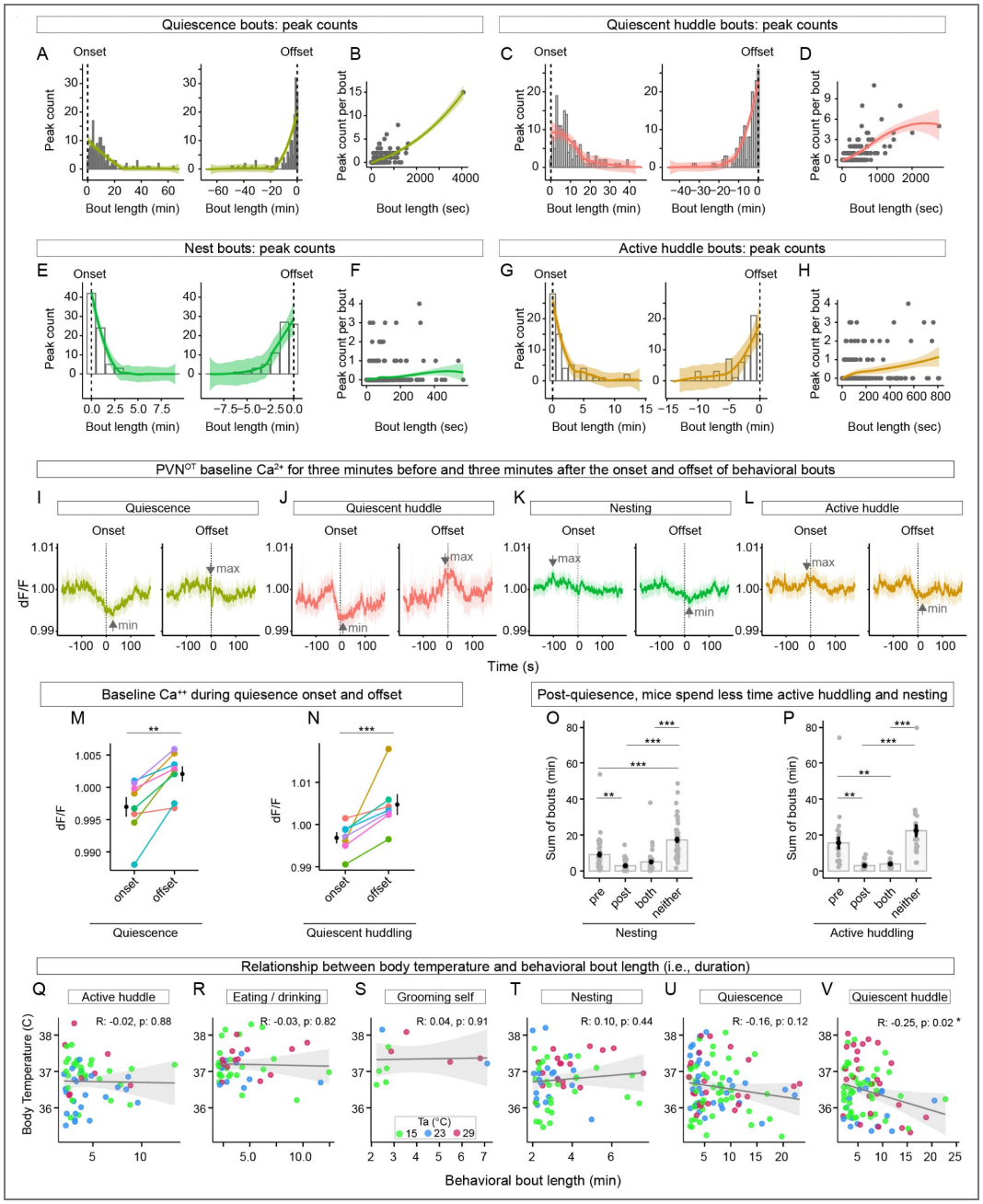

Figure S3. PVN^{OT} Ca^{2+} peaks during behavioral states and transitions.

Related to Figure 3. **(A - D)** Peak counts for bouts of resting behaviors. Quiescence onset/offset peak counts **(A)** and peak count per bout **(B)**. Quiescence huddle onset/offset peaks counts **(C)** and relationship between bout length and peak count **(D)**. **(E - H)** Peak counts for bouts of active behaviors. Nesting onset/offset peaks counts **(E)** and relationship between bout length and peak count **(F)**. Active huddle onset/offset peak counts **(G)** and relationship between bout length and peak count **(H)**. **(I-L)** Extended analysis of baseline PVNOT Ca2+ surrounding bout onsets and offsets. For each behavior, the minimum and maximum dF/F is indicated with an arrow. **(M - N)** Per-individual means of Ca++ dF/F during onset and offset (i.e., near-zero values) of two resting behaviors: quiescence **(M)** and quiescent huddle **(N)**. **(O - P)** Sum of bouts according to the phase of quiescence. "Neither" refers to bouts that did not adjoin bouts of quiescence. Nesting bouts **(O)**. Active huddling bouts **(P)**. Post quiescence nesting and active huddling is relatively rare. **(Q-V)** Regression analysis of bout length and Tb. Bouts <2min are excluded. Shown are the Pearson correlation (*R*) and associated p-value from a linear regression. Length of quiescent huddle bouts is negatively correlated with body temperature **(N)**. **M-P**: linear mixed models; N = 8 mice/50 recordings. **(Q-V): linear model;** N = 6 mice/27 recordings. All data shows mean ±SEM. P < 0.05 *, P < 0.01 **, P < 0.001 ***. Full statistical analysis in Table S1.

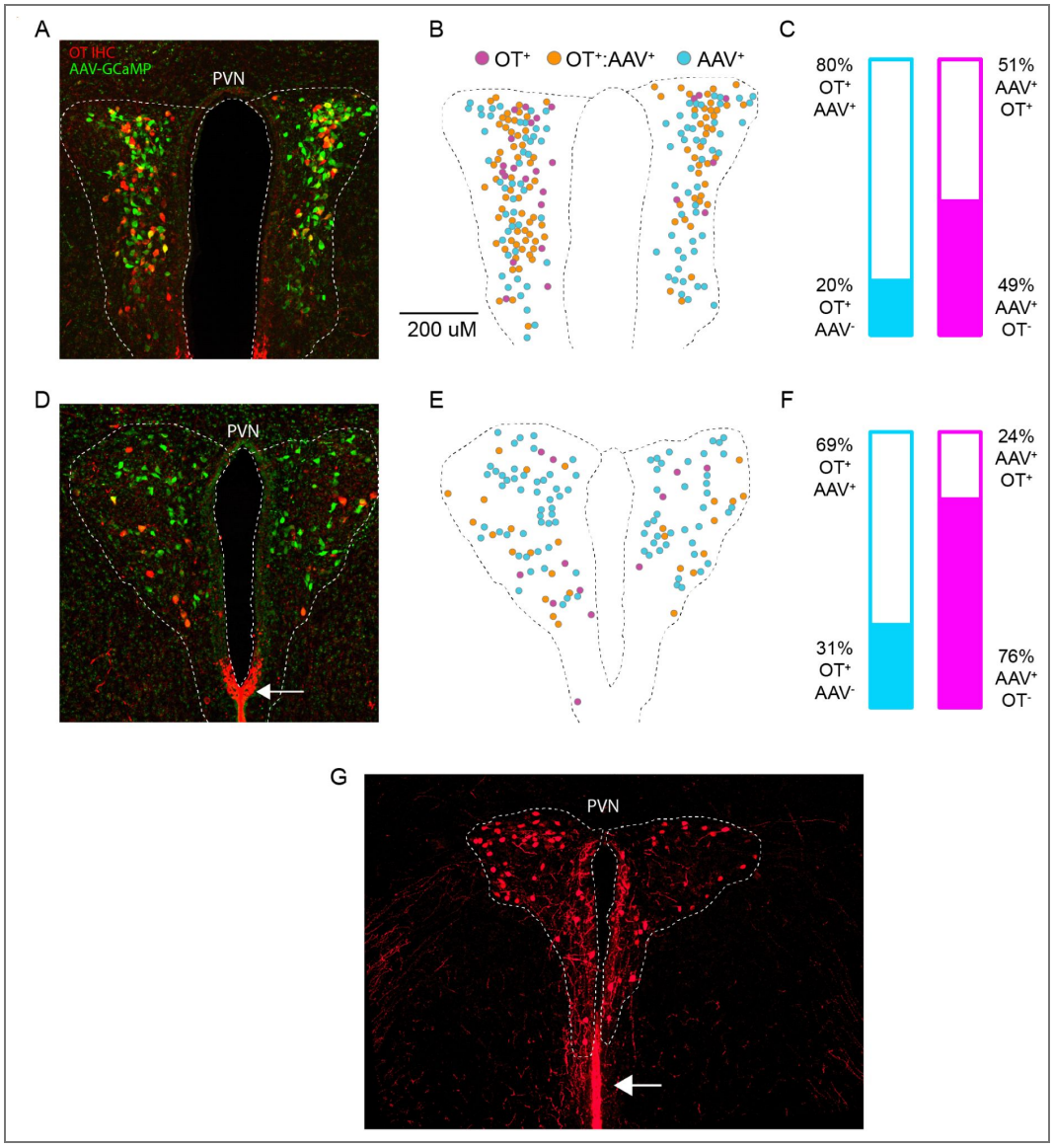

Figure S4. Intra-individual distribution and quantification of OT immunoreactivity and Cre-dependent GCaMP expression.

Related to Figure 4. **(A)** The paraventricular hypothalamus (PVN) showing oxytocin immunoreactivity (red) and Cre-dependent expression (green). **(B)** Re-construction of (A) showing the distribution of neurons with OT immunoreactivity, GCaMP expression, and their overlap. **(C)** Quantification of cellular overlap in (B). **(D)** An adjacent slice from the same animal as (A). Strong OT immunoreactivity or processes along the ventral third ventricle (white arrow). **(E)** Re-construction of (D) showing the distribution of neurons with OT immunoreactivity, GCaMP expression, and their overlap. **(F)** Quantification of cellular overlap in (E). **(G)** Image showing OT immunoreactivity in processes near the third ventricle, below the PVN.

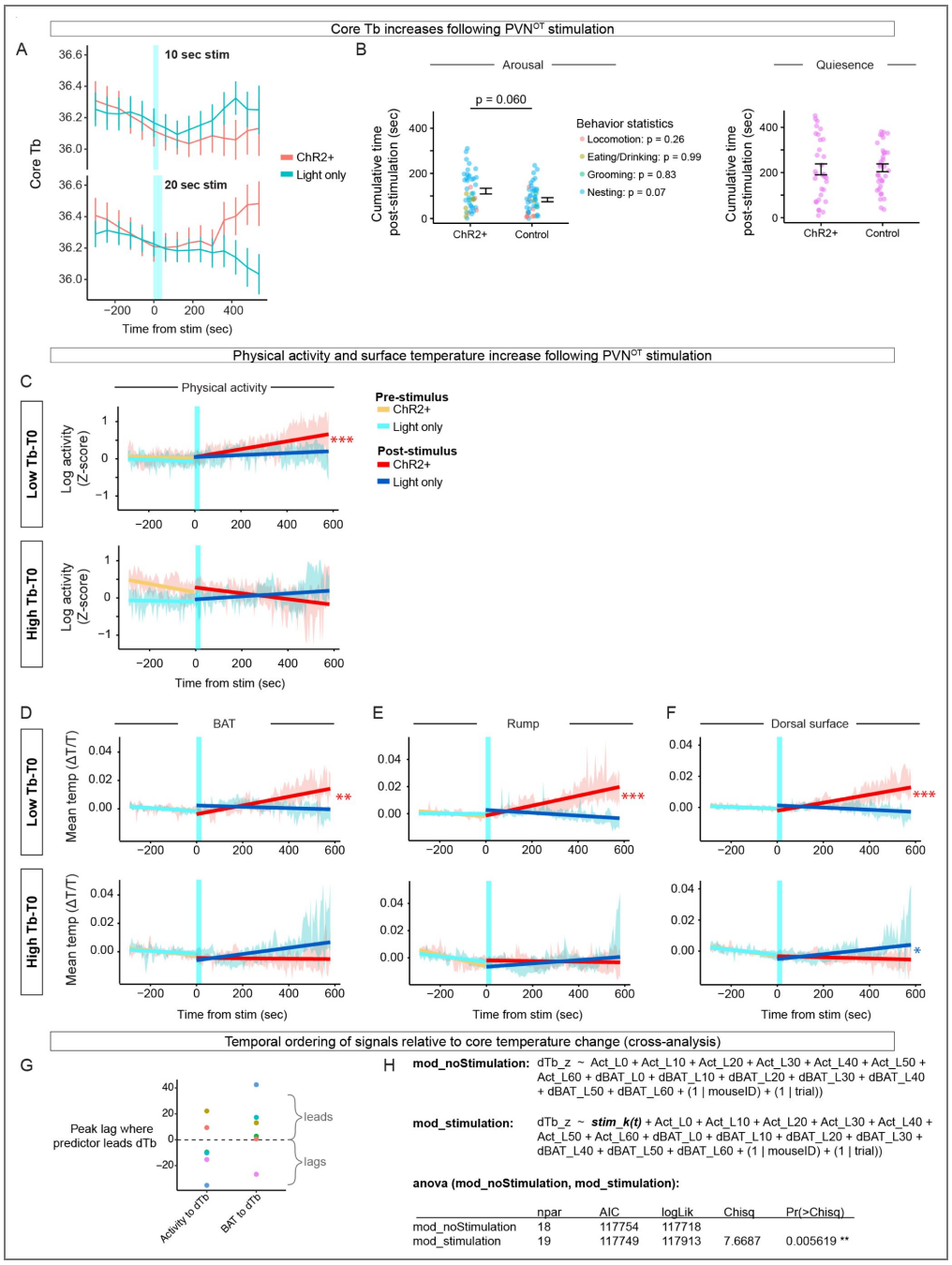

Figure S5.

(A) Blue light stimulation (time 0; shaded blue rectangle) during 20s vs. 10s stimulations in ChR2+ animals compared to light-only animals. **(B)** Cumulative time spent in arousal/awake (left) and rest/quiescent (right) behaviors following 20s PVNOT stimulation. Each point represents a trial, color-coded by behavior. Black bars show mean ± SEM. **(C)** Linear regression line ± SEM of physical activity (log-transformed Z-score) 5 min before and 10 min following 20s PVNOT stimulation. **(D - F)** Same analysis as in **(C)** for surface temperatures (ΔT/T) of BAT **(D)**, rump **(E)**, and dorsal surface **(F)**. Stimulation in ChR2+ animals significantly increased temperatures in the low Tb-T0 group, with opposite or no effect in the high Tb-T_0 group. P < 0.05 *, P < 0.01 **, P < 0.001 ***. Full statistical analysis in Table S1. **(G)** Mouse-level mean peak cross-correlation lags between dTb/dt and either dBAT/dt ("dBAT to dTb") or activity ("Activity to dTb") computed over a ±180 s window. Positive values indicate the predictor precedes dTb/dt; the dashed line marks zero lag. d/dt represents the derivative with respect to time (t). **(H)** Lagged regression model testing the effect of light stimulation on derivative Tb (dTb) while controlling for the effects of activity (Act) and derivative BAT-surface temperature (dBAT). Act and dBAT are represented as lags over 0-60 sec (10 sec increments). In the stimulation model, the light stimulation term (stim_k(t)) is represented as a decaying impulse-response using a 30 sec kernel.

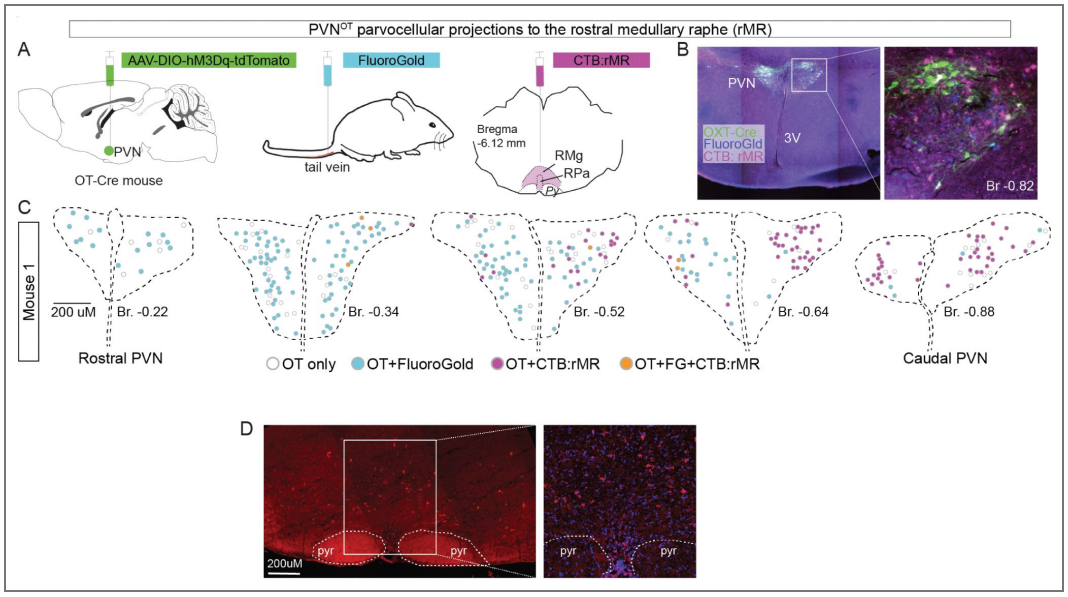

Figure S6. **PVN^{OT} parvocellular projections to the rostral medullary raphe.**

(A-D) PVN^{OT} parvocellular projections to the rostral medullary raphe (rMR). Scheme of injections to label magno- and parvocellular OT neurons **(A)**. Representative histology showing cells labeled for OXT-Cre, FluoroGold, and CTB **(B)**. Distribution of PVN^{OT} neurons retrogradely labeled with FluoroGold and CTB **(C)**. Each map was made from one coronal section. Cells double-labeled with FluoroGold and OT-Cre were mostly distributed in the rostral part of the PVN; cells double-labeled with CTB and OT-Cre were in the caudal part of the PVN **(C)**. Fluorescent in situ hybridization of OXTR (red) in the rMR region **(D)**.

Data availability

Data and code underlying this study are publicly available via the Open Science Framework (OSF) at *https://osf.io/x9kcj*. The repository includes the experimental datasets associated with the main fiber photometry experiments, lactation study, optogenetic experiments, and body temperature-linked photometry experiments, together with metadata files describing session- and animal-level information. Code used for data processing and analysis is also available at this repository.

Acknowledgements

We thank University of Wyoming Sensory Biology Center for input; Robert Carrol for assistance with animal husbandry; members of the Nelson and Bedford laboratory for input; Sean Harrington for coding assistance; the UW Engineering Shop for designing and building hardware. This work is funded by NIH COBRE Grant 5P20GM121310-07.

Additional information

Author contributions

M.V., J.G.L, J.F.R., N.L.B., and A.C.N. designed the study. M.V. performed the fiber photometry studies. M.V, J.G.L, and A.C.N. performed the optogenetic studies. M.V., J.G.L., B.A., C.P., and A.C.N. performed the histology studies. J.G.L, S.K. and G.J.T. performed code development. J.F.R. contributed to a previous draft of this manuscript. N.L.B. and A.C.N secured funding and provided expertise and feedback.

Author ORCID iDs

Adam C Nelson: https://orcid.org/0000-0002-7748-6497

Additional files

VideoS1 Photometry recording of virgin mouse in the homecage. A large-amplitude PVN^{OT} peak occurs at 0:00:03s. Video is sped up to 4x.

VideoS2 Photometry recording of a lactating dam in the homecage with pups on PPD 14. The first large-amplitude PVN^{OT} peaks occur at approximately 0:00:04s. An even larger peak typical of late-stage lactation occurs at 0:00:15s. Video is sped up to 4x.

VideoS3 SGBS enables real-time segmentation of thermally defined anatomical features in freely moving mice. Example video shows the output of the SGBS model, which accurately identifies and tracks three anatomical regions – BAT, rump, and dorsal surface – in a freely moving mouse in the homecage using thermal imaging. Video is sped up to 4x.

References

1. **Nixdorf-Miller A.**, Hunsaker D. M., Hunsaker Iii J. C (2006) Hypothermia and Hyperthermia Medicolegal Investigation of Morbidity and Mortality From Exposure to Environmental Temperature Extremes. *Archives of Pathology & Laboratory Medicine* **130**:1297-1304 https://doi.org/10.5858/2006-130-1297-hahmio | PubMed

2. **Blessing W.**, Ootsuka Y (2016) Timing of activities of daily life is jaggy: How episodic ultradian changes in body and brain temperature are integrated into this process. *Temperature* **3**:371-383 https://doi.org/10.1080/23328940.2016.1177159 | PubMed

3. **Refinetti R** (2020) Circadian rhythmicity of body temperature and metabolism. *Temperature* **7**:321-362 https://doi.org/10.1080/23328940.2020.1743605 | PubMed

4. **Refinetti R** (1999) Relationship between the daily rhythms of locomotor activity and body temperature in eight mammalian species. *American Journal of Physiology-Regulatory. Integrative and Comparative Physiology* **277**:R1493-R1500 https://doi.org/10.1152/ajpregu.1999.277.5.r1493 | PubMed
5. **Morrison S. F.,** Nakamura K (2019) Central Mechanisms for Thermoregulation. *Annu. Rev. Physiol* **81**:285-308 https://doi.org/10.1146/annurev-physiol-020518-114546 | PubMed
6. **Romanovsky A. A.** (2018) The thermoregulation system and how it works. In: Romanovsky A. A. (Ed). *Handbook of Clinical Neurology* **156** Elsevier. pp. 3-43 https://doi.org/10.1016/b978-0-444-63912-7.00001-1 | PubMed
7. **Škop V.,** et al. (2024) Beyond day and night: The importance of ultradian rhythms in mouse physiology. *Molecular Metabolism* **84**:101946 https://doi.org/10.1016/j.molmet.2024.101946 | PubMed
8. **Harding E. C.,** Franks N. P., Wisden W (2020) Sleep and thermoregulation. *Current Opinion in Physiology* **15**:7-13 https://doi.org/10.1016/j.cophys.2019.11.008 | PubMed
9. **Harding E. C.,** Franks N. P., Wisden W (2019) The Temperature Dependence of Sleep. *Frontiers in Neuroscience* **13** https://doi.org/10.3389/fnins.2019.00336 | PubMed
10. **Morrison S. F.,** Nakamura K (2011) Central neural pathways for thermoregulation. *Front Biosci* **16** https://doi.org/10.2741/3677 | PubMed
11. **Gordon C. J** (2012) Thermal physiology of laboratory mice: Defining thermoneutrality. *Journal of Thermal Biology* **37**:654-685 https://doi.org/10.1016/j.jtherbio.2012.08.004
12. **Landen J. G.,** Vandendoren M., Killmer S., Bedford N. L., Nelson A. C (2024) Huddling substates in mice facilitate dynamic changes in body temperature and are modulated by Shank3b and Trpm8 mutation. *Communications Biology* **7**:1186 https://doi.org/10.1038/s42003-024-06781-7 | PubMed
13. **Škop V.,** Xiao C., Liu N., Gavrilova O., Reitman M. L (2021) The effects of housing density on mouse thermal physiology depend on sex and ambient temperature. *Molecular Metabolism* **53**:101332 https://doi.org/10.1016/j.molmet.2021.101332 | PubMed
14. **Almeida M. C.,** Vizin R. C. L., Carrettiero D. C (2015) Current understanding on the neurophysiology of behavioral thermoregulation. *Temperature* **2**:483-490 https://doi.org/10.1080/23328940.2015.1095270 | PubMed
15. **Jung S.,** et al. (1998) A forebrain neural substrate for behavioral thermoregulation. *Neuron* **110**:266-279.e9 https://doi.org/10.1016/j.neuron.2021.09.039 | PubMed
16. **Sotelo M. I.,** et al. (2022) Lateral hypothalamic neuronal ensembles regulate pre-sleep nest-building behavior. *Current Biology* **32**:806-822.e7 https://doi.org/10.1016/j.cub.2021.12.053 | PubMed
17. **Tan C. L.,** Knight Z. A (2018) Regulation of Body Temperature by the Nervous System. *Neuron* **98**:31-48 https://doi.org/10.1016/j.neuron.2018.02.022 | PubMed
18. **Endo N.,** et al. (2018) Multiple animal positioning system shows that socially-reared mice influence the social proximity of isolation-reared cagemates. *Communications Biology* **1**:225 https://doi.org/10.1038/s42003-018-0213-5 | PubMed
19. **Gordon C. J.,** et al. (2014) Behaviorally mediated, warm adaptation: A physiological strategy when mice behaviorally thermoregulate. *Journal of Thermal Biology* **44**:41-46 https://doi.org/10.1016/j.jtherbio.2014.06.006 | PubMed
20. **Sotelo M. I.,** et al. (2024) Neurophysiological and behavioral synchronization in group-living and sleeping mice. *Current Biology* **34**:132-146.e5 https://doi.org/10.1016/j.cub.2023.11.065 | PubMed
21. **Alberts J. R** (1979) Huddling by rat pups: Group behavioral mechanisms of temperature regulation and energy conservation. *Journal of Comparative and Physiological Psychology* **92**:231 https://doi.org/10.1037/h0077459 | PubMed
22. **Fransson A.-L.,** Karlsson H., Nilsson K (2005) Temperature variation in newborn babies: importance of physical contact with the mother. *Archives of Disease in Childhood - Fetal and Neonatal Edition* **90**:F500-F504 https://doi.org/10.1136/adc.2004.066589 | PubMed

23. **Gilbert C.,** et al. (2010) One for all and all for one: the energetic benefits of huddling in endotherms. *Biological Reviews* **85**:545-569 https://doi.org/10.1111/j.1469-185x.2009.00115.x | PubMed

24. **Haig D.** (2008) Huddling: Brown Fat, Genomic Imprinting and the Warm Inner Glow. *Current Biology* **18**:R172-R174 https://doi.org/10.1016/j.cub.2007.12.040 | PubMed

25. **Gaskill B. N.,** et al. (2013) Impact of nesting material on mouse body temperature and physiology. *Physiology & Behavior* 110-111 https://doi.org/10.1016/j.physbeh.2012.12.018 | PubMed

26. **Gordon C. J** (1993) *Temperature Regulation in Laboratory Rodents* Cambridge: Cambridge University Press. https://doi.org/10.1017/CBO9780511565595

27. **Hankenson F. C.,** Marx J. O., Gordon C. J., David J. M (2018) Effects of Rodent Thermoregulation on Animal Models in the Research Environment. *comp med* **68**:425-438 https://doi.org/10.30802/aalas-cm-18-000049 | PubMed

28. **Rogers J. F.,** et al. (2024) Neural cell-types and circuits linking thermoregulation and social behavior. *Neuroscience & Biobehavioral Reviews* **161** https://doi.org/10.1016/j.neubiorev.2024.105667 | PubMed

29. **Chen C.-R.,** et al. (2021) Dysfunctions of the paraventricular hypothalamic nucleus induce hypersomnia in mice. *eLife* **10** https://doi.org/10.7554/elife.69909 | PubMed

30. **Noble E. E.,** Billington C. J., Kotz C. M., Wang C (2014) Oxytocin in the ventromedial hypothalamic nucleus reduces feeding and acutely increases energy expenditure. *American Journal of Physiology-Regulatory*. *Integrative and Comparative Physiology* **307**:R737-R745 https://doi.org/10.1152/ajpregu.00118.2014 | PubMed

31. **Fukushima A.,** Kataoka N., Nakamura K (2022) An oxytocinergic neural pathway that stimulates thermogenic and cardiac sympathetic outflow. *Cell Reports* **40** https://doi.org/10.1016/j.celrep.2022.111380 | PubMed

32. **Kasahara Y.,** et al. (2013) Oxytocin Receptor in the Hypothalamus Is Sufficient to Rescue Normal Thermoregulatory Function in Male Oxytocin Receptor Knockout Mice. *Endocrinology* **154**:4305-4315 https://doi.org/10.1210/en.2012-2206 | PubMed

33. **Sutton A. K.,** et al. (2014) Control of Food Intake and Energy Expenditure by Nos1 Neurons of the Paraventricular Hypothalamus. *J. Neurosci* **34**:15306-15318 https://doi.org/10.1523/jneurosci.0226-14.2014 | PubMed

34. **Froemke R. C.,** Young L. J. (2021) Oxytocin, Neural Plasticity, and Social Behavior. *Annu. Rev. Neurosci.* **44**:359-381 https://doi.org/10.1146/annurev-neuro-102320-102847 | PubMed

35. **Tang Y.,** et al. (2020) Social touch promotes interfemale communication via activation of parvocellular oxytocin neurons. *Nature Neuroscience* **23**:1125-1137 https://doi.org/10.1038/s41593-020-0674-y | PubMed

36. **Harshaw C.,** Leffel J. K., Alberts J. R (2018) Oxytocin and the warm outer glow: Thermoregulatory deficits cause huddling abnormalities in oxytocin-deficient mouse pups. *Hormones and Behavior* **98**:145-158 https://doi.org/10.1016/j.yhbeh.2017.12.007 | PubMed

37. **Yaguchi K.,** Miyamichi K., Tasaka G (2024) Flexible adjustment of oxytocin neuron activity in mouse dams revealed by microendoscopy. *Sci. Adv* **10** https://doi.org/10.1126/sciadv.adt1555 | PubMed

38. **Morrison S. F.,** Madden C. J., Tupone D (2014) Central Neural Regulation of Brown Adipose Tissue Thermogenesis and Energy Expenditure. *Cell Metabolism* **19**:741-756 https://doi.org/10.1016/j.cmet.2014.02.007 | PubMed

39. **Son Seoyoung,** et al. (2022) Whole-Brain Wiring Diagram of Oxytocin System in Adult Mice. *J. Neurosci* **42**:5021 https://doi.org/10.1523/jneurosci.0307-22.2022 | PubMed

40. **Besnard A.,** Leroy F (2022) Top-down regulation of motivated behaviors via lateral septum sub-circuits. *Mol Psychiatry* **27**:3119-3128 https://doi.org/10.1038/s41380-022-01599-3 | PubMed

41. **Rizzi-Wise C. A.,** Wang D. V (2021) Putting Together Pieces of the Lateral Septum: Multifaceted Functions and Its Neural Pathways. *eNeuro* **8**:ENEURO.0315-21.2021 https://doi.org/10.1523/eneuro.0315-21.2021 | PubMed

42. **Menon R.,** Süß T., Oliveira V. E. D. M., Neumann I. D., Bludau A (2022) Neurobiology of the lateral septum: regulation of social behavior. *Trends in Neurosciences* **45**:27-40 https://doi.org/10.1016/j.tins.2021.10.010 | PubMed

43. **Biag J.,** et al. (2012) Cyto- and chemoarchitecture of the hypothalamic paraventricular nucleus in the C57BL/6J male mouse: A study of immunostaining and multiple fluorescent tract tracing. *J of Comparative Neurology* **520**:6-33 https://doi.org/10.1002/cne.22698 | PubMed

44. **Li S.-B.,** et al. (2022) Hyperexcitable arousal circuits drive sleep instability during aging. *Science* **375**:eabh3021 https://doi.org/10.1126/science.abh3021 | PubMed

45. **McShane B. B.,** et al. (2010) Characterization of the bout durations of sleep and wakefulness. *Journal of Neuroscience Methods* **193**:321-333 https://doi.org/10.1016/j.jneumeth.2010.08.024 | PubMed

46. **Terrien J.,** Perret M., Aujard F (2011) Behavioral thermoregulation in mammals: a review. *Front Biosci (Landmark Ed)* **16**:1428-1444 https://doi.org/10.2741/3797 | PubMed

47. **Maloney S. K.,** Fuller A., Mitchell D., Gordon C., Overton J. M (2014) Translating Animal Model Research: Does It Matter That Our Rodents Are Cold?. *Physiology* **29**:413-420 https://doi.org/10.1152/physiol.00029.2014 | PubMed

48. **Škop V.,** et al. (2020) Mouse Thermoregulation: Introducing the Concept of the Thermoneutral Point. *Cell Reports* **31** https://doi.org/10.1016/j.celrep.2020.03.065 | PubMed

49. **Zhang Y.,** et al. (2023) Fast and sensitive GCaMP calcium indicators for imaging neural populations. *Nature* **615**:884-891 https://doi.org/10.1038/s41586-023-05828-9 | PubMed

50. **Resendez S. L.,** et al. (2020) Social Stimuli Induce Activation of Oxytocin Neurons Within the Paraventricular Nucleus of the Hypothalamus to Promote Social Behavior in Male Mice. *J. Neurosci* **40**:2282 https://doi.org/10.1523/jneurosci.1515-18.2020 | PubMed

51. **Yukinaga H.,** et al. (2022) Recording and manipulation of the maternal oxytocin neural activities in mice. *Current Biology* **32**:3821-3829.e6 https://doi.org/10.1016/j.cub.2022.06.083 | PubMed

52. **Zhan S.,** et al. (2024) Oxytocin neurons mediate stress-induced social memory impairment. *Current Biology* **34**:36-45.e4 https://doi.org/10.1016/j.cub.2023.11.037 | PubMed

53. **De Lecea L.,** Carter M. E., Adamantidis A (2012) Shining Light on Wakefulness and Arousal. *Biological Psychiatry* **71**:1046-1052 https://doi.org/10.1016/j.biopsych.2012.01.032 | PubMed

54. **Johnson Z. V.,** Walum H., Xiao Y., Riefkohl P. C., Young L. J (2017) Oxytocin receptors modulate a social salience neural network in male prairie voles. *Hormones and Behavior* **87**:16-24 https://doi.org/10.1016/j.yhbeh.2016.10.009 | PubMed

55. **Veening J. G.,** De Jong T., Barendregt H. P (2010) Oxytocin-messages via the cerebrospinal fluid: Behavioral effects; a review. *Physiology & Behavior* **101**:193-210 https://doi.org/10.1016/j.physbeh.2010.05.004 | PubMed

56. **Devarajan K.,** Marchant E. G., Rusak B (2005) Circadian and light regulation of oxytocin and parvalbumin protein levels in the ciliated ependymal layer of the third ventricle in the C57 mouse. *Neuroscience* **134**:539-547 https://doi.org/10.1016/j.neuroscience.2005.04.034 | PubMed

57. **Yukinaga H.,** Miyamichi K (2025) Oxytocin and neuroscience of lactation: Insights from the molecular genetic approach. *Neuroscience Research* https://doi.org/10.1016/j.neures.2025.01.002 | PubMed

58. **Perkinson M. R.,** Kim J. S., Iremonger K. J., Brown C. H (2021) Visualising oxytocin neurone activity in vivo: The key to unlocking central regulation of parturition and lactation. *J Neuroendocrinology* **33** https://doi.org/10.1111/jne.13012 | PubMed

59. **Mathis A.,** et al. (2018) DeepLabCut: markerless pose estimation of user-defined body parts with deep learning. *Nat Neurosci* **21**:1281-1289 https://doi.org/10.1038/s41593-018-0209-y | PubMed

60. **He K.,** Gkioxari G., Dollár P., Girshick R. (2017) Mask R-CNN. *arXiv* https://doi.org/10.48550/ARXIV.1703.06870

61. **TorchVision maintainers and contributors** (2016) TorchVision: PyTorch's Computer Vision library.

62. **Meyer C. W.,** Ootsuka Y., Romanovsky A. A (2017) Body Temperature Measurements for Metabolic Phenotyping in Mice. *Frontiers in Physiology* **8** https://doi.org/10.3389/fphys.2017.00520 | PubMed

63. **Ootsuka Y.,** et al. (2009) Brown adipose tissue thermogenesis heats brain and body as part of the brain-coordinated ultradian basic rest-activity cycle. *Neuroscience* **164**:849-861 https://doi.org/10.1016/j.neuroscience.2009.08.013 | PubMed

64. **Blessing W.,** McAllen R., McKinley M (2016) Control of the Cutaneous Circulation by the Central Nervous System. *Comprehensive Physiolog* 1161-1197 https://doi.org/10.1002/cphy.c150034 | PubMed

65. **Brownstone R. M.,** Chopek J. W (2018) Reticulospinal Systems for Tuning Motor Commands. *Front. Neural Circuits* **12**:30 https://doi.org/10.3389/fncir.2018.00030 | PubMed

66. **Engmann A. K.,** et al. (2020) The Gigantocellular Reticular Nucleus Plays a Significant Role in Locomotor Recovery after Incomplete Spinal Cord Injury. *J. Neurosci* **40**:8292-8305 https://doi.org/10.1523/jneurosci.0474-20.2020 | PubMed

67. **Althammer F.,** Grinevich V (2018) Diversity of oxytocin neurones: Beyond magno- and parvocellular cell types?. *J Neuroendocrinology* **30**:e12549 https://doi.org/10.1111/jne.12549 | PubMed

68. **Li H.,** et al. (2024) Single-neuron projectomes of mouse paraventricular hypothalamic nucleus oxytocin neurons reveal mutually exclusive projection patterns. *Neuron* **112**:1081-1099.e7 https://doi.org/10.1016/j.neuron.2023.12.022 | PubMed

69. **Yaguchi K.,** et al. (2023) Dynamic modulation of pulsatile activities of oxytocin neurons in lactating wild-type mice. *PLoS ONE* **18**:e0285589 https://doi.org/10.1371/journal.pone.0285589 | PubMed

70. **Chen S.,** Xu H., Dong S., Xiao L (2022) Morpho-Electric Properties and Diversity of Oxytocin Neurons in Paraventricular Nucleus of Hypothalamus in Female and Male Mice. *J. Neurosci* **42**:2885-2904 https://doi.org/10.1523/jneurosci.2494-21.2022 | PubMed

71. **Ludwig M.,** Leng G (2006) Dendritic peptide release and peptide-dependent behaviours. *Nat Rev Neurosci* **7**:126-136 https://doi.org/10.1038/nrn1845 | PubMed

72. **Sulaman B. A.,** Wang S., Tyan J., Eban-Rothschild A (2023) Neuro-orchestration of sleep and wakefulness. *Nat Neurosci* **26**:196-212 https://doi.org/10.1038/s41593-022-01236-w | PubMed

73. **Parmaksiz D.,** Kim Y (2025) Navigating Central Oxytocin Transport: Known Realms and Uncharted Territories. *Neuroscientist* **31**:234-261 https://doi.org/10.1177/10738584241268754 | PubMed

74. **Qian T.,** et al. (2023) A genetically encoded sensor measures temporal oxytocin release from different neuronal compartments. *Nat Biotechnol* **41**:944-957 https://doi.org/10.1038/s41587-022-01561-2 | PubMed

75. **Melón L. C.,** Hooper A., Yang X., Moss S. J., Maguire J (2018) Inability to suppress the stress-induced activation of the HPA axis during the peripartum period engenders deficits in postpartum behaviors in mice. *Psychoneuroendocrinology* **90**:182-193 https://doi.org/10.1016/j.psyneuen.2017.12.003 | PubMed

76. **Pedersen C. A.,** Caldwell J. D., McGuire M., Evans D. L (1991) Corticotronpin-releasing hormone inhibits maternal behavior and induces pup-killing. *Life Sciences* **48**:1537-1546 https://doi.org/10.1016/0024-3205(91)90278-j | PubMed

77. **Bendesky A.,** et al. (2017) The genetic basis of parental care evolution in monogamous mice. *Nature* **544**:434-439 https://doi.org/10.1038/nature22074 | PubMed

78. **Islam M. T.,** et al. (2022) Vasopressin neurons in the paraventricular hypothalamus promote wakefulness via lateral hypothalamic orexin neurons. *Current Biology* **32**:3871-3885.e4 https://doi.org/10.1016/j.cub.2022.07.020 | PubMed

79. **Adahman Z.,** et al. (2025) Hypothalamic Vasopressin Neurons Enable Maternal Thermoregulatory Behaviors. *bioRxiv* https://doi.org/10.1101/2025.01.23.634569 | PubMed

80. **Inada K.,** et al. (2025) Vasopressin-to-oxytocin receptor crosstalk in the preoptic area underlying parental behaviors in male mice. *Nat Commun* **16** https://doi.org/10.1038/s41467-025-66908-0 | PubMed

81. **Popescu I. R.,** Buraei Z., Haam J., Weng F., Tasker J. G (2019) Lactation induces increased IPSC bursting in oxytocinergic neurons. *Physiol Rep* **7**:e14047 https://doi.org/10.14814/phy2.14047 | PubMed

82. **Poulain D. A.,** Wakerley J. B., Dyball R. E. J (1977) Electrophysiological differentiation of oxytocin-and vasopressin-secreting neurones. *Proceedings of the Royal Society of London. Series B. Biological Sciences* **196**:367-384 https://doi.org/10.1098/rspb.1977.0046 | PubMed

83. **Wakerley J. B.,** Poulain D. A., Brown D (1978) Comparison of firing patterns in oxytocin- and vasopressin-releasing neurones during progressive dehydration. *Brain Research* **148**:425-440 https://doi.org/10.1016/0006-8993(78)90730-8 | PubMed

84. **Hrabovszky E.,** Liposits Z (2008) Novel Aspects of Glutamatergic Signalling in the Neuroendocrine System. *J Neuroendocrinology* **20**:743-751 https://doi.org/10.1111/j.1365-2826.2008.01719.x | PubMed

85. **Raam T.,** et al. (2024) Neural basis of collective social behavior during environmental challenge. *bioRxiv* https://doi.org/10.1101/2024.09.17.613378 | PubMed

86. **Son S.,** et al. (2022) Whole-Brain Wiring Diagram of Oxytocin System in Adult Mice. *J. Neurosci* **42**:5021-5033 https://doi.org/10.1523/jneurosci.0307-22.2022 | PubMed

87. **Hegoburu C.,** et al. (2024) Social buffering in rats reduces fear by oxytocin triggering sustained changes in central amygdala neuronal activity. *Nat Commun* **15** https://doi.org/10.1038/s41467-024-45626-z | PubMed

88. **Sun W.,** et al. (2025) Reviving-like prosocial behavior in response to unconscious or dead conspecifics in rodents. *Science* **387**:eadq2677 https://doi.org/10.1126/science.adq2677 | PubMed

89. **Carcea I.,** et al. (2021) Oxytocin neurons enable social transmission of maternal behaviour. *Nature* **596**:553-557 https://doi.org/10.1038/s41586-021-03814-7 | PubMed

90. **Borchers HW** (2011) pracma: Practical Numerical Math Functions. CRAN. https://doi.org/10.32614/CRAN.package.pracma

91. **Landen JG,** Vandendoren M, Killmer S, Bedford NL, Nelson AC (2024) Huddling substates in mice facilitate dynamic changes in body temperature and are modulated by Shank3b and Trpm8 mutation. *Communications Biology* **7**:1186 https://doi.org/10.1038/s42003-024-06781-7 | PubMed

92. **Liland KH,** Mevik B-H (2011) baseline: Baseline Correction of Spectra. CRAN. https://doi.org/10.32614/CRAN.package.baseline

93. **Lüdecke D** (2013) sjPlot: Data Visualization for Statistics in Social Science. CRAN. https://doi.org/10.32614/CRAN.package.sjPlot

94. **Tattersall G** (2019) gtatters/ThermImageJ: ThermImageJ. Zenodo. https://doi.org/10.5281/ZENODO.2652896

95. **Van Boxtel G,** Short T, Kienzle P (2021) gsignal: Signal Processing. CRAN. https://doi.org/10.32614/CRAN.package.gsignal

96. **Wu Z,** Xu Y, Zhu Y, Sutton AK, Zhao R, Lowell BB, Olson DP, Tong Q (2012) An Obligate Role of Oxytocin Neurons in Diet Induced Energy Expenditure. *PLOS One* **7**:e45167 https://doi.org/10.1371/journal.pone.0045167 | PubMed

97. **Zeileis A,** Grothendieck G, Ryan JA (2004) zoo: S3 Infrastructure for Regular and Irregular Time Series (Z's Ordered Observations). CRAN. https://doi.org/10.32614/CRAN.package.zoo

Nelson A (2025) Oxytocin Neurons Signal State-Dependent Transitions From Rest To Thermogenesis And Behavioral Arousal. OSF. ID x9kcj https://osf.io/x9kcj

Peer reviews

Reviewer #1 (Public review):

Summary:

The authors identify and investigate a specific population of PVNOT neurons (oxytocin neurons of the paraventricular hypothalamus) that seem to be involved in both behavioral and autonomic thermoregulation. These cells are activated by social thermoregulatory behaviors, but can influence thermoregulation in both social and social contexts, specifically during transitions and when mice are at low core body temperature (Tb).

Strengths:

The manuscript has many strengths.

This is a novel study, with a clear question that is addressed using an array of well-designed experiments employing integrative methods. Most of the Figures are well developed, and the analysis is generally rigorous and well detailed. The authors are clearly very experienced in this field, and indeed their scholarly introduction and discussion sections is in their credit.

The link between thermoregulation and the oxytocin system is well established, as is the link between social behavioral and the same broad system. However, the link between these three things is novel, if it can be well substantiated. I am not persuaded that was achieved here, but I do think this manuscript has many novel and useful offerings.

The authors use a cooling floor and only go town to 10 degrees Celsius. This is fine, but I would like to see the effects using ambient temperature also. This is not a crucial issue, as it is not necessary for the authors' interpretations, but it could improve measurement sensitivity.

Through an elegant behavioral experiment in Fig. 1, the authors identify c-Fos patterns in the PVN that are activated by active social huddling, and they show that at the RNA level these cells overlap with oxytocin, indicating that they are oxytocin producing cells. But this is not well discussed or indeed quantified.

The authors engage in deep analysis of fiber photometry experiments, first by observing PVNOT neuron overall activity during a variety of different behaviors in the context of three different temperatures. Activity was associated with nesting, quiescence, and both types of huddling (when social opportunities exist). Social situations did not strongly effect this, not did temperature conditions. These analyses indicate that the PVNOT neurons are involved in mediating specific behavioral outputs.

With more detailed analysis, the authors investigated how PVNOT neuronal activity relate to behavioral state transition. They found that the probability of peak PVNOT neural activity strongly predicts the offset of quiescence or quiescent huddling and therefore can be argued to signal an increase in physical activity, and as such increased metabolism. However, the opposite pattern was observed for huddling and nesting (onset being associated with PVNOT activity), again arguing for increased thermogenesis as a function.

What is particularly compelling is that these peaks of activity tend to occur during low Tb, again arguing for the function in increasing body warmth.

The authors then employ an impressive set-up where they image brown dispose tissue (BAT) in tandem with DeepLabCut (DLC) based animal tracking. Crucially, BAT activity and surface temperature correlated with the calcium peak of PVNOT neurons.

Lastly, optogenetic activation of PVNOT neurons increased Tb when it was in the lower range, but not when in the higher ranger. It also affected BAT and rump temperature, again at low Tb. However, there is no real affect on behavior, except a trend in activity.

The authors do some interesting tracing work at the end, though this is not functionally explored. That's not a criticism as it does seem like this would be a follow-up whole study.

Comments on revised version.

As discussed before, the authors employ a wide range of techniques (FOS IHC, FP for fine scale PVN OXT population dynamics, behavioural analysis, core and surface temperature tracking, physiological recordings to assess AAV specificity, optogenetic activation of PVN OXT neurons, and projection tracing) to address a clear question. The outcomes of these techniques seem to drive the same conclusion that PVN OXT neurons signal transitions from rest to arousal (behavioural and thermogenic) in a state-dependent manner:

- FOS data identifies PVN OXT population activity following behavioural onset

- Ca activity in these cells peaks at behavioural and thermogenic state transitions

- Rump temperature and BAT activity increase at state transition points

- Optogenetic stimulation of these cells recapitulates the thermogenic effects seen during physiological state transitions (in low body temperature animals) with a trending increase in physical activity

Despite the inconclusive IHC results when validating the specificity of their AAV, the virgin female/ lactation experiment is convincing that they are specifically targeting PVN OXT neurons. The rationale for this experiment is clearer in the revised manuscript.

Generally, in terms of the revised manuscript, the authors give strong responses to reviewer comments, either incorporating feedback, or giving clear explanations for the choices they made in the original manuscript. The revised manuscript is clearer about the question the authors aim to address, the reasons for their choice of experiments, and the limitations of the techniques used.

Criticisms:

I appreciate and agree with the authors' point that this manuscript is more fundamental than simply social basis oxytocin neuron function. This is point is well made by their data, and in the revised text. However, I still believe more behavioural analysis would be welcome to any reader.

They partly justify the lack of behavioural analysis in Figure 6 with the problem of "animal merging" on the SGBS images. However, in Figure 6C, they confirm that, in solo conditions, the SGBS readings are consistent with core body temperature readings. So why not stick to core body temperature, opto stimulate and analyse the social behaviour with DLC (with normal video recordings)?

The lactation validation still seems out of place in manuscript order. It is a very valuable validation, but it feels more like supplementary data for Figure 1. I feel the authors wanted it as a main figure because of how much work it must have been. In that case, it still makes more sense to include it in Figure 1.

Though their lactation experiment validates that they are targeting PVN OXT neurons, their optogenetic stimulation protocol may not be specifically inducing OXT release from these cells. PVN OXT neurons co-release glutamate but can also release glutamate independently of OXT following lower frequency tonic stimulation. OXT release from PVN neurons requires pulsatile stimulation at a higher frequency (Leithead et al., 2021; Piñol et al., 2014; Lincoln & Wakerley, 1975). In this paper, the authors use a low stimulation frequency (10Hz) and continuous pulse train (20s) to optogenetically manipulate the target PVN population which may bias the cells towards glutamate release over OXT. Therefore, though they find evidence that PVN OXT neurons are involved in driving the transition between states in their other experiments, their optogenetic stimulation may not necessarily involve OXT

release/signalling. It may be valuable to separate this out to identify the signalling molecule underlying this behavioural/ thermogenic transition. This could be done by using an opto protocol that recapitulates physiological OXT release.

The authors do however mention that isolating the specific contribution of OXT signalling compared to other co-transmitted molecules was not the aim of this study, so this is not an essential question for this manuscript.

A loss of function experiment to test for sufficiency would be a nice addition to further confirm their claims, but the authors mention that there were technical limitations to their attempts at inhibiting PVN OXT neurons. I appreciate the authors declaring that the DREADDs attempt suffered from unfortunate confounds. But for optogenetic attempts, I don't think they need a closed-loop system to get some useful results. They still can shine the light at "random" moments (that will correspond to random body temperatures) and then separate the data per body temperature.

Lastly, the mention of Raam et al. 2026 is insufficient. The authors just mention it regarding the potential differences with males, to be explored in future experiments. Even if not using males in the current study doesn't affect the stated conclusions, the fact that they chose females because "their thermo-behavioural states were readily discernible" is a considerable bias. Testing males in this very study might be out of scope, but more discussion is warranted.

References

Leithead, A. B., Tasker, J. G., & Harony-Nicolas, H. (2021). The interplay between glutamatergic circuits and oxytocin neurons in the hypothalamus and its relevance to neurodevelopmental disorders. Journal of neuroendocrinology, 33(12), e13061. *https://doi.org/10.1111/jne.13061*

Lincoln, D. W., & Wakerley, J. B. (1975). Factors governing the periodic activation of supraoptic and paraventricular neurosecretory cells during suckling in the rat. The Journal of physiology, 250(2), 443-461. *https://doi.org/10.1113/jphysiol.1975.sp011064*

Piñol, R. A., Jameson, H., Popratiloff, A., Lee, N. H., & Mendelowitz, D. (2014). Visualization of oxytocin release that mediates paired pulse facilitation in hypothalamic pathways to brainstem autonomic neurons. PloS one, 9(11), e112138. *https://doi.org/10.1371/journal.pone.0112138*

https://doi.org/10.7554/eLife.108212.2.sa3

Reviewer #2 (Public review):

This is a very interesting study from Vandendoren and colleagues examining the role of PVN oxytocin neurons during thermoregulatory behaviors, in particular during thermoregulatory huddling. The findings are important and have implications for the thermoregulation field as well as the social/naturalistic behavior field. The findings are compelling and use a combination of state-of-the-art tools (photometry, optogenetics, automated behavior tracking, thermal imaging, and core body temperature measurement), often in combination with each other, to produce a rigorous and high-dimensional dataset.

Comments on revised version.

I appreciate the effort the authors have put into addressing all of my questions, and I have no remaining concerns.

https://doi.org/10.7554/eLife.108212.2.sa2

Reviewer #3 (Public review):

Summary:

This study investigates how the activity of hypothalamic paraventricular oxytocin (PVNOT) neurons relates to physiological states in female mice, with a particular focus on behavioral states and thermogenic sympathetic activity. To address this question, the authors combined automated video-based behavioral classification with calcium imaging of PVNOT neuron activity. Sympathetic thermogenesis was inferred from surface temperature changes measured by infrared thermography, and the authors have made their custom analysis scripts available. The authors report that strong, pulsatile activation of PVNOT neurons was "occasionally" observed immediately before transitions from resting to active states. This observation suggests that PVNOT neuronal activity may facilitate the transition from rest to activity. This phenomenon was observed in both pair-housed and individually housed animals. Taken together, these findings raise the possibility that the oxytocinergic system contributes to naturalistic behavior transitions even in the absence of social interactions. However, concerns regarding the selectivity of GCaMP expression in oxytocin-expressing neurons call into question the validity of the recorded PVNOT neuronal activity.

Strengths:

The oxytocinergic neural system is believed to subserve a wide range of physiological functions. Elucidating these roles requires monitoring PVNOT neuronal activity under diverse behavioral contexts, as well as manipulating this activity to establish causal relationships. In this study, the authors present a technically sound experimental framework that integrates behavioral tracking in both individually and group-housed mice with the monitoring and manipulation of PVNOT neuron activity. This setup represents a valuable methodological resource for researchers investigating the physiological functions of oxytocin.

Weaknesses:

(1) Immunohistochemical validation of selective GCaMP expression in oxytocin-expressing neurons showed that only 24-51% of GCaMP-positive neurons expressed oxytocin. As an alternative approach, the authors demonstrate that GCaMP-expressing PVN neurons in virgin females exhibit calcium peaks during rest-wake transitions with kinetics similar to those observed in PVNOT neurons during early lactation. However, this comparison is based solely on population-level peak profiles and does not provide direct evidence for cell-type specificity of GCaMP expression in oxytocin neurons. This limitation substantially undermines the validity of the optical calcium imaging data. In situ hybridization targeting oxytocin mRNA, rather than immunohistochemistry, may provide a more reliable assessment of expression specificity.

(2) Although the authors' interpretation is generally consistent with the data presented, their main conclusions rely heavily on observational findings. Moreover, optogenetic stimulation of PVNOT neurons failed to robustly recapitulate behavioral state transitions (Figs. 6D and S5B). Further interventional experiments will be necessary to more rigorously test the authors' interpretation and to establish mechanistic insight into the causal relationship between PVNOT activity and rest-to-active transitions. In particular, loss-of-function approaches targeting the PVNOT system, such as OXTR antagonism, inhibitory DREADDs, or cell-type-specific ablation, will be essential to determine whether perturbation of this system alters behavioral state transitions These points should be addressed in future studies.

https://doi.org/10.7554/eLife.108212.2.sa1

Author response:

The following is the authors' response to the original reviews.

> ***Public Reviews:***
>
> ***Reviewer #1 (Public review):***
>
> *Summary:*
>
> *The authors identify and investigate a specific population of PVNOT neurons (oxytocin neurons of the paraventricular hypothalamus) that seem to be involved in both behavioral and autonomic thermoregulation. These cells are activated by social thermoregulatory behaviors, but can influence thermoregulation in both social and nonsocial contexts, specifically during transitions and when mice are at low core body temperature (Tb).*
>
> *Strengths:*
>
> *The manuscript has many strengths.*
>
> *This is a novel study, with a clear question that is addressed using an array of well-designed experiments employing integrative methods. Most of the figures are well-developed, and the analysis is generally rigorous and well-detailed. The authors are clearly very experienced in this field, and indeed, their scholarly introduction and discussion sections are to their credit.*

We are grateful for the reviewer's careful reading and positive assessment, including their remarks on the clarity of the question, experimental design, and analysis.

> *The link between thermoregulation and the oxytocin system is well established, as is the link between social behavior and the same broad system. However, the link between these three things is novel, if it can be well substantiated. I am not persuaded that was achieved here, but I do think this manuscript has many novel and useful offerings.*

We thank the reviewer for this thoughtful comment and for recognizing the novelty of the study. We wish to clarify the central goal of the manuscript: while social thermoregulation provided the initial influence for studying PVNOT neurons, our principal finding is that PVNOT activity during rest-to-arousal transitions is independent of social context. As stated in the manuscript, "To our surprise, these peaks were observed in both social and non-social contexts." Thus, our study demonstrates a broader role for PVNOT neurons in state-dependent thermoregulatory transitions—one that includes, but is not limited to, social contexts. We have revised the text to make this emphasis clearer throughout.

We also added a short piece to the Discussion on this point. This is the fourth and final paragraph of the Discussion section called "State-dependent PVNOT activity during thermo-behavioral transitions."

> *The authors use a cooling floor, and only go down to 10 degrees Celsius. This is fine, but I would like to see the effects using ambient temperature also. This is not a crucial issue, as it is not necessary for the authors' interpretations, but it could improve measurement sensitivity.*

Both Reviewer 1 and Reviewer 2 raise important and related points: manipulating floor temperature provides a thermal stimulus that is distinct from manipulating whole-chamber ambient air temperature, and these modalities could engage partially different sensory pathways and circuits. (Note this response is copy-pasted to other relevant comments).

We intentionally used floor cooling/heating because it provides a reliable, well-controlled stimulus that elicits thermoregulatory behaviors while keeping the experimental environment stable (e.g., avoiding changes in airflow/humidity that can accompany ambient cooling). To prevent conflation of these modalities, we revised the manuscript to consistently describe the manipulation as "floor temperature" (and not "ambient temperature"), and we added to the Discussion acknowledging that conductive floor temperature changes may differentially recruit peripheral thermoreceptors compared to ambient air temperature.

While extending these experiments to whole-chamber ambient temperature changes could be informative in future work, it is not required for the central interpretations here, which focus on PVNOT activity dynamics during thermoregulatory behavior under controlled thermal conditions.

> *Through an elegant behavioral experiment in Figure 1, the authors identify c-Fos patterns in the PVN that are activated by active social huddling, and they show that at the RNA level these cells overlap with oxytocin, indicating that they are oxytocin-producing cells. But this is not well discussed or indeed quantified.*

We thank the reviewer for catching this; Reviewer 2 made a similar comment. A typo in the figure legend led to this confusion. Figure 1I is in fact a quantification of the percent *Oxytocin*:*Fos* colocalized cells (not *Fos*:*DAPI*, as was written) in dorsal and ventral subregions of the PVN during active huddling and quiescent huddling. We have corrected the legend and clarified the quantification in the revised manuscript.

> *The authors engage in a deep analysis of fiber photometry experiments, first by observing PVNOT neuron overall activity during a variety of different behaviors in the context of three different temperatures. Activity was associated with nesting, quiescence, and both types of huddling (when social opportunities exist). Social situations did not strongly affect this, nor did temperature conditions. These analyses indicate that the PVNOT neurons are involved in mediating specific behavioral outputs.*
>
> *With more detailed analysis, the authors investigated how PVNOT neuronal activity relates to behavioral state transition. They found that the probability of peak PVNOT neural activity strongly predicts the offset of quiescence or quiescent huddling, and therefore can be argued to signal an increase in physical activity, and as such, increased metabolism. However, the opposite pattern was observed for huddling and nesting (onset being associated with PVNOT activity), again arguing for increased thermogenesis as a function.*
>
> *What is particularly compelling is that these peaks of activity tend to occur during low Tb, again arguing for the function in increasing body warmth.*
>
> *The authors then employ an impressive setup where they image brown adipose tissue (BAT) in tandem with DeepLabCut (DLC) based animal tracking. Crucially, BAT activity and surface temperature correlated with the calcium peak of PVNOT neurons.*
>
> *Lastly, optogenetic activation of PVNOT neurons increased Tb when it was in the lower range, but not when in the higher range. It also affected BAT and rump temperature, again at low Tb. However, there is no real effect on behavior, except a trend in activity.*
>
> *The authors do some interesting tracing work at the end, though this is not functionally explored. That is not a criticism, as it does seem like this would be a whole follow-up study.*
>
> *Weaknesses:*

> *While novel and valuable, the manuscript feels incomplete in its current form.*
>
> *The main evidence lacking is a loss of function of the experiment. Ideally, the authors would chronically and/or acutely inhibit PVNOT neurons to establish their necessity. I know this seems obvious, but I think it is important.*

We agree with the reviewer that loss-of-function experiments are a valuable component of circuit mapping and we appreciate this suggestion. For transparency, we did attempt a chronic chemogenetic inhibition experiment using DREADDs in PVNOT neurons. However, the results were inconclusive, primarily owing to the confounding effects of pharmacological injections: both drug and vehicle-treated animals exhibited stress-induced hyperthermia following injection, and because inhibition could not be delivered while animals were asleep/resting the experimental conditions did not recapitulate the low-Tb quiescent state during which PVNOT peaks naturally occur. Given these confounds, we do not believe these data meet the standard required for inclusion in this manuscript.

We did consider acute optogenetic inhibition. However, a clear prediction about inhibition was not as apparent in our model. Our photometry data identified a, testable hypothesis for activation: PVNOT peaks precede the exit from quiescence, therefore activation during quiescence should increase the transition, which it did (Figures 5 and 6).

That said, new analyses of our data, driven by these reviews, have now uncovered what might be inhibition of PVNOT neurons during the approximate 60 seconds prior to entry to resting states (i.e., quiescence and quiescent huddling); see the new Fig. S3I-L. This raises the possibility that an appropriately timed photoinhibition of PVNOT neurons could facilitate the establishment of resting states. We believe that, in light of our chemogenetic and optogenetic activation experiments, for an inhibition experiment to be done appropriately would require a real-time, closed loop setup that is currently not available in our laboratory.

We have added a caveat to the Discussion acknowledging the lack of LOF data as a limitation and have identified this as an important direction for future investigation.

> *The relative lack of behavioral analysis following optogenetic activation of PVNOT neurons is puzzling. The authors must surely want to study what this intervention does to behavioral state transitions. I feel that the current level of analysis limits the overall conclusions of this study to a large extent.*

We appreciate this concern and wish to clarify two points.

First, our decision to perform optogenetic activation in isolated (solo-housed) animals was driven by our initial finding that PVNOT activity profiles are mostly social-context independent during the transition from rest to arousal (Figures 2 and 3). By studying isolated animals, we could test the fundamental relationship between PVNOT activation and the rest-to-active transition without confounding social feedback. Additionally, we encountered technical challenges when using the SGBS thermographic model in paired contexts: the high thermal intensity at the point of contact between huddling mice created a thermal merging artifact that prevented accurate segmentation of individual body regions (BAT vs. rump).

Second, we did examine the post-stimulation behaviors of solo-housed animals (Fig. S5B). While PVNOT activation significantly increased the probability of exiting quiescence, it did not trigger a singular, stereotyped behavioral output. Instead, it facilitated a generalized transition to an active state, within which animals engaged in various context-appropriate actions (nesting, grooming, locomotion). We note in the discussion that “Analysis of manually-annotated behaviors suggested that PVNOT stimulation did not activate a specific motor pattern output but instead resulted in combined increases in the time spent in nesting (linear

mixed model estimate coefficient of ChR2+ stimulation: +38.0 sec), locomotion (+54.0 sec), and grooming (+14.5 sec), but not in eating/drinking (-0.4 sec) (Fig. S4B)."

That photostimulation had relatively larger effects on nesting and locomotion is consistent with our model.

Last, in the Discussion we acknowledge that future experiments should seek to disentangle the effects of PVNOT light simulation in the non-social vs social context (last paragraph of the Discussion section called "State-dependent PVNOT activity during thermo-behavioral transitions").

> *A broader criticism is that the social dimension of this manuscript seems overplayed. Naturally, oxytocin signaling can be implicated in social behavior based on a large literature. However, the focus on social thermogenesis seems like a crude integration of social behavior and thermogenesis. Given that the authors see their effects in both social and nonsocial cases of thermoregulation, I am not sure the attempts at integrating social functions and thermogenic functions of PVNOT neurons are warranted. That is, unless the authors have further experiments or analysis that can convincingly justify this link.*

We thank the reviewer for this comment. We understand the concern and wish to reframe our position. We argue that the equivalence of PVNOT signals across social and non-social contexts is itself a central finding. While the oxytocin system is widely regarded as a mediator of social bonding, and therefore a candidate mechanism underlying huddling, our data demonstrate that PVNOT neurons provide a signal for state-dependent thermoregulatory transitions that is unbiased by social context. Rather than overplaying the social dimension, we believe our study contextualizes the social function within a broader homeostatic role: PVNOT neurons facilitate transitions from rest to thermogenesis and arousal regardless of whether the resting state involves social huddling or solitary quiescence.

While the thermoregulatory transitions are present in both contexts, we note that social context appears to modestly enhance some PVNOT downstream effects. Specifically, peak probability and frequency were slightly higher in the paired compared to solo context (Fig. 3F-I, Fig. S2D), and peaks were associated with a somewhat stronger increase in physical activity when a cagemate was present (Fig. 3B-E). Additionally, quiescent huddling (paired) bouts were associated with stronger body temperature regulation compared to solo quiescence (Fig. S3Q-V). This nuance supports that the social dimension is not overplayed but rather situated within a broader homeostatic function.

We have revised the manuscript to ensure that this framing is consistent and clear. We emphasize that our goal was to uncover neural mechanisms underlying physiological transitions across behavioral and arousal states, using our social thermoregulation assay as a starting point (based on our previous publication). Counter to our initial hypothesis, the PVNOT signals generalized beyond the social setting.

> *In addition, the analysis of virgin females and lactating mothers seems out of place in Figure 4.*

This point was echoed by Reviewers 1 and 3, and one we have taken several actions to address this. (Note this response is copy-pasted to the other reviewers).

We agree with the reviewers that the rationale for the lactation data should be made more explicit. The primary purpose of this experiment was to validate the identity of oxytocinergic neurons of the PVN.

Our efforts to use IHC to validate the identity of AAV-transfected cells were inconclusive, and we have now added new data to illustrate this point. We have added Fig. S4 that includes

quantitative data on expression specificity. We observed significant variability in co-staining (OT+/GCaMP+) across brain slices, likely reflecting the dynamic nature of oxytocin peptide synthesis and storage, particularly with respect to processes lining the third ventricle. This finding is in accordance with other studies that are now cited in the text.

We now emphasize that, because IHC provided variable co-localization, we employed the lactation model as an independent physiological validation of the identity of the recorded neurons.

It is well established that PVNOT neurons undergo dramatic changes in firing dynamics and synchrony during lactation to support milk ejection (Yaguchi et al., 2023; Yukinaga et al., 2022). Conversely, AVP and CRF cell populations in the PVN do not appear to display synchronized pulsatile bursting during lactation (see response to Reviewer-2 comment-2 in 'Recommendation for authors' and our updated Discussion). Observing these characteristic changes in our recorded population provides high-confidence functional evidence that we are targeting oxytocin neurons. We have revised the text to clarify that Figure 4 serves primarily as a functional verification of genetic targeting.

We also acknowledge in the Discussion the possibility that our Cre-line may capture a small percentage of nonoxytocinergic neurons, while noting that the dramatic shift in calcium dynamics during lactation (Figure 4I–L) strongly suggests the recorded population is dominated by oxytocin neurons.

> *The c-Fos/oxytocin overlap needs to be quantified.*

We thank the reviewer for catching this; Reviewer 2 made a similar comment. A typo in the figure legend led to this confusion. Figure 1I is in fact a quantification of the percent *Oxytocin*:*Fos* colocalized cells (not *Fos*:*DAPI*, as was written) in dorsal and ventral subregions of the PVN during active huddling and quiescent huddling. We have corrected the legend and clarified the quantification in the revised manuscript. (Note this response is copy-pasted to other relevant comments).

> *The methods section could be improved by explaining how the authors exclude animals that exhibit both types of huddling, if they occur within a 90-minute time window. This seems like it could cause significant confounds.*

We have clarified in the Methods that animals were not excluded if they exhibited both active and quiescent huddling during the recording session. Importantly, a prerequisite for inclusion in the FOS study was that animals had to be continually engaged in the target behavior for a minimum of 15 consecutive minutes from behavior onset, an established approach for behavior-driven immediate early gene mapping. The 90-minute window was then counted from that same onset for FOS IHC. Because active huddling frequently transitions directly into quiescent huddling (and vice versa), excluding such animals would have eliminated the majority of recordings. The heterogeneity of behavioral states within the FOS integration windows is precisely why we turned to fiber photometry, a technique with the temporal resolution necessary to dissociate neural signals associated with each behavioral state.

> *The computer vision model is not well-explained. The authors need to be far more explicit here about how it was validated.*

We thank the reviewer for this comment and agree that the original manuscript did not sufficiently detail the validation framework. We have revised both the Methods and Results to explicitly detail how SGBS was evaluated.

First, we now clearly describe model validation on a held-out dataset (20% of manually annotated images not used for training), reporting standard segmentation metrics (per-class

IoU and Dice/F1) and directly comparing SGBS to an unmodified Mask R-CNN trained under identical conditions (same backbone initialization, dataset split, and training schedule). As shown in Fig. 5D, the skeleton-guided model converged more rapidly and achieved a lower final loss than the baseline network, demonstrating improved segmentation performance in occlusion-rich thermographic recordings.

Second, we more explicitly describe an independent physiological validation step. SGBS-derived surface temperature trajectories were temporally aligned with simultaneously recorded implanted thermologger measurements, which were not used during model training. As shown in Fig. 5E, SGBS-derived signals strongly corresponded with core body temperature dynamics and reproduced expected thermophysiological relationships (e.g., BAT warming preceding core temperature rise). This establishes external validity beyond pixel-level segmentation metrics.

> *The authors should cite and consider this preprint:*
> *https://www.biorxiv.org/content/10.1101/2024.09.17.613378v1*

We have cited this preprint (Raam et al., 2024) in the revised manuscript and integrated relevant findings into the Discussion, in the section called “Limitations and caveats”.

> ***Reviewer #2 (Public review):***
>
> *Summary:*
>
> *This is a very interesting study from Vandendoren and colleagues examining the role of PVN oxytocin neurons during thermoregulatory behaviors, in particular during thermoregulatory huddling. The findings are important and compelling, and have implications for the thermoregulation field as well as the social/naturalistic behavior field.*
>
> *Strengths:*
>
> *The study is very creative and tackles a challenging task to examine how natural and social behavior influences neural circuits for a homeostatic system such as thermoregulation. The authors use a combination of state-of-the-art tools (photometry, optogenetics, automated behavior tracking, thermal imaging, and core body temperature measurement), often in combination with each other, to produce a rigorous and high-dimensional dataset. Carrying out tightly temperature-controlled experiments and examining natural behavior, neural activity, and body physiology simultaneously is quite a feat. I applaud the authors for taking this on in a rigorous and detailed manner. This paper will be valuable for both the thermoregulation field as well as for researchers interested in naturalistic social behaviors. The conclusions are supported by the data.*

We appreciate the reviewer’s careful read and positive assessment of our integrated behavioral, neural, and physiological measurements and their relevance to both thermoregulation and social behavior.

> *Weaknesses:*
>
> *I have a number of questions and suggestions for clarification that would help improve the interpretation of the findings.*

(1) Figure 1D-F: It would be helpful to include representative images of cFos expression in the PVN, LS, and DMH during both quiescent and solo huddling conditions, to better illustrate the reported differences.

We have now addressed this in the revised manuscript. We had originally shown active huddle FOS expression in Fig. 1D-F and quiescent huddle in Fig. S1A-C. We have now added

solo groom FOS expression to Fig. S1D-F.

> *(2) Figure 1C: The data suggest a general suppression of neural activity during sleep-associated quiescent huddling, which somewhat complicates the interpretation of what specifically the active huddling cells are responding to. A more informative control might have been a comparison between huddling and a more generic form of social engagement (e.g., dyadic sniffing) to assess whether huddling-responsive neurons are broadly tuned to social stimuli. While it may not be feasible to add this experimentally at this time, a brief discussion of this limitation in the main text would be valuable.*

We thank the reviewer for this thoughtful suggestion. We agree that comparing huddling-responsive neurons with a more generic social engagement is an important consideration.

We first note that the FOS study required animals to be continuously engaged in the target behavior for a minimum of 15 consecutive minutes, ensuring that FOS expression reflects sustained behavioral engagement rather than brief social contact. Furthermore, we believe the FOS association with active huddling in Figure 1C is likely driven by preceding bouts of quiescent huddling. Because these experiments were conducted during the light phase, active huddling bouts were almost always preceded by bouts of quiescent huddling.

Given that FOS protein often integrates neural activity over ~60-90 minutes, the FOS signal during active huddling may reflect cumulative PVNOT activity during the quiescent to active transition, rather than active huddling by itself. This interpretation aligns with our fiber photometry data, which show that PVNOT peaks are concentrated at the offset of quiescent states and the onset of active states. Moreover, a broad-scale analysis of calcium data driven by these reviews, now shows there is a local minimum of PVNOT neurons during the transition into quiescent states and a local maximum of calcium activity during the offset of resting states and the onset of nesting and active huddling (Fig. S3I-L).

To directly address whether PVNOT neurons are broadly tuned to social engagement or specifically associated with thermoregulatory state transitions, we examined neural activity during "Contact Initiated" (ConI) and "Contact Received" (ConR) events—brief social interactions (e.g., dyadic sniffing) that occur outside the context of huddling. These interactions, which typically last less than one second, did not trigger the large-amplitude calcium peaks observed during rest-to-arousal transitions. Specifically, there was no significant association between ConI or ConR events and PVNOT peak frequency or amplitude (Fig. S2H; Table S1; $p = 0.505$, $p = 0.575$, respectively). This reinforces our conclusion that PVNOT peaks are not a generic response to social stimuli but are specifically aligned with the coordinated autonomic and behavioral transitions required to exit a low-temperature quiescent state. We have added a clarifying paragraph to the Discussion.

> *(3) Figure 2H-J vs. Figure 1: The fiber photometry data suggest increased PVN activity during quiescent huddling vs active huddling, which appears to contrast with the cFos results from Figure 1. It would be helpful for the authors to comment on possible reasons for this discrepancy-e.g., methodological differences, temporal resolution, or cell-type specificity.*

We agree that this apparent contrast deserves explicit discussion. The difference arises from the dramatically different temporal resolutions of the two techniques. Fiber photometry captures real-time neural dynamics at subsecond resolution, revealing that PVNOT neurons exhibit high-amplitude bursts primarily during the offset of quiescence (and to a lesser extent the onset of post-quiescence behaviors) (Figs. 3 and 5). Because these peaks occur while the animal is categorized as "quiescent," they appear as quiescence-associated activity in the photometry ethogram.

Conversely, FOS integrates neural activity over ~30–90 minutes. In retrospect, and in light of

our photometry data, an animal categorized as "Active Huddling" in the FOS study is one that has likely experienced PVNOT bursts and subsequently transitioned to an active state. The higher FOS signal in active animals therefore likely represents the cumulative activity of the transition itself and sustained activity in the active state.

We have added a clarifying statement to the Discussion section, in the section called “State-dependent PVNOT activity during thermo-behavioral transitions”.

> *(4) Figure 2O: A comparable linear regression for active huddling would be informative to assess whether the observed relationships extend across behavioral states.*

We agree. We have added linear regression analyses for active huddling and nesting to Fig. S2K-N including rsquared values, to complement the resting analyses in Figure 2O and 2L.

This analysis shows that active huddling peak counts are also positively correlated with active huddle duration (but not nesting duration). The text has been updated accordingly.

> *(5) Temperature manipulation: The use of floor temperature changes presents a distinct physiological and sensory experience from, for example, manipulation of ambient temperature. A discussion of how this choice may affect neural circuit engagement or interpretation of thermoregulatory responses would be beneficial.*

Both Reviewer 1 and Reviewer 2 raise important and related points: manipulating floor temperature provides a thermal stimulus that is distinct from manipulating whole-chamber ambient air temperature, and these modalities could engage partially different sensory pathways and circuits. (Note this response is copy-pasted to other relevant comments).

We intentionally used floor cooling/heating because it provides a reliable, well-controlled stimulus that elicits thermoregulatory behaviors while keeping the experimental environment stable (e.g., avoiding changes in airflow/humidity that can accompany ambient cooling). To prevent conflation of these modalities, we revised the manuscript to consistently describe the manipulation as “floor temperature” (and not “ambient temperature”), and we added Discussion acknowledging that conductive floor temperature changes may differentially recruit peripheral thermoreceptors compared to ambient air temperature.

While extending these experiments to whole-chamber ambient temperature changes could be informative in future work, it is not required for the central interpretations here, which focus on PVNOT activity dynamics during thermoregulatory behavior under controlled thermal conditions.

> *(6) Correlations with behavior: Across the manuscript, it would be informative to see correlations between huddle duration and neural activity (e.g., cFos expression, calcium signal magnitude). Similarly, do longer huddles produce greater thermogenic effects?*

This is a great suggestion. The first point about huddle duration and neural activity echoes the Reviewer’s comment (4) above. For this point, we now show that the duration of active huddling is positively correlated with PVNOT peak count (Fig. S2K), which is similar to what we had shown for quiescence and quiescent huddling (Fig. 2K-P).

Next, the point about huddle duration and thermogenic effects is also helpful. We have now added new analysis and panels to address this (Fig. S3M-R). We find that the duration of quiescent huddle bouts is negatively correlated with Tb (Fig. S3V). The other behaviors examined did not show correlations between duration and Tb. This finding supports our previous demonstration that quiescent huddling is an energy saving state in mice (Landen et al., 2024).

Finally, we note that longitudinal correlations between bout length and peak counts are already reported in Fig. S3A-H.

> *(7) Lactating vs. virgin mothers: The inclusion of maternal data is intriguing but feels somewhat disconnected from the central huddling-thermoregulation narrative. If these experiments are to remain, additional explanation of their rationale and how they fit into the broader story would help clarify their relevance.*

This point was echoed by Reviewers 1 and 3, and one we have taken several actions to address this.

We agree with the reviewers that the rationale for the lactation data should be made more explicit. The primary purpose of this experiment was to validate the identity of oxytocinergic neurons of the PVN.

Our efforts to use IHC to validate the identity of AAV-transfected cells were inconclusive, and we have now added new data to illustrate this point. We have added Fig. S4 that includes quantitative data on expression specificity. We observed significant variability in co-staining (OT+/GCaMP+) across brain slices, likely reflecting the dynamic nature of oxytocin peptide synthesis and storage, particularly with respect to processes lining the third ventricle. This finding is in accordance with other studies that are now cited in the text.

We now emphasize that, because IHC provided variable co-localization, we employed the lactation model as an independent physiological validation of the identity of the recorded neurons.

It is well established that PVNOT neurons undergo dramatic changes in firing dynamics and synchrony during lactation to support milk ejection (Yaguchi et al., 2023; Yukinaga et al., 2022). Conversely, AVP and CRF cell populations in the PVN do not appear to display synchronized pulsatile bursting during lactation (see response to Reviewer-2 comment-2 in 'Recommendation for authors' and our updated Discussion). Observing these characteristic changes in our recorded population provides high-confidence functional evidence that we are targeting oxytocin neurons. We have revised the text to clarify that Figure 4 serves primarily as a functional verification of genetic targeting.

We also acknowledge in the Discussion the possibility that our Cre-line may capture a small percentage of non-oxytocinergic neurons, while noting that the dramatic shift in calcium dynamics during lactation (Figure 4I–L) strongly suggests the recorded population is dominated by oxytocin neurons.

> *(8) Optogenetic manipulation: Have the authors tested the effect of PVN OT neuron stimulation or inhibition during huddling? Even a negative result would be of interest to the field. If these data exist (main or supplementary), I apologize for missing them. If not, the authors might consider including them or commenting briefly on any attempts or challenges in carrying out these experiments.*

We thank the reviewer for this question. We have not performed optogenetic manipulation during huddling. Our decision to perform optogenetic activation in solo-housed animals was driven by our fiber photometry finding that PVNOT activity profiles during the rest-to-arousal transition are social-context independent (Figures 2 and 3). Had the GCaMP data suggested that PVNOT peaks were specific to social huddling, optogenetic manipulation during huddling would have been the natural next experiment. However, because peaks aligned with thermoregulation broadly, rather than social behavior specifically, we designed our functional experiments to test the circuit's role in driving the autonomic and behavioral arousal transition.

We also note that our experience with chemogenetic manipulation suggests that pharmacological approaches to study the rest-arousal transitions during huddling are not currently feasible. As described to our response to Reviewer 1, our DREADD inhibition experiments were confounded by stress-induced hyperthermia following injection, and because drug delivery could not occur while animals were asleep and resting, the experimental conditions failed to recapitulate the low-Tb quiescent state during which PVNOT peaks naturally occur. We share this experience because we believe it will be informative for others in the field considering similar approaches.

Additionally, as described above (Reviewer 1, #5), the SGBS thermographic model encounters artifacts in paired contexts due to thermal merging between huddling mice. We have added a note in the Discussion addressing this, in the section called “Limitations and caveats”.

> ***Reviewer #3 (Public review):***
>
> *Summary:*
>
> *The authors aimed to elucidate the relationship between physiological state (i.e., behavioral status and thermogenic sympathetic activity) and the activity of hypothalamic paraventricular oxytocin (PVNOT) neurons in female mice. They studied this by combining automated classification of mouse behavior via video-based analysis with calcium imaging of PVNOT neuron activity. Sympathetic thermogenesis was inferred from surface temperature changes captured by infrared thermography, and the authors provided their custom analysis scripts in the manuscript. Notably, they found that a strong, pulsatile activation of PVNOT neurons was "occasionally" observed immediately before the animals transitioned from a resting to an active state. This pulsatile activity was observed in both pair-housed and individually housed animals. While PVNOT neurons are often associated with social behaviors, this finding suggests that the oxytocinergic system is also engaged during naturalistic behaviors, even in the absence of social interactions. If experiments were more convincingly performed and presented, the results would point to a broader physiological role of central oxytocin, including in the regulation of fundamental brain states and homeostatic processes, and offer a new perspective on the functional significance of central oxytocin signaling.*
>
> *Strengths:*
>
> *The oxytocinergic neural system is believed to subserve a wide range of physiological functions, and elucidating these roles requires monitoring PVNOT neuronal activity under various behavioral contexts, as well as manipulating this activity to establish causal links. In the present study, the authors show a technically sound experimental framework that integrates behavioral tracking in both individually and group-housed mice with the observation and manipulation of PVNOT neuron activity. This experimental setup represents a valuable methodological resource for researchers investigating the physiological functions of oxytocin.*

We thank the reviewer for the thoughtful review and for recognizing the value of our integrated framework for monitoring and manipulating PVNOT neuronal activity across behavioral contexts.

> *Weaknesses:*
>
> *While this study successfully established a new experimental setup for simultaneous analyses of behavior and PVNOT neuronal activity, there are several concerns regarding the interpretation of the results and the robustness of the conclusions, which should be more thoroughly addressed.*

(1) The study relies on the assumption that calcium imaging and optogenetic manipulation were restricted only to PVNOT neurons. However, the specificity of AAV-mediated gene expression was not verified quantitatively. A fair number of cell bodies in the PVN expressed GCaMP8s, but not OT, indicating potential off-target expression (see Figure S2A, B). The lack of quantitative validation weakens confidence in the causal interpretation of the results.

This point was echoed by Reviewers 1 and 3, and one we have taken several actions to address this.

We agree with the reviewers that the rationale for the lactation data should be made more explicit. The primary purpose of this experiment was to validate the identity of oxytocinergic neurons of the PVN.

Our efforts to use IHC to validate the identity of AAV-transfected cells were inconclusive, and we have now added new data to illustrate this point. We have added Fig. S4 that includes quantitative data on expression specificity. We observed significant variability in co-staining (OT+/GCaMP+) across brain slices, likely reflecting the dynamic nature of oxytocin peptide synthesis and storage, particularly with respect to processes lining the third ventricle. This finding is in accordance with other studies that are now cited in the text.

We now emphasize that, because IHC provided variable co-localization, we employed the lactation model as an independent physiological validation of the identity of the recorded neurons.

It is well established that PVNOT neurons undergo dramatic changes in firing dynamics and synchrony during lactation to support milk ejection (Yaguchi et al., 2023; Yukinaga et al., 2022). Conversely, AVP and CRF cell populations in the PVN do not appear to display synchronized pulsatile bursting during lactation (see response to Reviewer-2 comment-2 in 'Recommendation for authors' and our updated Discussion). Observing these characteristic changes in our recorded population provides high-confidence functional evidence that we are targeting oxytocin neurons. We have revised the text to clarify that Figure 4 serves primarily as a functional verification of genetic targeting.

We also acknowledge in the Discussion the possibility that our Cre-line may capture a small percentage of nonoxytocinergic neurons, while noting that the dramatic shift in calcium dynamics during lactation (Figure 4I–L) strongly suggests the recorded population is dominated by oxytocin neurons.

(Note, we have updated Figure S2A,B to more accurately reflect the extent of co-localization in this image).

> *(2) The study focuses on the transition from rest to active states following pulsatile activity of PVNOT neurons. However, the physiological significance of this pulsatile activity remains unclear. According to the authors, pulsatile activity occurred with an approximately 20% probability within 100 seconds prior to the end of the resting state. This implies that, in the remaining 80% of rest-to-active transitions, pulsatile PVNOT activity did not occur, suggesting that it is not essential for initiating the transition. A comparative analysis of behavioral and thermogenic changes between transitions with and without pulsatile PVNOT activity would help to further clarify the functional relevance of this phenomenon and strengthen the authors' interpretation of the findings.*

These are excellent points, and here we address them separately.

(1) probability of transitions.

We agree that our wording could be misread and we have revised the text for clarity. The "~20%" value is not the fraction of rest-to-active transitions that exhibit pulsatile PVNOT

activity within a 100-s window. Instead, Fig. 3F,H report an instantaneous (per-second) probability of observing a calcium peak as a function of time-to-bout offset (logistic regression). In other words, the probability of a peak increases sharply as the animal approaches rest offset (e.g., from ~2–3%/s near onset to ~14%/s for quiescence and ~25%/s for quiescent huddling near offset), indicating a strong state-dependent increase in peak likelihood rather than an all-or-none trigger.

We further clarify in the Discussion that we do not claim PVNOT peaks are essential for initiating every transition; rather, PVNOT activity biases or enhances the probability of transition toward thermogenesis and behavioral arousal (added to section called “State-dependent PVNOT activity during thermo-behavioral transitions”).

(2) the effect of peaks on transitions

This is a very helpful suggestion and we agree that directly comparing transitions with vs. without pre-offset pulsatile PVNOT activity could strengthen interpretation of the functional relevance of these events. We have therefore added a new transition-aligned analysis of thermogenic dynamics at rest-to-active transitions (new Fig. 3P&S; and corresponding text in the Results and Statistics sections).

Briefly, we extracted peri-transition body temperature (Tb) traces (−300 to +300 s) aligned to the offset of quiescence and quiescent-huddling bouts and classified each transition as Peak+ if it contained one or more calcium peaks in the 100 s preceding bout offset, and Peak− otherwise. To account for inter-individual differences in “balance point,” Tb was z-scored within mouse. We then quantified the post-offset thermogenic rise for each transition as the change in scaled temperature from a pre-offset baseline (−60 to 0 s) to the post-offset interval (0 to 300 s) and tested Peak+ vs Peak− differences using linear mixed-effects models. This revealed that Peak+ transitions exhibited significantly larger post-offset increases in scaled Tb than Peak− transitions for both quiescence offsets and quiescent-huddling offsets.

Together, these results indicate that while pulsatile PVNOT activity is not present prior to every rest-to-active transition, when it occurs it is associated with a stronger thermogenic rise, consistent with a probabilistic modulatory role in promoting the transition rather than being strictly required to initiate it.

We are grateful for this suggestion as this new data is very informative in the context of our model.

> *(3) The study identifies a correlation between pulsatile activity of PVNOT neurons and rest-to-active transitions, and tests for a causal relationship using optogenetic stimulation. However, since PVNOT neurons are known to co-release other neurotransmitters such as glutamate, it remains unclear whether the observed effects are mediated specifically through oxytocin receptor signaling. To address this question, functional intervention experiments using oxytocin receptor antagonists or receptor knockout mice are necessary.*

We agree with the reviewer that PVNOT neurons co-release glutamate and that isolating the specific contribution of oxytocin signaling versus co-transmitted signals is an important question. However, our study was designed to identify the functional role of the PVNOT cell type during thermoregulatory state transitions, not to dissect the molecular mechanism of signaling at downstream targets. By demonstrating that the endogenous activity of this specific population aligns with the rest-arousal window and that their activation is sufficient to drive the phenotype, we provide an anatomical and functional framework for future mechanistic investigations.

We also note that we provide anatomical evidence supporting a possible peptidergic mechanism: PVNOT neuron projections to the rostral medullary raphe (rMR), a key

thermogenic control site, alongside oxytocin receptor mRNA expression in this region (Fig. S5). This anatomical link suggests a plausible pathway for oxytocinergic modulation of thermogenesis, but of course does not rule in/out glutamatergic signaling. We acknowledge this limitation in the Discussion and frame pharmacological and receptor knockout studies as important next steps.

We address these points in the Discussion, in the section called “Limitations and caveats.”

> *(4) The authors attempted to detect BAT thermogenesis and skin vasomotion using infrared thermography. This technique measures only skin hair temperatures (since the skin was not shaved), but does not measure "BAT temperature" or "vasomotor tone". As seen in Figure 5E, the temperatures of the body surface areas ("BAT", "Rump", and "Dorsal surface") mostly changed in parallel, indicating that these temperatures are strongly affected by body core temperature. Therefore, the thermographic measurements in this study did not provide convincing information on BAT thermogenesis or skin vasomotion. To avoid misleading reports, the authors need to use other techniques to directly measure temperatures, such as telemetry.*

We agree that infrared thermography measures surface radiance rather than internal tissue temperature. We have revised the manuscript to use more precise language (e.g., "surface temperature over the interscapular BAT region" rather than "BAT temperature"). However, surface measurements are not merely passive reflections of core temperature. Here we add background and explanation about our thermography data:

Background on our approach

Infrared thermography provides a non-invasive readout of heat emission over the interscapular region and has been validated as reporting UCP1-dependent BAT thermogenesis in mice under adrenergic stimulation (Crane et al., 2014). That said, there are known confounds (insulation/adiposity, blood flow, protocol variability) and standardized protocols are needed (Law et al., 2018). Direct telemetry or implanted thermocouples offer superior precision for measuring BAT temperature, so long as the probe is sutured to BAT itself or to Sulzer’s vein–a technical challenge because probes tend to drift over time (e.g., (Dodson et al., 2024)).

Our BAT findings in context:

Using SGBS, we demonstrate that the interscapular BAT region is significantly warmer than the adjacent rump surface (Fig. 5C). If surface temperature were purely a reflection of uniform core temperature, this consistent regional hotspot would not be observed.

Our cross-correlation analysis from the photometry (Fig. 5E) shows the rise in BAT surface temperature precedes changes in other body regions by approximately 90 seconds, suggesting that BAT acts as a primary heat source during rest-to-arousal transitions rather than passively following core temperature. This finding is consistent with another study, using telemetric probes placed in BAT, finding that episodic onset of BAT temperature started to increase 3 minutes before body temperature (Ootsuka et al., 2009).

Based on this Reviewer’s comment here and the subsequent one (5), we have now added a new analysis of the temporal patterning of arousal and thermogenesis in the optogenetic cohort of animals; see below for details.

Vasomotor tone

We agree that infrared thermography does not directly measure vasomotor tone. We have revised the text to remove language implying that our measurements directly quantify vasomotor tone, vasodilation or vasoconstriction.

We note that the established approach for non-invasive assessment of vasomotion uses glabrous skin of the tail and ears (Garami et al., 2011; Meyer et al., 2017; Škop et al., 2020). Rump surface temperature measured over hairy, non-glabrous skin correlates more closely with core body temperature than with cutaneous vasomotor tone (Meyer et al., 2017; Škop et al., 2020) and is used in the literature as a reference point for calculating BAT thermogenesis.

In our data, rump surface temperature decreased following PVNOT calcium peaks while BAT and dorsal surface temperatures increased (Fig. 5L-M). This pattern is consistent with sympathetically-driven thermogenesis in which peripheral heat loss is reduced while BAT drives core temperature upwards. We now acknowledge that our rump measurements do not isolate vasomotor contributions. We have revised the manuscript accordingly, replacing references to rump vasoconstriction with language describing the observed thermal pattern while avoiding attribution to a specific thermoeffector mechanism.

Finally, we note that telemetry would strengthen deep-body temperature interpretation, but telemetry does not itself quantify vasomotor tone; the same distal heat-loss readouts described above would be required regardless of core Tb methodology.

In sum, infrared thermography enables non-invasive, simultaneous tracking of multiple thermal features in freely moving, undisturbed animals—a requirement for studying the naturalistic state transitions central to this study. We have added a section to the Discussion acknowledging the limitations of surface infrared thermography.

> *(5) Photostimulation of PVNOT neurons increased Tb after 400 sec (6.6 min) (Figure 5). This latency is too long to conclude that the neuronal stimulation elicited BAT thermogenesis. A more reasonable explanation is that the increase in Tb was caused by the induction of physical activity (Figure S4C), which slowly generates heat and contributes to the elevation of Tb. However, this view contradicts the authors' claim. To address this concern, the authors should directly measure BAT thermogenesis and compare it with the rate of Tb elevation. If BAT thermogenesis occurs, the rate at which the BAT temperature increases must exceed the rate at which Tb rises.*

We thank the reviewer for this thoughtful critique. With this response we first provide additional context about the timeline of temperature increases, and second add a new analysis addressing the relative contributions of activity and BAT-surface to Tb changes.

(1) Additional context on the temporal progression

First, the observed timescale does not, per se, rule out a contribution of BAT thermogenesis. While the kinetics of BAT activation and associated Tb increases can operate on a fast timescale in anesthetized animals, *in vivo* activation of BAT thermogenesis pathways can take several minutes to yield a statistically detectable difference. For example, activation of DMH→rMR glutamatergic signaling, a canonical thermogenic command pathway, takes several minutes to produce a significant increase in both Tb and BAT using telemetric temperature probes (Kataoka et al., 2014).

This timescale could also be consistent with peptidergic neuromodulation by PVNOT neurons, which are more likely to be modulators (and not drivers) of the canonical thermogenic pathway. Oxytocin is known to act via volume transmission and metabotropic receptor signaling, which operate on slower timescales than ionotropic neurotransmission (Ludwig and Leng, 2006). Downstream recruitment of sympathetic outflow and BAT thermogenesis is likewise a multistep autonomic process, not an immediate synaptic event.

Next, the thermal dynamics reported in Figure 5 and Figure S4 are not consistent with activity-induced heat production alone. Specifically:

- Thermal increases were spatially localized to interscapular/dorsal regions corresponding to BAT depots before generalized surface warming.

- Importantly, photostimulation-induced warming was observed even during behavioral states characterized by low baseline activity, suggesting that thermogenic activation was not simply a byproduct of movement.

While we did not directly measure BAT sympathetic nerve activity, our surface thermography approach was designed specifically to resolve regional temperature dynamics over the interscapular BAT area. The spatial specificity and temporal profile of the warming are consistent with BAT thermogenesis rather than uniform musclegenerated heat.

We acknowledge that direct measurement of BAT sympathetic activity or oxygen consumption would provide additional mechanistic resolution. However, given (i) the known role of PVN oxytocin neurons in autonomic regulation, (ii) the spatially localized dorsal temperature increase, and (iii) the temporal dissociation between stimulation onset and gradual systemic Tb rise, we conclude that BAT thermogenesis remains the most parsimonious explanation.

We have revised the Discussion to more explicitly acknowledge these temporal dynamics by clarifying that photostimulation likely follows the timescales of peptidergic neuromodulation.

(2) New analysis

We have added a new analysis to address the relationship between Tb and BAT-surface temperature and locomotion the optogenetic cohort. In short, we show that across all mice changes in BAT typically precede changes in Tb, and that the effect of optogenetic stimulation on core Tb can't be explained by physical activity (nor can it be explained by BAT-surface temperature).

First, cross-correlation of derivatives suggested BAT surface temperature changes typically precede changes in dTb/dt across mice, whereas physical activity changes did not consistently precede dTb/dt. This result, now shown in Fig. S5G, is consistent with our cross-correlation analysis of the fiber-photometry cohort.

Next, we used a lagged regression analysis to test whether photostimulation-evoked increases in core temperature are fully mediated by physical activity. Specifically, we modeled the derivative of core Tb (dTb/dt) using an impulseresponse representation of photostimulation, while controlling for distributed lags (0–120 s) of physical activity and BAT surface temperature derivative, with random effects for mouse and trial. Photostimulation remained a significant predictor of dTb/dt while controlling for activity and BAT-surface (likelihood ratio test, χ^2=7.66, p=0.0056), indicating that the relationship between stimulation and Tb is not fully explained by activity.

> ***Recommendations for the authors:***
>
> ***Editors note:***
>
> *We suggest including key statistical support for the claims in the main text (e.g., results or figure legends).*

We have added statistical support for key claims in the main text results. We have also added references to Table S1 where appropriate (e.g., where there is a long list of statistical results); we hope this aids the readability of the report.

> ***Reviewer #1 (Recommendations for the authors):***

> *See above - the authors should decide what to prioritize, but I only mention significant concerns above. The manuscript could be improved to 'Convincing' or even 'Compelling' with sufficient effort.*

Thanks for the careful reading of the manuscript. We've addressed many of these points, and feel the manuscript has been strengthened as a result.

> *There were also some text errors here and there.*

Several text errors were identified and fixed. Thank you.

> ***Reviewer #2 (Recommendations for the authors):***
>
> *(1) Figure 1I: The quantification shown here is a bit unclear from the figure and legend - are the authors reporting the percentage of cFos+ cells within the OXT+ population, or within the general DAPI+ population? If the latter, including a co-localization analysis to estimate the proportion of OXT+ cells activated would strengthen the interpretation.*

We thank the reviewer for catching this; Reviewer 1 made a similar comment. A typo in the figure legend led to this confusion. Figure 1I is in fact a quantification of the percent *Oxytocin*:*Fos* colocalized cells (not *Fos*:*DAPI*, as was written) in dorsal and ventral subregions of the PVN during active huddling and quiescent huddling. We have corrected the legend and clarified the quantification in the revised manuscript. (Note this response is copy-pasted to other relevant comments).

> *(2) PVN cell types: It would be useful to briefly discuss the potential involvement of other PVN populations (e.g., CRF, AVP neurons) in huddling, given their known roles in social behavior, stress, and thermoregulation.*

Thank you for the insightful comment. We address these points in two parts.

(1) PVN cell types and huddling

Regarding the specific connection between these cell types and huddling: to our knowledge, no study has directly tested the effect of PVN CRF or PVN AVP neuron manipulation on huddling behavior. The most relevant data come from Bendesky et al. (Bendesky et al., 2017), who found that intracerebroventricular administration of AVP in *Peromyscus* inhibited nest building but had no effect on huddling, licking, or pup retrieval (though this pharmacological approach does not isolate PVN AVP neurons specifically). Their chemogenetic manipulation of PVN AVP neurons in *Mus musculus* confirmed the nest-building effect but did not assess huddling. For CRF, the available evidence suggests an opposing role to OT in social care contexts: chemogenetic activation of PVN CRF neurons impairs maternal behavior in postpartum mice (Melón et al., 2018), and intracerebroventricular CRF administration suppresses maternal care and can induce pup-killing in virgin rats (Pedersen et al., 1991).

That said, PVN AVP neurons do promote wakefulness via lateral hypothalamic orexin neurons (Islam et al., 2022) and a recent preprint has implicated PVN AVP neurons in temperature-dependent maternal thermoregulatory behaviors, including co-nesting and shepherding, via projections to the central amygdala (Adahman et al., 2025). Notably, while that study focused on AVP neurons, their c-Fos data also revealed significant temperature-dependent modulation of PVNOT neurons (Fig. 3B), with suppressed activity at thermoneutrality relative to cooler conditions, a pattern suggesting that OT neurons are active under conditions where thermoregulatory effort is required. This data is consistent with our findings on PVNOT neuron involvement in rest-to-arousal transitions driven by thermoregulatory need.

Additionally, Inada et al. (Inada et al., 2025) used an elegant series of viral-genetic experiments to demonstrate that PVN AVP neurons facilitate paternal caregiving behaviors via AVP to oxytocin receptor crosstalk in the preoptic area. Critically, their fiber photometry and circuit mapping data showed that chemogenetic activation of PVN AVP neurons did not recruit PVN OT neurons (Fig. 4), indicating that these populations operate independently in this context. We believe this finding is consistent with our interpretation that the thermoregulatory signals we observe reflect a cell-type specific property of PVNOT neurons. Future work examining how PVNOT, AVP, and CRF population interact during thermoregulatory state transitions would be valuable.

(2) PVN cell types and stress and thermoregulation

PVN CRF and AVP neurons have established roles in stress responses and social behavior, and future studies examining their involvement in huddling would be valuable. However, their direct roles in thermoregulation are limited. PVN CRF neurons are primarily stress-axis regulators whose thermoregulatory influence is mediated indirectly through downstream targets such as the DMH (reviewed in (Morrison and Nakamura, 2019)). AVP's thermoregulatory role is principally as an endogenous antipyretic acting via preoptic area neurons (Tabarean, 2021), rather than through PVN magnocellular AVP neurons.

Importantly, the synchronized pulsatile bursting pattern that is characteristic of OT neurons during lactation (which serves as a key validation benchmark for our PVNOT calcium peaks), appears to be specific to OT neurons and does not generalize to other PVN populations. One study (Popescu et al., 2019) directly demonstrated that lactation-induced IPSC burst upregulation occurs selectively in OT magnocellular neurons, with no change in VP neurons within the same nucleus. VP neurons do exhibit phasic bursting, but these patterns are asynchronous, of longer duration, and serve antidiuretic rather than neuroendocrine-pulsatile functions (De Mota et al., 2004; Poulain et al., 1977; Wakerley et al., 1978). To our knowledge, no studies have reported synchronized burst activity in PVN CRF neurons during lactation or at rest. We have added a brief discussion of these points to the manuscript.

> *(3) Figure 2B: Several behavioral abbreviations (e.g., LMA) are not intuitive and are missing from the legend. Spelling them out or including schematic illustrations would improve clarity.*

We have expanded the figure legends to define all behavioral abbreviations: LMA (Locomotor Activity), EaDr (Eating or Drinking), Groom (Grooming), Nest (Nesting or Nest Building), Quies (Quiescence), Sta (Stationary), ConI (Contact Initiated), ConR (Contact Received), AHud (Active Huddle), QHud (Quiescent Huddle).

> ***Reviewer #3 (Recommendations for the authors):***
>
> *(1) Figures 1D-F and S1A-C: The current magnification is insufficient to clearly resolve the distribution of FOS signals. FOS fluorescence is generally expected to be localized within cell nuclei. However, particularly in Figure 1F, the signals exhibit punctate or fibrous staining in addition to nuclear localization.*
>
> *This raises concerns about the quality of the tissue staining and the reliability of subsequent analyses. Including higher-magnification images would strengthen the credibility of the data presented.*

Thanks for the careful observation. We used a well-validated FOS protocol (see Methods; c-Fos (9F6) Rabbit mAb, Cell Signaling, 14609, 1:1000 dilution in block solution).

To address this issue, in Figure 1 we have included better images of the regions of interest (DMH, LS, and PVN). We also show an inset with DAPI and the FOS IHC. These inset images

show that the FOS signal does co-localize with nuclei.

The reviewer notes that there is a fibrous staining in the PVN. We too noted this type of staining, due to clusters of bright dots in the PVN but not in other regions. This pattern was reproducible across several histological experiments. Fortunately, these bright dots were easily removed in our image processing routine using a selective median filter (pixel radius < 2.0 and and pixel intensity > 50).

> *(2) Figures 2A, 4C, and 6A: As mentioned in the Public Review, the specificity of AAV-mediated gene expression is critical for the strength of the conclusions. Quantitative data demonstrating the expression specificity should be included.*

This point was echoed by Reviewers 1 and 3, and one we have taken several actions to address this. (Note this response is copy-pasted to the other reviewers).

We agree with the reviewers that the rationale for the lactation data should be made more explicit. The primary purpose of this experiment was to validate the identity of oxytocinergic neurons of the PVN.

Our efforts to use IHC to validate the identity of AAV-transfected cells were inconclusive, and we have now added new data to illustrate this point. We have added Fig. S4 that includes quantitative data on expression specificity. We observed significant variability in co-staining (OT+/GCaMP+) across brain slices, likely reflecting the dynamic nature of oxytocin peptide synthesis and storage, particularly with respect to processes lining the third ventricle. This finding is in accordance with other studies that are now cited in the text.

We now emphasize that, because IHC provided variable co-localization, we employed the lactation model as an independent physiological validation of the identity of the recorded neurons.

It is well established that PVNOT neurons undergo dramatic changes in firing dynamics and synchrony during lactation to support milk ejection (Yaguchi et al., 2023; Yukinaga et al., 2022). Conversely, AVP and CRF cell populations in the PVN do not appear to display synchronized pulsatile bursting during lactation (see response to Reviewer-2 comment-2 in 'Recommendation for authors' and our updated Discussion). Observing these characteristic changes in our recorded population provides high-confidence functional evidence that we are targeting oxytocin neurons. We have revised the text to clarify that Figure 4 serves primarily as a functional verification of genetic targeting.

We also acknowledge in the Discussion the possibility that our Cre-line may capture a small percentage of non-oxytocinergic neurons, while noting that the dramatic shift in calcium dynamics during lactation (Figure 4I–L) strongly suggests the recorded population is dominated by oxytocin neurons.

> *(3) Figure 2D: The authors should show an expanded view of a representative "PVNOT peak" from the spikes presented.*

We have added a representative peak to Fig. 2D.

> *(4) Figure 2E-J: All the abbreviations of the behavioral states must be defined in the figure or legend.*

We added these abbreviations to the legend, and a text box reading "See legend for abbreviations" to the schematic.

> *(5) Figure 2F, G, I, and J: The units on the y-axis should be indicated to facilitate interpretation.*

We have added these units. Thanks.

> *(6) Figure 3A: Three large PVNOT peaks occurred between 01:30 and 02:00. However, these peaks did not cause an obvious transition in behavioral states or an increase in Tb within several minutes. Therefore, statements such as "PVNOT neurons predict transitions towards thermogenesis and behavioral arousal" in the text and subheading (pages 7 and 9) are questionable.*

We thank the reviewer for this careful observation. The three peaks between 01:30 and 02:00 that do not immediately lead to a behavioral transition illustrate a key aspect of our findings: the relationship between PVNOT activity and state transitions is probabilistic and state-dependent, not deterministic. Our logistic regression analysis (Fig. 3F, H, J, L) demonstrates that peaks increase the probability of a transition (up to ~20% per second) rather than acting as an obligatory "on switch." While individual variability exists in any single trace, the group-level analysis reveals a statistically significant increase in physical activity following PVNOT peaks (Fig. 3B–E).

We therefore use ‘predict’ in a probabilistic sense: PVNOT peaks increase the conditional probability of impending state transitions in a manner that depends on behavioral context, rather than acting as an obligate trigger in every instance. We have taken care to not claim that PVNOT neurons are a necessary causal factor for transitions towards thermogenesis and arousal.

We have updated the figure legend to clarify that Figure 3A shows an individual example trace, and revised the subheading on page 7 to more accurately reflect the probabilistic nature of this relationship: "PVNOT neurons predict increased likelihood of transitions towards thermogenesis and behavioral arousal in social and non-social contexts".

We qualified the word “predicts” with “probabilistically” in the third paragraph of this section.

Finally, this comment is related to the Reviewer’s comment-2 in the Public Reviews. To address that comment, we added a new analysis (now Fig. 3P&S) which shows that the presence of a peak in a bout of rest increases the thermogenic trajectory compared to bouts without a peak.

> *(7) Figure 3F and H: If PVNOT peaks contribute to the initiation of transitions into the active state, the probability of peak occurrence should reach its maximum prior to the quiescence offset. However, the figures do not present the probability trajectory after the offset, which limits the ability to evaluate the authors' interpretation. Reanalysis extending to 150 seconds post-offset would be needed to clarify this issue.*

Thank you for this suggestion. We agree that examining PVNOT dynamics around the period following quiescence (and quiescent huddling) offset can further inform how PVNOT activity relates to rest-to-active transitions, and this has led to new insights within the manuscript.

For background, in the original analysis (Fig. 3F,H), we used logistic regression to quantify how peak probability differs between bout onset versus near bout offset. We focused these analyses on the the timeframe of the bouts themselves (plus a small margin) because, in freely behaving animals, the pre-onset and post-offset period is heterogeneously composed of multiple potential subsequent behaviors (e.g., brief re-entry into quiescence, nesting, active huddling, locomotion, etc), which would confound a single post-offset probability trajectory (unless offsets are stratified by the identity of the subsequent behavioral state–beyond the scope of this paper).

To address this concern, we now expand our peri-event baseline calcium analysis to include three minutes before and three minutes after both bout onset and bout offset for all four behaviors (new Fig. S3I–L). These extended traces show that for the two resting states (quiescence and quiescent huddling), baseline PVNOT calcium reaches a minimum near bout onset and a maximum near bout offset, whereas for the two active states (nesting and active huddling) baseline calcium shows the opposite pattern (maximum near onset, minimum near offset). Thus, the expanded post-offset analyses provide a more complete view of PVNOT calcium dynamics across the requested post-offset epoch and further support the conclusion that PVNOT activity is aligned with (and elevated around) behavioral transitions in a state-dependent manner. We have updated the Results text accordingly and now explicitly reference these new extended peri-event baseline analyses.

> *(8) Figures 4H and I: Figure 4H shows that the waveform in the PPD2-7 group has a narrower FWHM than the Virgin group, which is the opposite of the group data in Figure 4I. Presenting scaled waveforms in parallel would allow for a clearer comparison across groups.*

Thank you for pointing out the inconsistency between the representative waveform in Fig. 4H and the group summary in Fig. 4I. You were correct: the PPD2–7 and Virgin waveforms in Fig. 4H had been mislabeled. We have corrected the labeling. (We verified that the underlying data are correct).

As suggested, to enable visual comparison of waveform width across groups independent of amplitude differences, we derived peak-normalized average waveforms using a normalization procedure for every peak prior to averaging. Specifically, for each peak we (1) baseline-subtracted the trace by subtracting the mean fluorescence in a pre-peak baseline window, and then (2) divided the baseline-subtracted waveform by its own maximum value to scale the event amplitude to 1. We then computed the mean ± SEM of these peak-normalized waveforms across events within each group.

We believe these changes resolve the discrepancy and improve the clarity of the figure, consistent with your suggestion.

> *(9) Figure 5: In studies of thermoregulatory processes, tail blood flow or temperature is commonly used as an indicator of vasomotor responses. Is it feasible to track tail temperature using the SGBS system? If not, it may be helpful to acknowledge this as a technical limitation.*

We agree that tail temperature is a commonly used indicator of vasomotor responses. While SGBS could in principle be trained to segment the tail, the current model was optimized for dorsal body regions viewed from an overhead perspective. Reliable tail tracking presents substantial technical challenges in our configuration of homecage recordings. The tail's thin geometry and rapid, multidirectional movement frequently result in partial or complete occlusion (e.g., beneath bedding or the animal's body). In addition, during vasoconstriction the tail temperature approaches ambient floor temperature, reducing thermal contrast and making segmentation unreliable with the current thermal resolution limited by our camera. We have acknowledged this as a technical limitation in the Discussion, in the section called "Thermal tracking and validation of PVNOT recording specificity".

> *(10) Figure S5: Please describe the reason and histological background for the intravenous injection of FluoroGold.*

Intravenous injection of FluoroGold (FG) was used to histologically differentiate between magnocellular and parvicellular oxytocin neurons in the PVN. Because the posterior pituitary is located outside the blood-brain barrier,

i.v. FG is selectively taken up by terminals of magnocellular neurons and retrogradely transported to their cell bodies. This allows us to infer the neuroanatomical identity (magno- vs. parvicellular) of the PVNOT neurons of interest. We have updated the Methods with a detailed description of the FG injection protocol as follows:

"To distinguish between peripheral-projecting magnocellular and central-projecting parvicellular neurons, mice received 15 uL intravenous injection of 4% Fluoro-Gold (Fluorochrome) diluted in 100 uL of sterile saline. Prior to injection, mice were given an analgesic dose of carprofen (20 mg/kg, s.c.). Mice were briefly restrained using a modified 50 mL conical tube, in which holes were drilled to allow for proper air flow and respiration. Mouse tails were interposed between two heating pads to enhance visibility of the tail vein. Tails were wiped down with 70% ethanol and FG was administered via either right or left lateral tail vein using a 0.5 mL 28G syringe. Mice were sacrificed 24- 48 hours post-FG administration."

> *The following are minor points.*
>
> *(11) Figure 2E-G, Figure 3F,G, Figure S2G,I, Figure S3A: "quiesence" > "quiescence". This typo may appear elsewhere in the manuscript as well.*

Thanks. These edits have been made.

> *(12) Page 7, line 14: Peaks were NOT significantly increased at 29{degree sign}C in Figure 2N.*

Thanks for the very careful read. By way of explanation: this difference had been significant in an earlier draft; however, when we added more replicates, the difference went away. We have corrected this sentence.

> *(13) There are mislabeled figure numbers in the main text. The authors should carefully check this throughout the manuscript.*

We found mislabeled figure numbers and have corrected them.

> *(14) Page 13, lines 1- 2: To make the description clearer, it might be better to rephrase the part that says, "some blue light stimulations occurred." As it stands, it could give the impression that the stimulations happened spontaneously. Using a phrase like "were delivered" would more clearly indicate that these were intentional, experimenter-controlled events.*

Agreed. Thanks. The edit has been made.

> *Additional comments:*
>
> *The oxytocin system is thought to support a wide range of physiological and behavioral functions, and the circuits involving oxytocin neurons are likely to be regulated in complex and dynamic ways. As oxytocin research continues to expand, the growing body of evidence not only deepens our understanding but also highlights the system's complexity. In this context, the development of an approach that enables the observation of oxytocinergic neuron activity in parallel with naturalistic behavior represents a promising methodological contribution. It is likely that similar experimental frameworks will become increasingly common in future studies. While reading this manuscript, as a reader rather than a reviewer, I was wondering how OXT neurons detect or define the "rest balance-point," and how they might contribute to shifting the brain toward an "awake balance-point" (Figure 7). Given that eLife allows authors to include an "Ideas and Speculation" subsection within the Discussion, it would be appreciated - though not*

> *essential - if the authors could briefly share their perspective on this point. I believe such mechanistic insight would make the manuscript more intellectually stimulating.*

This is a great suggestion. We have added a new “Ideas and Speculation” section of the Discussion.

References

Adahman Z, Ooyama R, Gashi DB, Medik ZZ, Hollosi HK, Sahoo B, Akowuah ND, Riceberg JS, Carcea I. 2025. Hypothalamic Vasopressin Neurons Enable Maternal Thermoregulatory Behaviors. DOI: *https://doi.org/10.1101/2025.01.23.634569*

Bendesky A, Kwon Y-M, Lassance J-M, Lewarch CL, Yao S, Peterson BK, He MX, Dulac C, Hoekstra HE. 2017. The genetic basis of parental care evolution in monogamous mice. Nature 544:434–439. DOI: *https://doi.org/10.1038/nature22074*

Crane JD, Mottillo EP, Farncombe TH, Morrison KM, Steinberg GR. 2014. A standardized infrared imaging technique that specifically detects UCP1-mediated thermogenesis in vivo. Molecular Metabolism 3:490– 494. DOI: *https://doi.org/10.1016/j.molmet.2014.04.007*

De Mota N, Reaux-Le Goazigo A, El Messari S, Chartrel N, Roesch D, Dujardin C, Kordon C, Vaudry H, Moos F, Llorens-Cortes C. 2004. Apelin, a potent diuretic neuropeptide counteracting vasopressin actions through inhibition of vasopressin neuron activity and vasopressin release. Proceedings of the National Academy of Sciences 101:10464–10469. DOI: *https://doi.org/10.1073/pnas.0403518101*

Dodson AD, Herbertson AJ, Honeycutt MK, Vered R, Slattery JD, Goldberg M, Tsui E, Wolden-Hanson T, Graham JL, Wietecha TA, O’Brien KD, Havel PJ, Sikkema CL, Peskind ER, Mundinger TO, Taborsky GJ, Blevins JE. 2024. Sympathetic Innervation of Interscapular Brown Adipose Tissue Is Not a Predominant Mediator of Oxytocin-Induced Brown Adipose Tissue Thermogenesis in Female High Fat Diet-Fed Rats. Current Issues in Molecular Biology 46:11394–11424. DOI: *https://doi.org/10.3390/cimb46100679*

Garami A, Pakai E, Oliveira DL, Steiner AA, Wanner SP, Almeida MC, Lesnikov VA, Gavva NR, Romanovsky AA. 2011. Thermoregulatory Phenotype of the Trpv1 Knockout Mouse: Thermoeffector Dysbalance with Hyperkinesis. The Journal of Neuroscience 31:1721–1733. DOI: *https://doi.org/10.1523/JNEUROSCI.4671-10.2011*

Inada K, Hagihara M, Yaguchi K, Irie S, Inoue YU, Inoue T, Miyamichi K. 2025. Vasopressin-to-oxytocin receptor crosstalk in the preoptic area underlying parental behaviors in male mice. Nature Communications 16:10844. DOI: *https://doi.org/10.1038/s41467-025-66908-0*

Islam MT, Rumpf F, Tsuno Y, Kodani S, Sakurai T, Matsui A, Maejima T, Mieda M. 2022. Vasopressin neurons in the paraventricular hypothalamus promote wakefulness via lateral hypothalamic orexin neurons. Current Biology 32:3871-3885.e4. DOI: *https://doi.org/10.1016/j.cub.2022.07.020*

Kataoka N, Hioki H, Kaneko T, Nakamura K. 2014. Psychological Stress Activates a Dorsomedial HypothalamusMedullary Raphe Circuit Driving Brown Adipose Tissue Thermogenesis and Hyperthermia. Cell Metabolism 20:346–358. DOI: *https://doi.org/10.1016/j.cmet.2014.05.018*

Landen JG, Vandendoren M, Killmer S, Bedford NL, Nelson AC. 2024. Huddling substates in mice facilitate dynamic changes in body temperature and are modulated by Shank3b and Trpm8 mutation. Communications Biology 7:1186. DOI: *https://doi.org/10.1038/s42003-024-06781-7*

Law J, Chalmers J, Morris DE, Robinson L, Budge H, Symonds ME. 2018. The use of infrared thermography in the measurement and characterization of brown adipose tissue activation. Temperature 5:147–161. DOI: *https://doi.org/10.1080/23328940.2017.1397085*

Ludwig M, Leng G. 2006. Dendritic peptide release and peptide-dependent behaviours. Nature Reviews Neuroscience 7:126–136. DOI: *https://doi.org/10.1038/nrn1845*

Melón LC, Hooper A, Yang X, Moss SJ, Maguire J. 2018. Inability to suppress the stress-induced activation of the HPA axis during the peripartum period engenders deficits in postpartum behaviors in mice. Psychoneuroendocrinology 90:182–193. DOI: *https://doi.org/10.1016/j.psyneuen.2017.12.003*

Meyer CW, Ootsuka Y, Romanovsky AA. 2017. Body Temperature Measurements for Metabolic Phenotyping in Mice. Frontiers in Physiology 8:520. DOI: *https://doi.org/10.3389/fphys.2017.00520*

Morrison SF, Nakamura K. 2019. Central Mechanisms for Thermoregulation. Annual Review of Physiology 81:285– 308. DOI: *https://doi.org/10.1146/annurev-physiol-020518-114546*

Ootsuka Y, de Menezes RC, Zaretsky DV, Alimoradian A, Hunt J, Stefanidis A, Oldfield BJ, Blessing WW. 2009. Brown adipose tissue thermogenesis heats brain and body as part of the brain-coordinated ultradian basic rest-activity cycle. Neuroscience 164:849–861. DOI: *https://doi.org/10.1016/j.neuroscience.2009.08.013*

Pedersen CA, Caldwell JD, McGuire M, Evans DL. 1991. Corticotronpin-releasing hormone inhibits maternal behavior and induces pup-killing. Life Sciences 48:1537–1546. DOI: *https://doi.org/10.1016/00243205(91)90278-J*

Popescu IR, Buraei Z, Haam J, Weng F, Tasker JG. 2019. Lactation induces increased IPSC bursting in oxytocinergic neurons. Physiological Reports 7:e14047. DOI: *https://doi.org/10.14814/phy2.14047*

Poulain DA, Wakerley JB, Dyball REJ. 1977. Electrophysiological differentiation of oxytocin- and vasopressinsecreting neurones. Proceedings of the Royal Society of London. Series B. Biological Sciences 196:367– 384. DOI: *https://doi.org/10.1098/rspb.1977.0046*

Škop V, Guo J, Liu N, Xiao C, Hall KD, Gavrilova O, Reitman ML. 2020. Mouse Thermoregulation: Introducing the Concept of the Thermoneutral Point. Cell Reports 31:107501. DOI: *https://doi.org/10.1016/j.celrep.2020.03.065*

Tabarean IV. 2021. Activation of Preoptic Arginine Vasopressin Neurons Induces Hyperthermia in Male Mice. Endocrinology 162:bqaa217. DOI: *https://doi.org/10.1210/endocr/bqaa217*

Wakerley JB, Poulain DA, Brown D. 1978. Comparison of firing patterns in oxytocin- and vasopressin-releasing neurones during progressive dehydration. Brain Research 148:425–440. DOI: *https://doi.org/10.1016/00068993(78)90730-8*

Yaguchi K, Hagihara M, Konno A, Hirai H, Yukinaga H, Miyamichi K. 2023. Dynamic modulation of pulsatile activities of oxytocin neurons in lactating wild-type mice. PLOS ONE 18:e0285589. DOI: *https://doi.org/10.1371/journal.pone.0285589*

Yukinaga H, Hagihara M, Tsujimoto K, Chiang H-L, Kato S, Kobayashi K, Miyamichi K. 2022. Recording and manipulation of the maternal oxytocin neural activities in mice. Current Biology 32:3821-3829.e6. DOI: *https://doi.org/10.1016/j.cub.2022.06.083*

https://doi.org/10.7554/eLife.108212.2.sa0